

國立交通大學

機械工程學系

博士論文

新型腰椎獨立式融合器的生物力學分析

Biomechanical Analysis of A New Stand-alone Lumbar Cage

研究生：江銘傑

指導教授：洪景華 教授

中華民國 102 年 11 月

新型腰椎獨立式融合器的生物力學分析

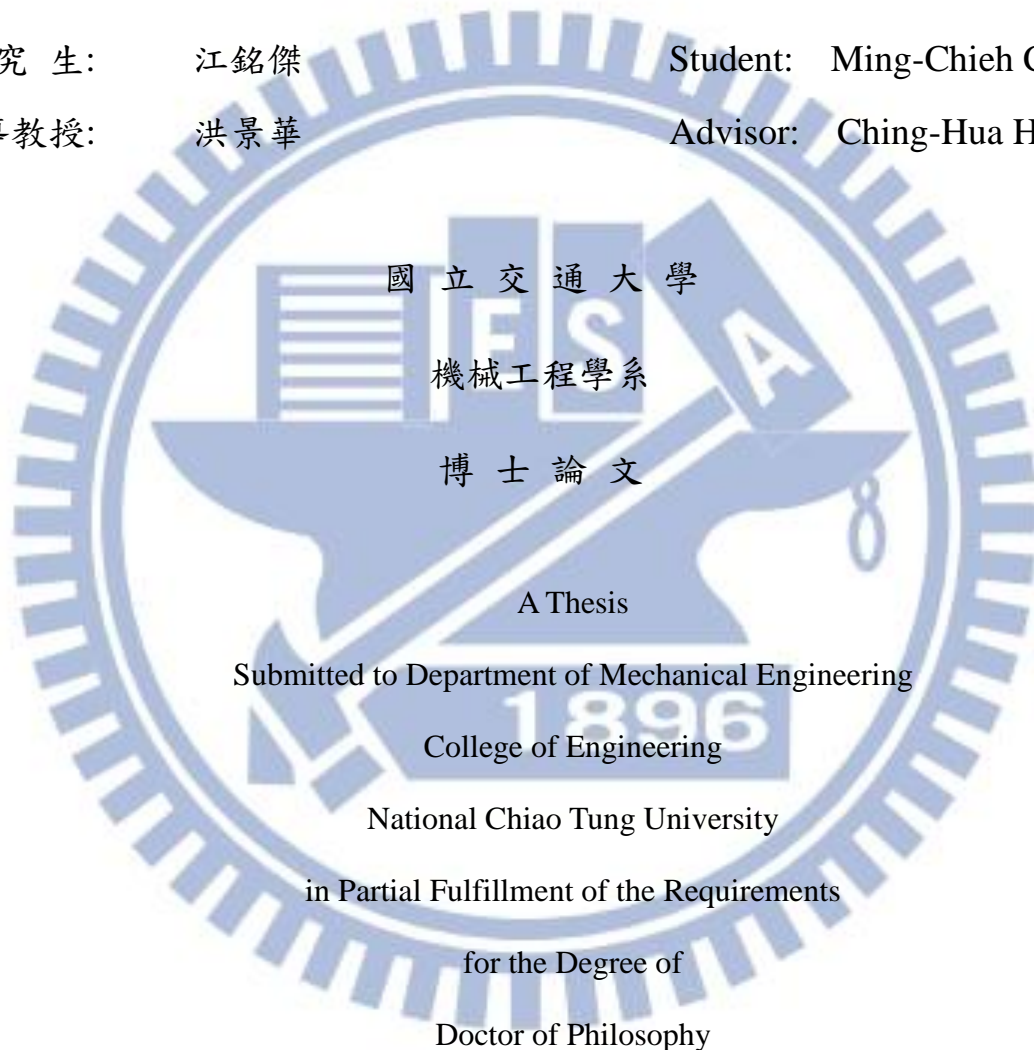
Biomechanical Analysis of A New Stand-alone Lumbar Cage

研究生: 江銘傑

Student: Ming-Chieh Chiang

指導教授: 洪景華

Advisor: Ching-Hua Hung



國立交通大學

機械工程學系

博士論文

A Thesis

Submitted to Department of Mechanical Engineering

College of Engineering

National Chiao Tung University

in Partial Fulfillment of the Requirements

for the Degree of

Doctor of Philosophy

in

Mechanical Engineering

November 2013

Hsinchu, Taiwan, Republic of China

中華民國 102 年 11 月

新型腰椎獨立式融合器的生物力學分析

研究生：江銘傑

指導教授：洪景華 教授

國立交通大學機械工程學系

摘 要

腰椎間盤退化和其所引發的各種併發症是目前世界常遭遇的脊椎病變之一，其治療方式分為保守與手術治療，其中，腰椎間融合術是手術治療方式之一，其方法是清除發生病變的腰椎間盤，再將自體或異體骨植入，且合併使用椎間融合器，以達到去除病源、提供穩定脊椎、避免神經壓迫等治療效果。研究指出，在前腰椎融合術(Anterior lumbar interbody fusion, ALIF)單獨使用融合器，無法提供脊椎在後彎動作下足夠的穩定性，必須搭配後位內固定器才能有良好穩性效果，達成椎間融合的目的。但植入後位內固定器需增開後方傷口，會損壞肌肉血管組織甚至傷及脊神經。因此，一種具備自我穩定能力的獨立椎間融合器(Self-stabilizing stand-alone fusion cage)設計發展出來，期望透過特殊的幾何設計，在融合手術時無需搭配後位內固定器就能達成椎間融合的融合效果。

本研究利用一個經過驗證的五節腰椎有限元素模型，在施加伴隨負荷(Follower load)的情形進行分析，共分為兩個部分，第一部分進行三款 Self-stabilizing stand-alone cage：新型 Latero 融合器，與兩種舊有的 ALIF 融合器(SynFix, Stabilis)，對比傳統 ALIF 融合器搭配後位內固定器的穩定效果比較，並藉由多種生物評估參數包括：穩定性、環帶應力、小面關節受力以及植入物應力，來探討三款 Stand-alone 融合器的椎間穩定度與此三種融合器對於腰椎界面造成的影響。第二部分則對 Latero 融合器提出後續設計建議並加以分析。

本研究第一部分結果發現，新型 Stand-alone 融合器 Latero 的穩定效果相似於和傳統 ALIF 融合器搭配後位內固定器，若在考量避免增開後方傷口對病患造成影響的情形下，建議使用 Latero 融合器，就可提供腰椎間足夠的穩定性與適合融合的環境。第二部分結果則提出針對 Latero 融合器的後續設計建議。

關鍵字： 前位融合; 獨立式融合器; 有限元素分析。

Biomechanical Analysis of A New Stand-alone Lumbar Cage

Student: Ming-Chieh Chiang

Advisor: Prof. Ching-Hua Hung

Department of Mechanical Engineering

National Chiao Tung University

ABSTRACT

For anterior lumbar interbody fusion (ALIF), stand-alone cages can be supplemented with vertebral plate, locking screws, or threaded cylinder to avoid the use of posterior fixation. Intuitively, the plate, screw, and cylinder aim to be embedded into the vertebral bodies to effectively immobilize the cage itself. The kinematic and mechanical effects of these integrated components on the lumbar construct have not been extensively studied. In the part-1 of this study, a nonlinearly lumbar finite-element model was developed and validated to investigate the biomechanical differences between three stand-alone (Latero, SynFix, and Stabilis) and SynCage-Open plus transpedicular fixation. All four cages were instrumented at the L3-4 level. In the part-2 of this study, the Latero was analyzed for different design parameters.

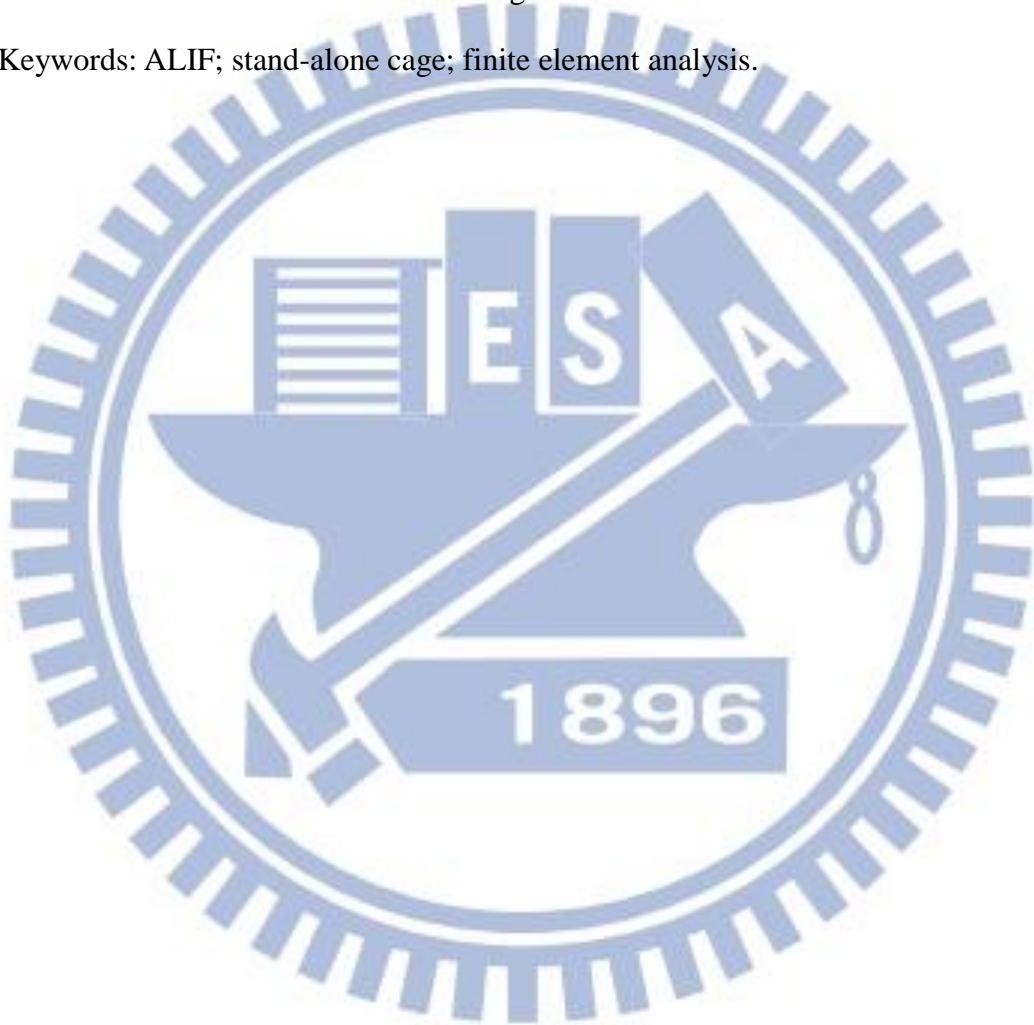
The lumbar models were subject to the follower load along the lumbar column and the moment at the lumbar top to produce flexion (FL), extension (EX), left/right lateral bending (LLB, RLB), and left/right axial rotation (LAR, RAR). A 10 Nm moment was applied to obtain the six physiological motions in all models. The comparison indices included disc ROM, facet contact force, and stresses of the annulus and implants.

At the surgical level, the SynCage-open model supplemented with transpedicular fixation decreased ROM (>76%) greatly; while the SynFix model decreased ROM 56-72%, the Latero model decreased ROM 36-91%, in all motions as compared with the INT model. However, the

Stabilis model decreased ROM slightly in extension (11%), lateral bending (21%), and axial rotation (34%). At the adjacent levels, there were no obvious differences in ROM and annulus stress among all instrumented models.

ALIF instrumentation with the Latero or SynFix cage provides an acceptable stability for clinical use without the requirement of additional posterior fixation. However, the Stabilis cage is not favored in extension and lateral bending because of insufficient stabilization.

Keywords: ALIF; stand-alone cage; finite element analysis.



誌謝

首先要衷心地感謝指導教授洪景華老師，願意耗費許多時間教導學生，使學生遭遇研究瓶頸時，不僅能迎刃而解，且能適時給予信心與鼓勵，引導學生培養獨立研究的態度與創新構想的思維，讓學生盡情的發揮。

特別感謝陳世豪醫師、林君甫醫師以及林上智教授，在研究上提供了專業智識與寶貴建議。

感謝廖建忠博士、陳振昇教授、林上智教授、楊秉祥教授、林君甫醫師在百忙之中挪出時間參加學生口試給於意見，讓學生的論文更加完整。

回首研究所期間，特別感謝實驗室政成學長、正展學長，在遇到困難時，適時剖析建議與協助；感謝研究室夥伴在學業及生活中的指導與關懷，特別是實驗室生醫組的同學，在研究生涯中的陪伴，所建立的深厚友誼與每一句歡笑將成為美好的回憶。期間，也受到交大機械所許多師長、助教的教導與提攜，同樣致上最誠摯的謝意。

最後，僅以此論文獻給我最敬愛的雙親與家人，感恩他們多年來不辭辛勞的養育、栽培與無怨無悔的付出。

作者：江銘傑 謹誌

中華民國 102 年 11 月

Table of Contents

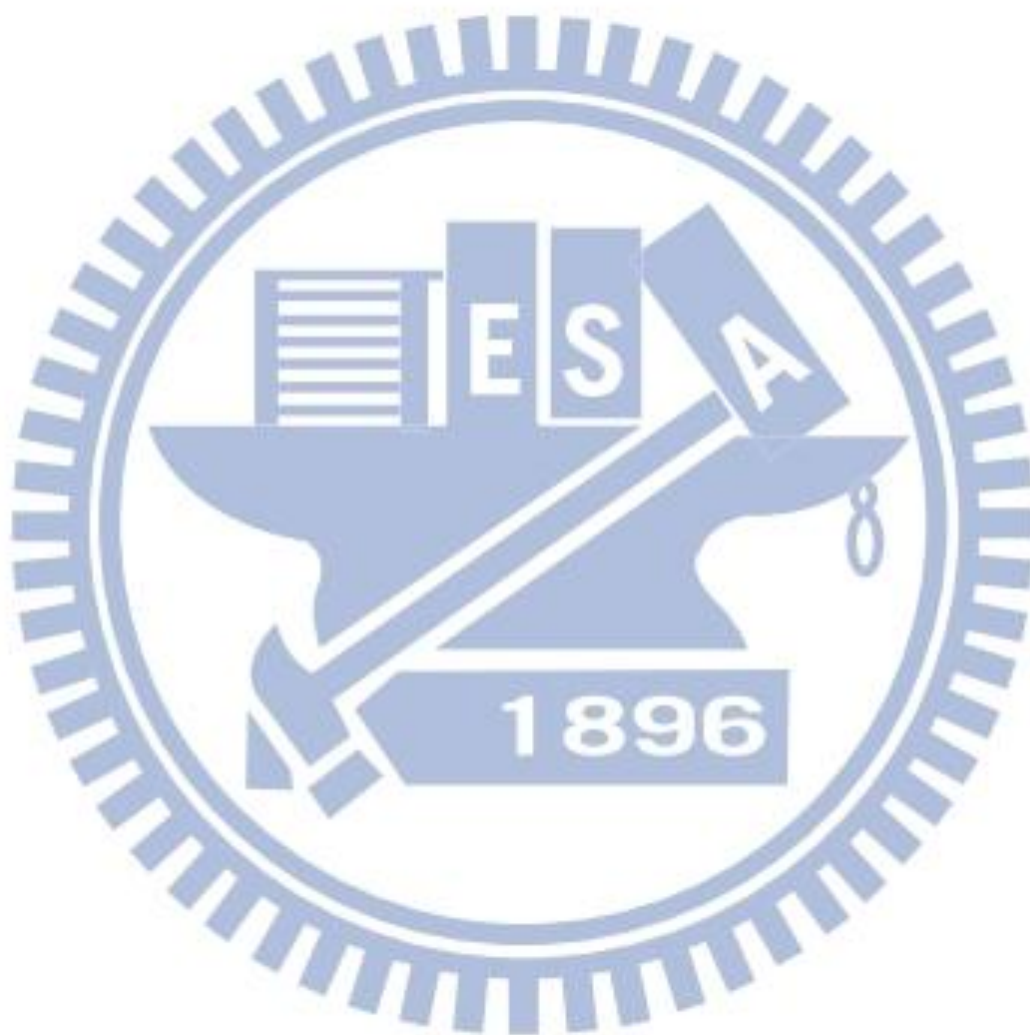
Chapter 1 Introduction.....	1
1.1. Overview.....	1
1.2. Motivation and objectives.....	1
1.3. Outline	3
Chapter 2 Background.....	5
2.1. Spine anatomy and biomechanics.....	5
2.1.1. Vertebra.....	7
2.1.2. Intervertebral disc	8
2.1.3. Facet joint	9
2.1.4. Spinal ligaments.....	10
2.1.5. Neural foramen	11
2.1.6. Spinal cord and nerve roots	11
2.2. Spinal pathology and treatments.....	12
2.2.1. Lumbar spinal stenosis.....	13
2.2.2. Conservative therapy	16
2.2.3. Decompression surgery.....	17
2.2.4. Fusion surgery.....	18
2.2.5. Lumbar interbody fusion cages.....	21
2.2.6. Minimally invasive techniques and stand-alone implant.....	23
Chapter 3 Materials and Methods.....	26
3.1 Part-1 of this study	26
3.1.1. The establishment of intact lumbar spine model (INT model).....	26
3.1.2. The establishment of implant models	40
3.2 Part-2.....	46

3.2.1. The different insert positions of Latero model.....	46
3.2.2. Different angle of the lateral plate of the Latero.....	47
3.3. Boundary and loading conditions	49
Chapter 4 Results.....	51
4.1. Part-1.....	51
4.1.1. ROM	51
4.1.2. Annulus stress	54
4.1.3. Facet contact force	57
4.1.4. Implant stress	59
4.1.5. Endplate stress	61
4.2. Part-2.....	62
4.2.1. ROM of different positions.....	62
4.2.2. ROM of different lateral plate angles	64
Chapter 5 Discussion.....	66
5.1. Part-1: Comparison with stand-alone implants and conventional fixation method	66
5.1.1. ROM	66
5.1.2. von-Mises stress at the vertebra.....	68
5.1.3. Facet contact force	69
5.1.4. Stress distribution at the annulus	70
5.2. Part-2: The effects of different design factors for Latero device.....	70
5.3. Limitations	71
Chapter 6 Conclusion and Future Work	73
6.1 Part-1: Conclusion	73
6.2 Part-2: Conclusion	74
6.3 Future work.....	74

References 76

Vita..... 88

Publication List..... 88



List of Tables

Table 3. 1: Material properties used in the FE model.....	30
Table 3. 2: Material properties of the implants.....	45



List of Figures

Figure 2. 1: Vertebral column: Anterior, left lateral and posterior views of the major regions of the spine [15].	6
Figure 2. 2: The motion segment in the lumbar spine, which composed of two vertebrae and surrounding soft tissue [16].	7
Figure 2. 3: The Shape of a human vertebra: (A) Superior view of the typical lumbar vertebra [16]. (B) The trabecular structure of a lumbar vertebral body in sagittal section [18].	8
Figure 2. 4: In the intervertebral disc, the annulus fibrosus, made up of laminar layers of criss-crossed collagen fibers, surrounds the nucleus pulposus [16].	9
Figure 2. 5: Orientation of lumbar facet to the transverse plane (left) and the frontal plane (right) [16].	10
Figure 2. 6: The major ligaments of the spine [27].	11
Figure 2. 7: Spinal Cord and Nerve Roots [28].	12
Figure 2. 8: The radiograph shows the spinal instability [34].	14
Figure 2. 9: Mono-segmental lumbar spinal stenosis at L4-L5 segment [35].	15
Figure 2. 10: Multi-segmental lumbar spinal stenosis at L3-L5 segment [35].	15
Figure 2. 11: Pathoanatomical illustration of lumbar spine stenosis [35].	16
Figure 2. 12: Pedicle screw instrumentation [51].	18
Figure 2. 13: This radiograph demonstrates a solid bony union between L3 and L4 [53].	19
Figure 2. 14: Common surgical techniques for insertion of a spinal cage. The black arrow indicates the ALIF approach, the red arrow indicates the PLIF approach, and the blue arrow indicates the TLIF approach, and the green arrow indicated the lateral approach.	20
Figure 2. 15: Interbody fusion combined with posterior pedicle screw fixation [57].	21

Figure 2. 16: Various lumbar interbody fusion cages: (A) SynCage-Open (Synthes Spine, Inc., PA, USA); (B) O.I.C. (Stryker Spine, Mahwah, New Jersey, USA); (C) AVS-TL (Stryker Spine, Mahwah, New Jersey, USA).	22
Figure 2. 17: Front and left side views of the four ALIF cages were used in this study. (A) Latero. (B) SynFix. (C) Stabilis. (D) SynCage-Open.....	25
Figure 3. 1: Each spinal component was selected from computed tomography scan DICOM file to create material-related contours.	28
Figure 3. 2: Modeling process of the L3 vertebra: (A) surface geometries of vertebra were reconstructed through sequential processed computed tomography scan DICOM file; (B) surface geometry was exported to the DXF file; (C) FE model of the L3 vertebra.	29
Figure 3. 3: The lumbar finite element model used in this study (Intact model from L1 to L5 levels)	29
Figure 3. 4: Convergence test of the intact model: (A) result of motion changes under flexion; (B) result of motion changes under extension; (C) result of motion changes under axial rotation; (D) result of motion changes under lateral bending.	31
Figure 3. 5: (A)The illustration of applying follower load; The experiment setting of follower load ((B) lateral view and(C) front view) [14].	32
Figure 3. 6: Lumbar spine specimen mounted in a spine tester and loaded with a pure moment plus a follower load [109].....	33
Figure 3. 7: (A)The illustration of wrapping element; (B)the wrapping element applied on the five levels lumbar spine [110,111].....	34
Figure 3. 8: Lateral view of Renner's[112] finite element model showing follower load trusses at each vertebra.	35
Figure 3. 9: Finite element model of the lumbar spine with the loads applied in Rollhman's study[113].	36

Figure 3. 10: The illustration of follower load of Rolhman's model [113].	37
Figure 3. 11: The illustration of follower load (simplified: applied in the center).	38
Figure 3. 12: The illustration of follower load (bilateral: applied bilaterally)	38
Figure 3. 13: Range of motion (ROM) calculated for the L1-L5 segments of intact lumbar spine is compared to four kinds of preload condition.	39
Figure 3. 14: Range of motion (ROM) calculated for the L1-L5 segments of intact lumbar spine is compared to previous <i>in vitro</i> experiments. (A)Intact lumbar spine without follower load; (B)intact lumbar spine with simplified follower load.	40
Figure 3. 15: The implant devices used in this study. (A)Latero. (B) SynFix. (C)Stabilis. (D)SynCage-Open	41
Figure 3. 16: The vertical view and lateral cross-sectional view of Latero implanted into L3-L4 segment	42
Figure 3. 17: The vertical view and lateral cross-sectional view of (A) SynFix and (B) Stabilis implanted into L3-L4 segment	43
Figure 3. 18: The vertical view and rear view of SynCage-Open and the pedicle screws implanted into L3-L4 segment	44
Figure 3. 19: The different positions of Latero model:(A)Anterior; (B)Middle; (C)Posterior	47
Figure 3. 20: The lateral view of (A)Latero-A and (B)Latero-P	47
Figure 3. 21: The lateral view of Latero-(30).	48
Figure 3. 22: The different bending angle of lateral plate:(A)Oblique view of original plate; (B)Lateral view of original plate; (C) Lateral view of modified plate.	48
Figure 3. 23: The boundary and loading conditions of the simulation were that the inferior surface of L5 vertebra was fixed, and 10 Nm moment and a 400 N follower load were applied to the superior surface of L1 vertebra.	50
Figure 4. 1: Comparison of the normalized intersegmental ROM among all models under six motions. (A) Surgical level. (B) Upper adjacent levels. (C) Lower adjacent level.	53

Figure 4. 2: Stress comparison of the normalized stress among all models under six motions. (A) Annulus stress. (B) Implant stress.	55
Figure 4. 3: Distribution of the annulus stress for the four models. (A) Extension (B) Left lateral bending. (C) Right lateral bending.	56
Figure 4. 4: Comparison of facet contact force among all models. (A) Extension. (B) Left axial rotation. (C) Right axial rotation. Middle bars are the surgical level (L3-L4); left and right bars are the adjacent levels (L2-L3 and L4-L5).....	58
Figure 4. 5: Distribution of implant stress for the Latero, SynFix, and Stabilis models. (A) Extension. (B) Left axial rotation. (C) Right axial rotation.....	60
Figure 4. 6: Comparison of endplate stress on the lower surface of the L3 vertebra for all models.	61
Figure 4. 7: Comparison of the normalized intersegmental ROM among Latero models under six motions. (A) Surgical level. (B) Upper adjacent levels. (C) Lower adjacent level	63
Figure 4. 8: Comparison of the normalized intersegmental ROM among different lateral plate angles of Latero models under six motions. (A) Surgical level. (B) Upper adjacent levels. (C) Lower adjacent level	65
Figure 5. 1: Distribution of endplate stress on the upper surface of the L4 vertebra for all models. (A) Flexion. (B) Extension. (C) Left lateral bending. (D) Left axial rotation.....	69

Chapter 1 Introduction

1.1. Overview

Degenerative disc disease (DDD) in the lumbar spine can be associated with displacement of the vertebral body. DDD with concomitant spinal stenosis is among the most frequent conditions in the aging adults. Treatment options for spinal stenosis continue to be discussed among spine professionals, but several studies have shown that surgical procedures provided better improvement in pain and function compared to usual nonoperative care [1, 2]. Various surgical options have been studied to evaluate safety and optimal radiological and clinical options. A new minimally invasive, stand-alone alternative different to conservative and standard surgical implants has been developed. The new Latero (Latero; A-Spine Asia, Taipei, Taiwan) device uses the vertebrae as the fulcrums. The lateral vertebral plate utilizes a stabilizing mechanism which is dissimilar from those of other devices. This technique is novel in that it can be used to gain access to the lumbar spine via a lateral approach. Hence, the potential complications with an anterior approach to the lumbar spine can be avoided.

1.2. Motivation and objectives

Interbody cages have been certified to restore disc height and to increase stability of the spinal segment, and thereby enhance fusion in the surgical treatment of low back pain, spondylolisthesis and degenerative lumbar disc disease. Since 1991, Obenchain described the first laparoscopic lumbar discectomy [3], the field of minimally invasive spine surgery has continued to evolve. Surgeon and patient alike have been attracted by the advantages of minimally invasive surgery, including less tissue trauma during the surgical approach, less postoperative pain, shorter hospital stays, and faster return to activities of daily living. These reported advantages led to the laparoscopic anterior lumbar approach and mini-open anterior

lumbar interbody fusion becoming commonly performed procedures [4, 5]. Therefore, surgical options turn to minimize collateral muscle/bone damage while achieving excellent clinical results, with minimal risk and complication rates.

In this study, a novel stand-alone implant Latero is investigated. As a minimally invasive option, the lateral approach to interbody fusion avoids related complications from posterior-approach and anterior-approach, achieves spinal stabilization and provides indirect decompression [6-11]. Additionally, the lateral approach preserves the inherent biomechanical integrity of the motion segment through maintenance of all the ligamentous structures, including the anterior longitudinal ligament (ALL) [6, 12, 13], which is considered to be one of the major stabilizing components of the lumbar spine.

The loading conditions for the spinal motions are highly complex, therefore, not been fully characterized. Various simplifications have been made in experimental and numerical studies. It is not clear which loading condition deliver more realistic results. An experimental technique, called follower load, developed by Patwardhan et al. [14], applied compressive preload along a path following the lordotic curve of the lumbar spine, and allowed the *in vitro* spinal models to support higher physiologic loads without damage or instability. The follower load was applied on the lumbar spine to permit a certain amount of shear force in the three-dimensional FE models. It was shown that the load carrying capacity of the spine was significantly increased with little change in the shape of the spine at all vertebrae in comparison with the vertical direction loading. In this study, the follower load setting was investigated using the finite element (FE) method.

This study focused on the analysis of Latero design. The study was separated into two parts. In the part-1 of the study, it was focused on comparison of Latero implant with respect to other stand-alone implants. The finite element models inserting of conventional fusion devices were created for the evaluation the new implant. These finite element models were used to compare different stand-alone implants in all physiological motions including flexion,

extension, lateral bending and axial rotation. In the part-2 of the study, in order to improve the design of Latero implant, two improvement parameters were proposed: position of implant and bending angle of lateral plate. The evaluation results derived from finite element models data were focused on ROM for stability assessment.

1.3. Outline

This dissertation is divided into six chapters:

Introduction:

This chapter introduces the overview, objectives, and outline of this dissertation.

Background:

This chapter reviews the spine anatomy and biomechanics, spinal pathology and treatments, and follower load settings.

Materials and methods:

The first subject of the chapter includes FE modeling of the five-segment intact lumbar spine and the validation of follower load setting in FE analysis.

The second subject of the chapter includes the four implant models: Latero, SynFix (SynFix; Synthes Spine Inc., PA, USA), Stabilis (Stabilis; Stryker, Michigan, USA), and SynCage-Open (Synthes Spine, Inc., PA, USA) with pedicle screws fixation.

The third subject of the chapter includes the three implant models: Latero inserted in anterior position, Latero inserted in posterior position and Latero with modified lateral plate.

The fourth subject includes the boundary and loading conditions.

Results:

The first subject includes data of Latero implantation, SynFix implantation, Stabilis implantation, and SynCage-Open with pedicle Screws Fixation models.

The second subject includes data of Latero implantations with different implant

modifications.

Discussion:

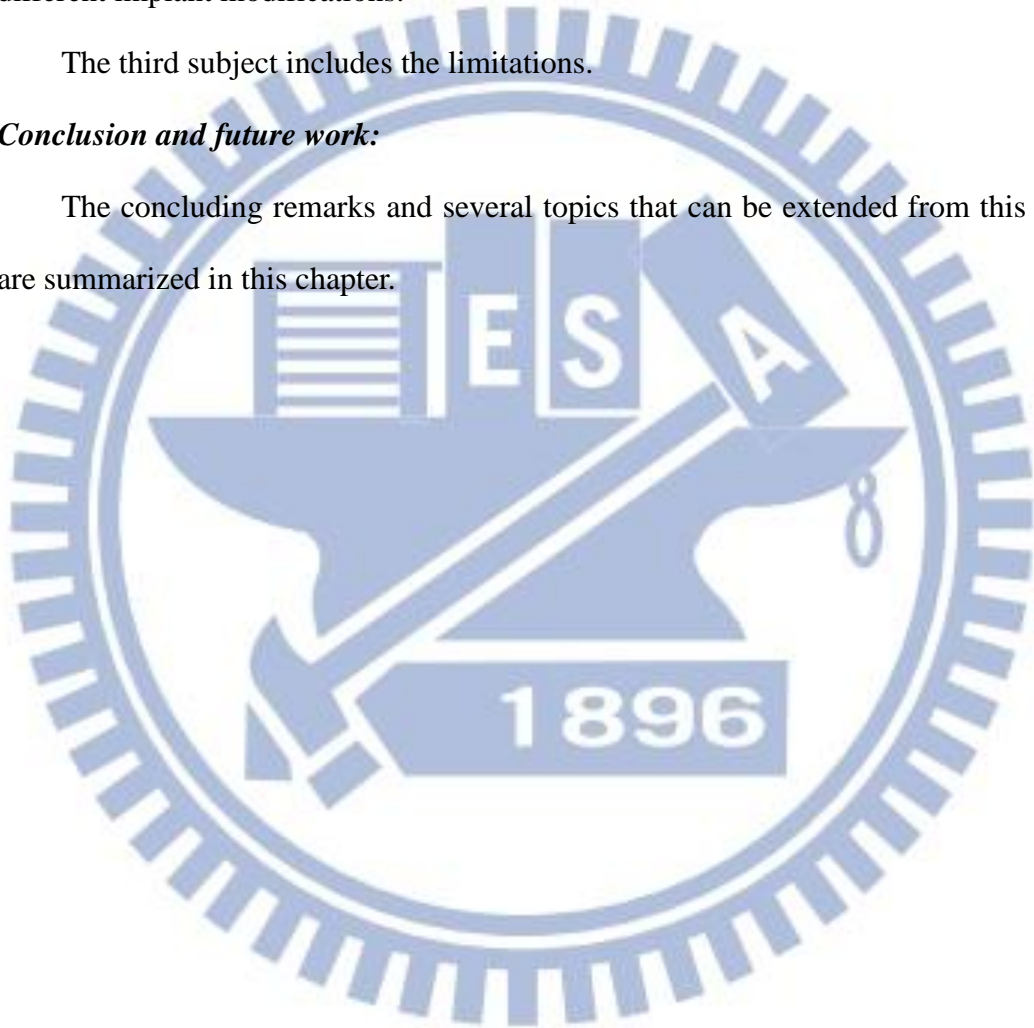
The first subject discusses biomechanical effect of Latero implantation compared with traditional implantations.

The second subject discusses biomechanical effect of Latero implantation with different implant modifications.

The third subject includes the limitations.

Conclusion and future work:

The concluding remarks and several topics that can be extended from this research are summarized in this chapter.



Chapter 2 Background

The following sections contain a literature review of the anatomy of the spine, spine biomechanics, spine pathology, treatments and follower load settings.

2.1. Spine anatomy and biomechanics

The spine consists of a curved stack of 33 vertebra divided structurally into five regions (Figure 2.1). Proceeding from superior to inferior, there are seven cervical vertebrae (C1-C7), twelve thoracic vertebrae (T1-T12), five lumbar vertebrae (L1-L5), five fused sacrum vertebrae (S1-S5), and four small fused coccygeal vertebrae. The vertebrae from each region have similar parts, but the shapes of vertebrae vary considerably from region to region in the spine.

Because of structural differences and the ribs, varying amounts of movement are permitted between adjacent vertebrae in the cervical, thoracic, and lumbar portions of the spine. Within these regions, two adjacent vertebrae and the soft tissues between them are known as a motion segment. The motion segment is considered to be the functional unit of the spine (Figure 2.2).

Each motion segment contains three joints. The vertebral bodies separated by the intervertebral disc form a symphysis type of amphiarthrosis. The right and left facet joints between the superior and inferior articular processes are diarthroses of the gliding type that are lined with articular cartilage.

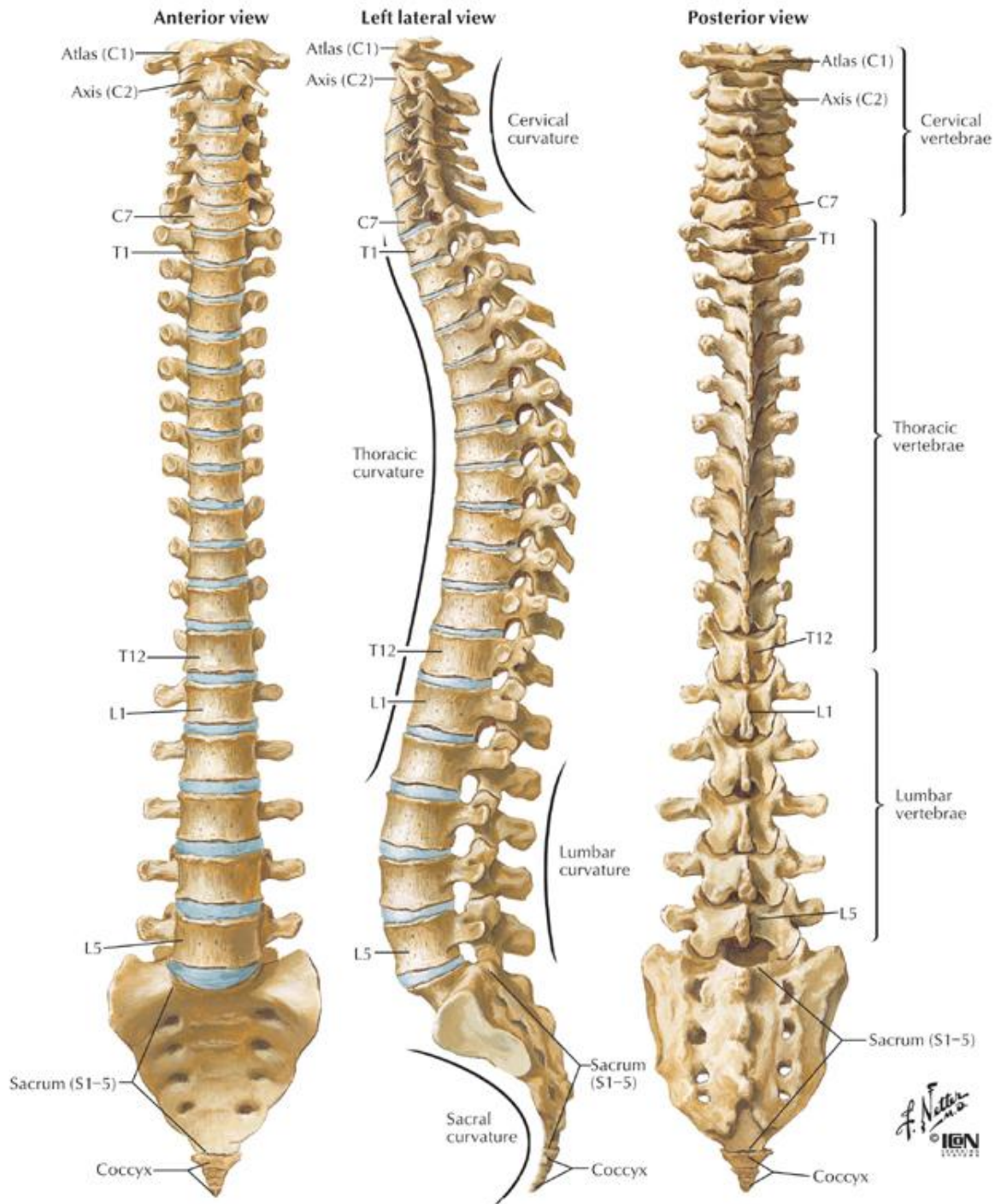


Figure 2. 1: Vertebral column: Anterior, left lateral and posterior views of the major regions of the spine [15].

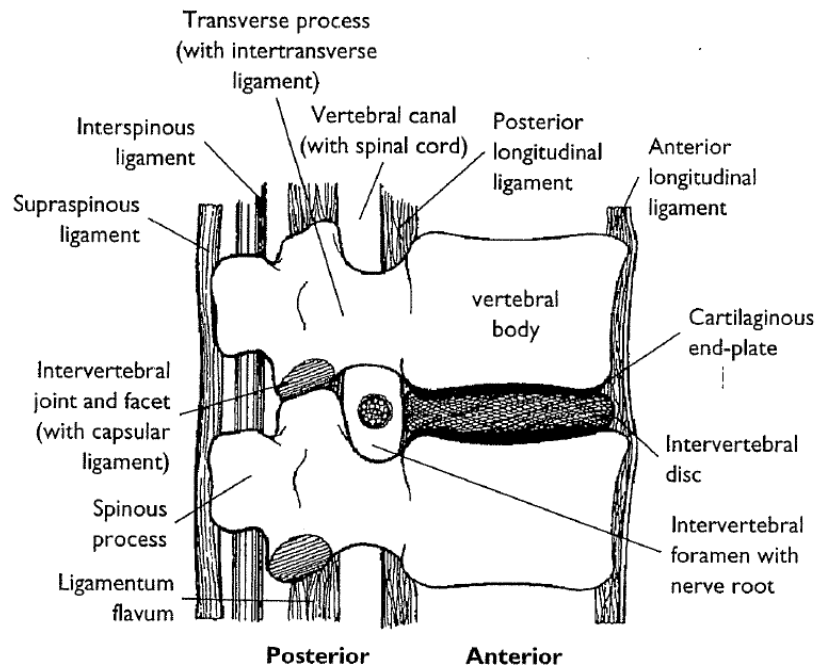


Figure 2. 2: The motion segment in the lumbar spine, which composed of two vertebrae and surrounding soft tissue [16].

2.1.1. Vertebra

A typical vertebra consists of a body, a hollow ring, and several bony processes, such as the pedicle, lamina, spinous process, and transverse process, as shown in Figure 2.3(A). Each vertebral body consists of an outer shell of cortical bone and an inner core of cancellous bone. The vertical and horizontal structure of bone in the cancellous core is called trabecular bone (Figure 2.3 B). Most of the compressive force acting down the long axis of the spine is resisted by the cancellous bone because of its dense network of trabecular bone [17]. In general, the vertebral size is progressively increased from the cervical region to the lumbar region.

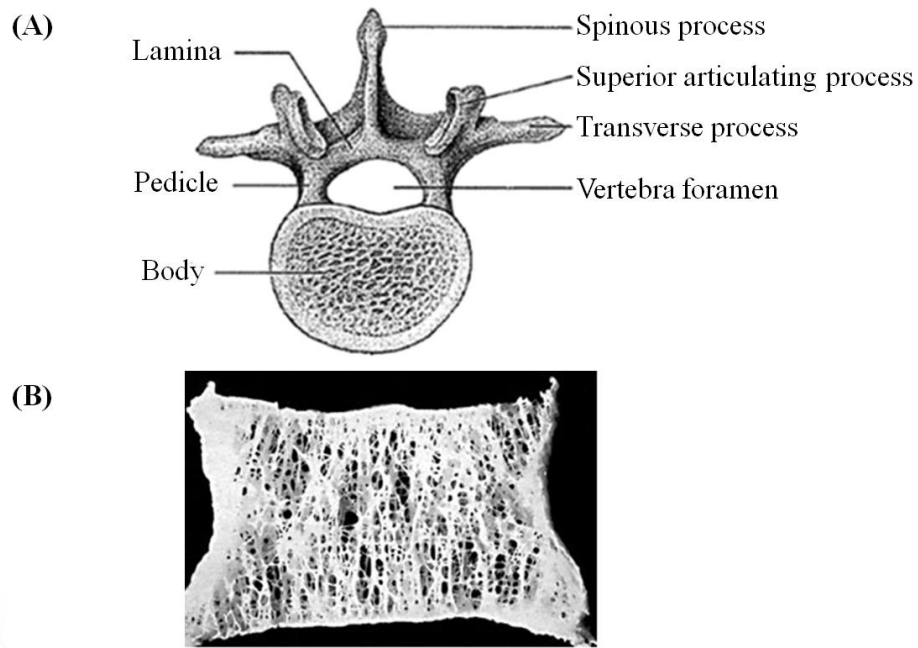


Figure 2. 3: The Shape of a human vertebra: (A) Superior view of the typical lumbar vertebra [16]. (B) The trabecular structure of a lumbar vertebral body in sagittal section [18].

2.1.2. Intervertebral disc

The intervertebral disc is composed of two parts: the nucleus pulposus and annulus fibrosus (Figure 2.4). The nucleus pulposus located in the central of each disc which is only slightly compressible and with 80 % to 88 % water content [19]. In general, the lumbar nucleus fills 30 % to 50 % of the total disc area in cross-section [20]. The annulus fibrosus consists of approximately 15-25 concentric lamellae in the circumferential around the nucleus which contain collagen fibers [21]. The collagen fibers are oriented approximately 30° angle to the horizontal plane and crisscross to each other in the adjacent lamella. The superior and inferior cartilaginous endplates cover disc and connect with adjacent vertebrae bodies.

The primary function of the disc is transfer compressive forces evenly from one vertebral body to the next, while allowing for small-amplitude twisting and sliding movements [22]. The tensile properties of the annulus are stiffer in anterior than the posterolateral regions, with the outer region being stiffer than the inner regions [23]. The outer lamellae resist excessive

bending and twisting of adjacent vertebrae, while the innermost lamellae are deformable and normally behave like a fluid. The endplate not only helps to equalize loading of the vertebral body but also prevents rapid fluid loss from the nucleus [24].

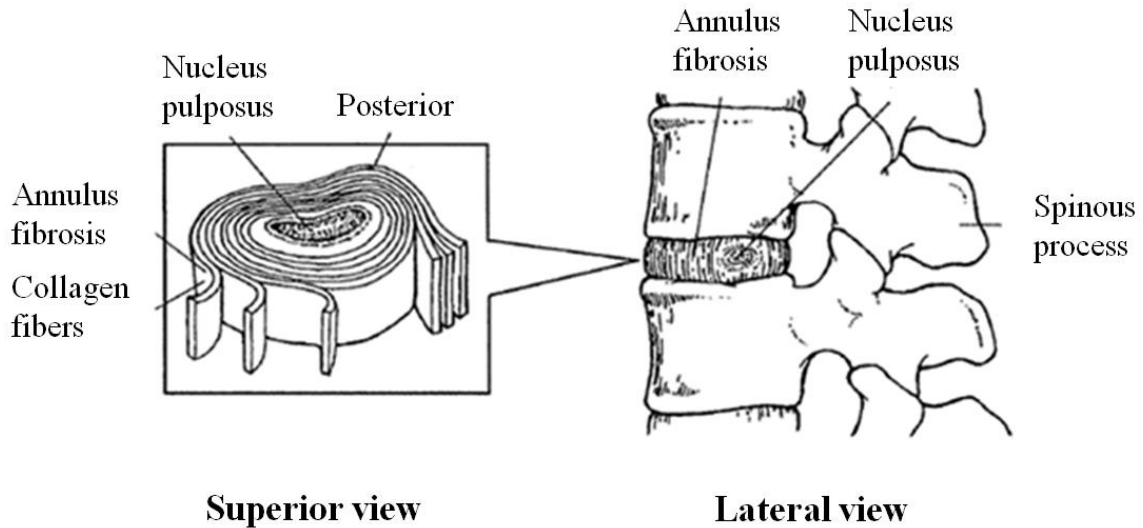


Figure 2. 4: In the intervertebral disc, the annulus fibrosus, made up of laminar layers of criss-crossed collagen fibers, surrounds the nucleus pulposus [16].

2.1.3. Facet joint

The size and angulation of the vertebral processes vary throughout the spinal column (Figure 2.5). This changes the orientation of the facet joints, which limit ROM in the different spinal regions. In addition to channeling the movement of the motion segment, the facet joints assist in load bearing. The facet joints and discs provide about 80 % of the spine's ability to resist rotational torsion and shear, with half of this contribution from the facet joints [25, 26].

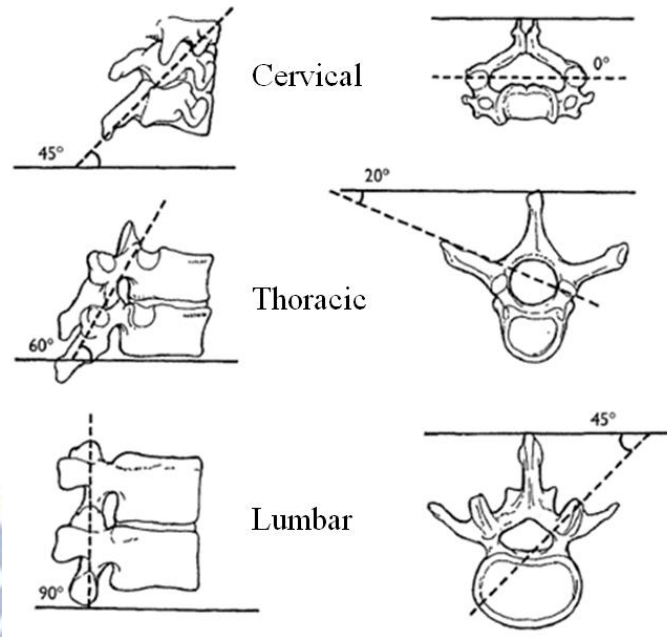


Figure 2. 5: Orientation of lumbar facet to the transverse plane (left) and the frontal plane (right)

[16].

2.1.4. Spinal ligaments

There are a series of ligaments that are important to the stability of the vertebral column. Important to the lumbar spine are seven types of ligaments (Figure 2.6): ALL and posterior longitudinal ligament (PLL) are associated with each joint between the vertebrae. The ALL runs along the front and outer surfaces of the vertebral bodies. It has the most significant effect for the stability under extension. However, in the ALIF surgery, it was moved out from the surgical level. The posterior longitudinal ligament runs within the vertebral canal along the back surface of the vertebral bodies. The ligamentum flavum (LF) is located on the back surface of the canal where the spinal cord or cauda equina runs. The interspinous ligament (ISL) runs from the base of one spinous process (the projections at the back of each vertebra) to another. Intertransverse ligament (ITL) and supraspinous ligaments (SSL) run along the tips of the spinous processes. Joint-related structures called facet capsular ligament (CL) also play an important role in stabilization and movement.

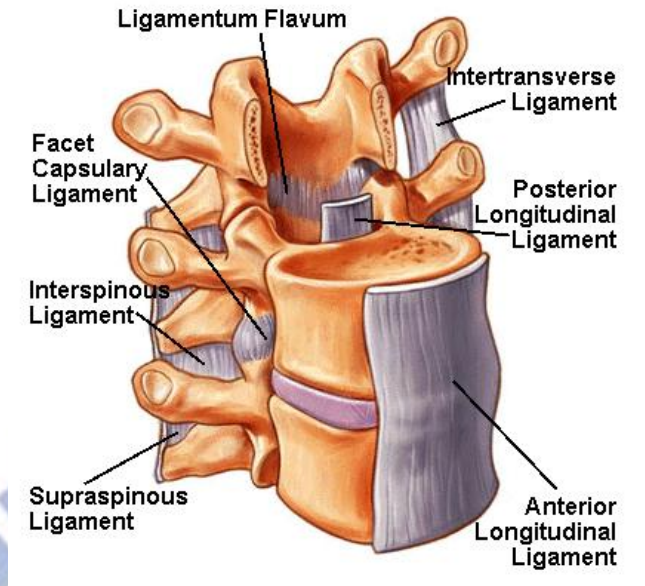


Figure 2. 6: The major ligaments of the spine [27].

2.1.5. Neural foramen

The segmental spinal nerve roots exit through the intervertebral foramen (Figure 2.2). The intervertebral foramen is bounded by the pedicles superiorly and inferiorly, and ventrally and dorsally by two major intervertebral articulations. It is bounded ventrally by the dorsum of the intervertebral disc and the lateral expansion of the posterior longitudinal ligament. Foraminal disc herniations can impinge on the exiting nerve root, causing radiculopathy. The joint capsule of the articular facets and the ligament flavum make up the dorsal boundary of the intervertebral foramen. The remaining space is composed of loose areolar tissue and fat.

2.1.6. Spinal cord and nerve roots

The spinal cord is a column of millions of nerve fibers that run through spinal canal (Figure 2.7). It extends from the brain to the area between the end of first lumbar vertebra and top of second lumbar vertebra. At the second lumbar vertebra, the spinal cord divides into several different groups of fibers that form the nerves that will go to the lower half of the body. For a small distance, the nerves actually travel through the spinal canal before exiting out the

neural foramen. This collection of nerves is called the cauda equina while it is still inside the spinal canal.

A protective membrane called the dura mater covers the spinal cord. The dura mater forms a watertight sack around the spinal cord and the spinal nerves. Inside this sack, the spinal cord is surrounded by spinal fluid.

The nerve fibers in spinal cord branch off to form pairs of nerve roots that travel through the small openings (foramina) between vertebrae and vertebrae. The nerves in each area of the spinal cord connect to specific parts of body. This is why damage to the spinal cord can cause paralysis in certain areas and not others; it depends on which spinal nerves are affected. The nerves of the cervical spine go to the upper chest and arms. The nerves in the thoracic spine go to chest and abdomen. The nerves of the lumbar spine then reach to legs, bowel, and bladder. These nerves coordinate and control all the body's organs and parts, and body muscles.

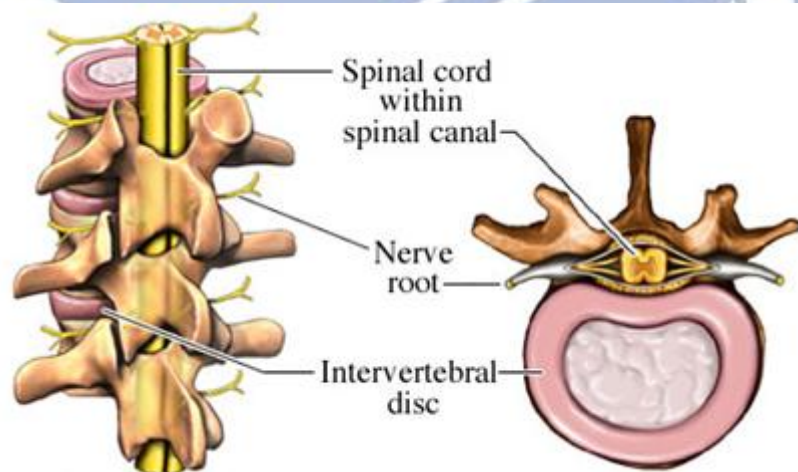


Figure 2. 7: Spinal Cord and Nerve Roots [28].

2.2. Spinal pathology and treatments

The functions of spine are to provide the longitudinal weight support, limit excessive movement, and protect posterior spinal cord. However, the spinal instability may induce due to several pathological changes, such as DDD, spinal deformity, tumor, infection, trauma,

congenital anomaly, inflammatory, etc (Figure 2.8). Thus spinal nerve roots or spinal cord may be compressed and leading low back pain (Figure 2.9). The first choice of treatment for low back pain is conservative therapy, such as physical therapy or medication. When conservative treatments fail, spine surgeons may perform either fusion or non-fusion surgery, with the aim of reducing pain and decreasing disability [29].

2.2.1. Lumbar spinal stenosis

The most common cause of lumbar spinal stenosis (LSS) is initial stage of degeneration intervertebral disc. LSS defined as narrowing of the spinal canal or intervertebral foramina, is a common cause of pain, numbness, and weakness. Early descriptions of neurogenic claudication secondary to lumbar stenosis have been attributed to Verbiest [30]. This syndrome is displayed by radicular pain, which is exacerbated by standing, walking, and other positions that place the lumbar spine in extension. A flexed posture improves or relieves the symptoms. In severe cases, sensory loss or motor deficits are evident. Although several theories have been postulated to explain the occurrence of these symptoms, the precise mechanism remains unclear [31]. It is obvious that the pathological progression begins with degeneration of disc, which finally leads to loss of disc height. Resultant instability may worsen the spondylosis by inducing facet joint hypertrophy [32]. Furthermore, hypertrophy of the ligamentum flavum, particularly during extension, contribute to the reduction in size of the thecal sac limiting the space available for the cauda equine [33].

LSS can be mono-segmental or multi-segmental (Figure 2.9 and 2.10), and unilateral or bilateral. Anatomically, the stenosis can be classified as central, lateral or foraminal [34]. Depending on the degree of degeneration, central, lateral and foraminal stenosis can occur alone or in combination. The L4-L5 spinal discs are most frequently affected by LSS, followed by L3-L4, L5-S1, and S1-S2 [35]. Degeneration of disc often causes a protrusion, which leads to ventral narrowing of the spinal canal (Figure 2.11). As a consequence of disc degeneration,

the height of intervertebral space is reduced, which causes the intervertebral foramina to narrow (foraminal stenosis), exerting strain on the facet joints. Such an increase in load can lead to facet joint arthrosis, hypertrophy of the joint capsules and the development of expanding joint cysts (lateral stenosis), which in combination propagate spinal instability [35, 36]. The reduced height of the segment leads the ligamentum flavum to form creases, which exert pressure on the spinal dura from the dorsal side (central stenosis). Concomitant instability due to loosened tendons (ligamentum flavum) further propagates preexisting hypertrophic changes in the soft tissue and osteophytes, creating the characteristic trefoil-shaped narrowing of the central canal [35-43].



Figure 2. 8: The radiograph shows the spinal instability [34].



Figure 2. 9: Mono-segmental lumbar spinal stenosis at L4-L5 segment [35].

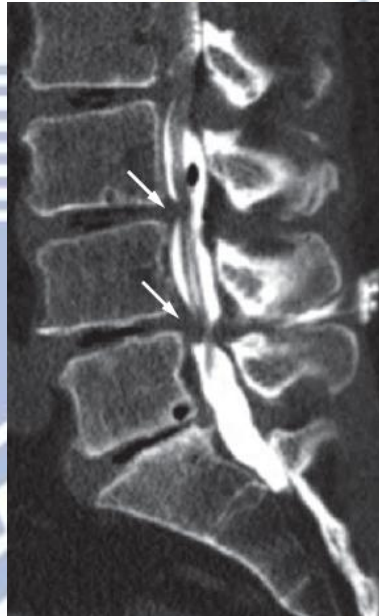


Figure 2. 10: Multi-segmental lumbar spinal stenosis at L3-L5 segment [35].

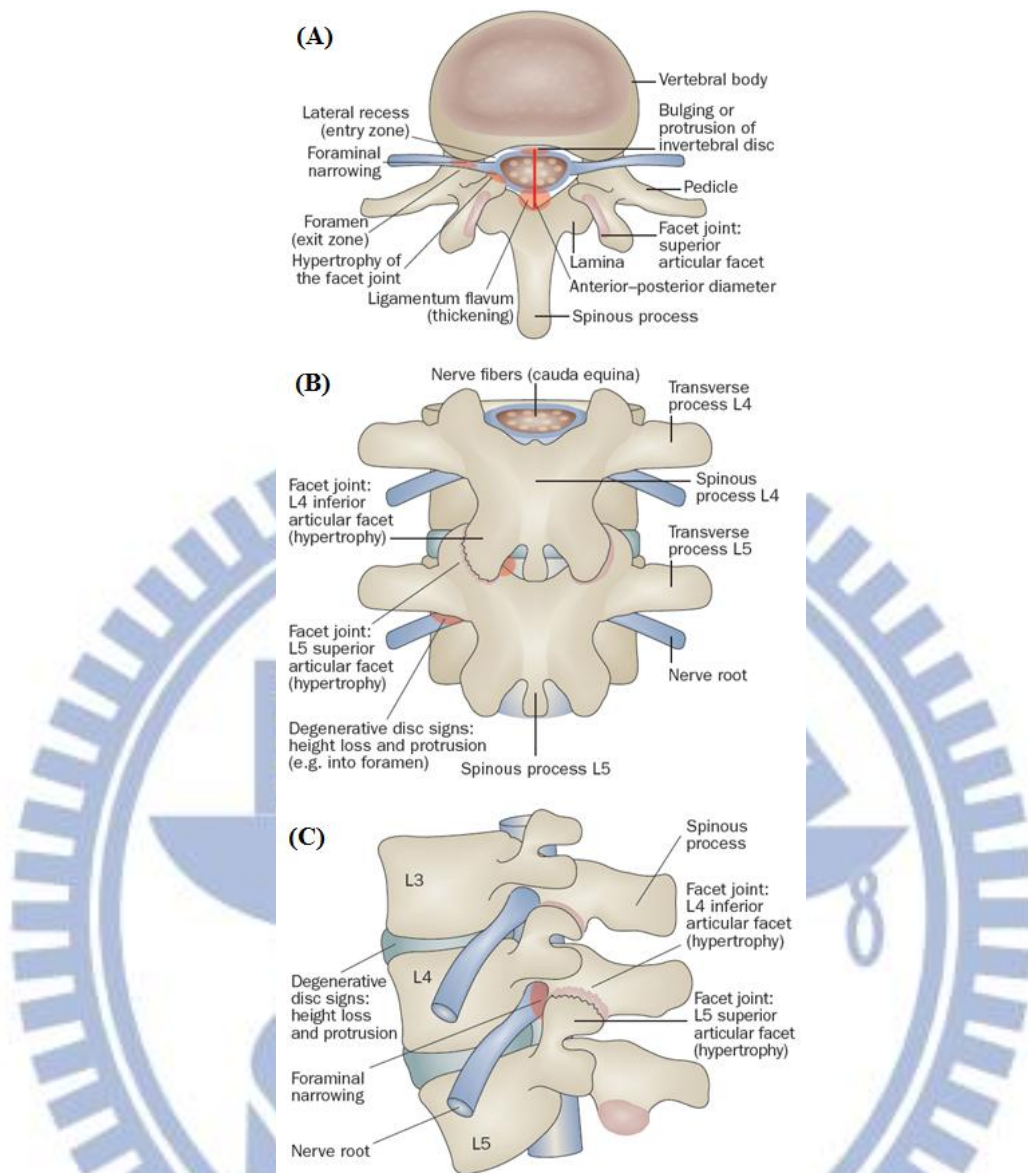


Figure 2. 11: Pathoanatomical illustration of lumbar spine stenosis [35].

2.2.2. Conservative therapy

The conservative treatment of LSS comprises a wide variety of methods, such as ergotherapy, physical therapy, behavioral therapy, girdles, acupuncture, manual therapy and pharmacological intervention. Few studies have been conducted to demonstrate the effectiveness of conservative therapy in treating LSS, although those that reported had success rates of up to 70 % [35, 37, 38, 39]. However, none of the available studies provide sufficient data to support the effectiveness, or any one of the wide range of conservative treatments [40].

In the absence of evidence-based clinical guidelines, multidisciplinary approach should be given preference over a significant therapy [40, 41].

2.2.3. Decompression surgery

Decompression surgery used in LSS aim to decompress the neural elements, without occur instability of the segment. Such decompression surgery usually leads to relief of pain in the legs and low back pain [42]. Decompressive surgical procedures include laminectomy and hemilaminectomy, hemilaminotomy, fenestration, and foraminotomy [43]. The complication rates for decompression surgery range from 14 % to 35 % or more [44-47]. Typical complications of decompression surgery include inadequate decompression with significant residual stenosis, instability of segment, renewed nerve compression, and reossification. All of these complications result in renewed nerve compression [46-49].

Decompression surgery may cause complication as mentioned above if weight bearing structures are compromised. Therefore, instrumented is necessary when preexisting or surgically induced instability is present. Pedicle screw instrumentation is a popular method of strong fixation to achieve stabilization rate (Figure 2.12). For stabilization of one spinal functional unit, four pedicle screws are usually used.

However, the use of pedicle screws is technically demanding and associated with certain risks. Complications were divided into three categories: 1. Infections: deep infections. 2. Neurological complications: postoperative neurapraxias or permanent neurological disorders. 3. Implant failures: malposition, breakage or loss of correction [50].

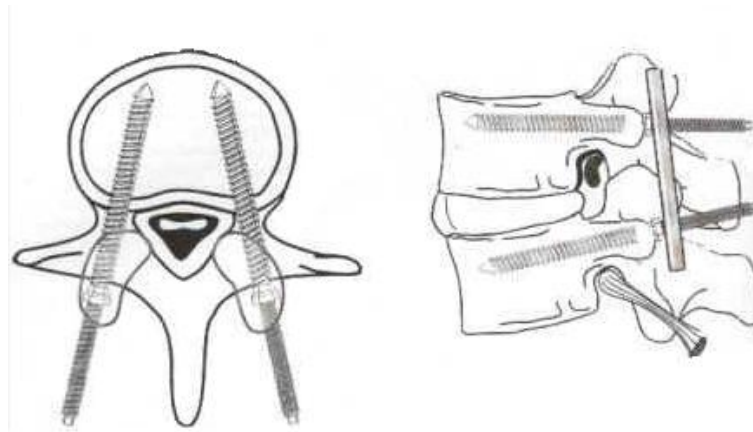


Figure 2. 12: Pedicle screw instrumentation [51].

2.2.4. Fusion surgery

Fusion surgery is needed in cases of severe degeneration disc, instability (rotational or vertical mobility of the vertebral body >3 mm), spondylolisthesis (>5 mm forward movement of a lumbar vertebra relative to one below) or scoliosis (lateral curvature of the spine $>20^\circ$), because instability can make nerve root compression [52-59].

Spinal fusion is defined as a bony union between two vertebrae spaces following surgical manipulation [52, 60], and aims to completely eliminate movement by the motion segment (Figure 2.13). It is an effective technique for treating degenerative spinal instability, and the final goal of the procedure is to restore disc height, enlarge the stenotic foramen, and support the anterior spinal column. To maintain the disc height, the fusion surgery requires the use of an interbody spacer. Although titanium cages are used in this capacity, the two most common spacers are cortical allografts and polyetheretherketone (PEEK) cages. In general, bone grafts are placed into the interface between vertebral bodies to maintain disc height and to accelerate bone growth into neighboring vertebrae. These bone grafts may be autografts, allografts or synthetic materials which can be adopted from fibulae, illia, the iliac crest, or ribs.



Figure 2. 13: This radiograph demonstrates a solid bony union between L3 and L4 [61].

The surgical techniques can be classified as the anterior lumbar interbody fusion (ALIF) approach, posterior lumbar interbody fusion (PLIF) approach, transforaminal lumbar interbody fusion (TLIF) approach, and lateral approach by the insertion of the spinal cages (Figure 2.14). In general, the ALIF approach includes the removal of the ALL, the anterior portions of the disc annulus, and the nucleus before implanting an interbody fusion cage (Figure 2.14; black arrow) [62]. For the PLIF approach, a partial laminectomy, discectomy and nucleotomy are performed, which includes the removal of the ISL, SSL, LF, posterior portions of the disc annulus, and the total nucleus. In addition, a certain portion of the facet joint can be removed to give the nerve roots more space (Figure 2.14; red arrow) [63]. The TLIF approach was modified from the PLIF approach. The TLIF procedure preserves the ISL of the lumbar spine and preserves the contralateral laminar surface as an additional surface for bone graft. (Figure 2.14; blue arrow) [64]. Lateral approach is performed through a lateral, retroperitoneal, transpsoas approach to the anterior column, and uses real-time directional neuromonitoring to ensure safe passage through the psoas muscle, avoiding the nerves of the lumbar plexus (Figure 2.14; green arrow).

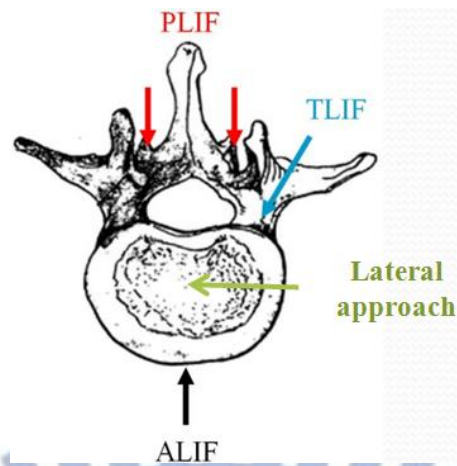


Figure 2. 14: Common surgical techniques for insertion of a spinal cage. The black arrow indicates the ALIF approach, the red arrow indicates the PLIF approach, and the blue arrow indicates the TLIF approach, and the green arrow indicated the lateral approach.

The fusion surgery is very successful in the treatment of deformity as well as degenerative conditions of the lumbar spine. Fusion provides stabilization of the spine, protection of neural elements, maintenance of neural decompression. Historically, spine surgery was performed through a posterior approach as it was the most direct pathway to the bony structures. All types of fusion surgery approaches are recommended for combination with traditional pedicle screw fixation to increase stabilization and fusion rates (Figure 2.15). The pedicle screw can be used for unilateral or bilateral pedicle screw fixation. Unilateral pedicle screw fixation was used with the TLIF surgery to provide stability in minimally invasive surgery, but the asymmetric construct will result in spine segment destabilization and a decrease in spine stiffness. However, the use of pedicle screws is technically demanding and associated with certain risks. Typical complications of pedicle screws surgery include infections, neurological risk and implant failures [50]. At present, ALIF combined with posterior pedicle screw fixation can provide better stability than other fusion techniques. Therefore, SynCage-Opne (Figure 2.16A) interbody cage supplementation with posterior pedicle screw fixation was selected to represent the traditional fusion model in this study.

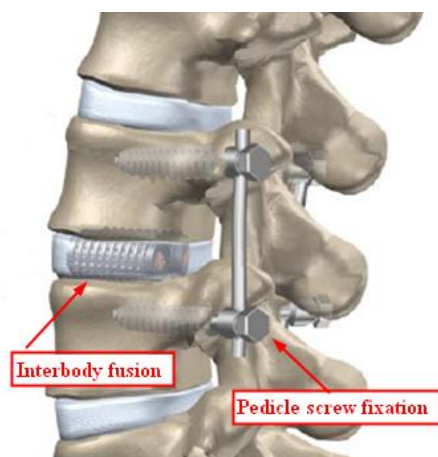


Figure 2. 15: Interbody fusion combined with posterior pedicle screw fixation [65].

2.2.5. Lumbar interbody fusion cages

A problem associated with the use of autologous bone grafts in interbody fusion is the high morbidity of the donor site. Many attempts have been made to avoid the use of tricortical autologous grafts. This has resulted in the use of different materials such as bioceramics, corals, allografts, and constructs made from carbon fibre or metal. The most popular method to achieve interbody fusion has been autologous bone grafts, but the use of instrumentation has increased. Using slightly oversized cages, a distraction between the vertebral bodies would occur so that intervertebral height is restored. The end result would be bone ingrowth from the endplates through the fenestrations of the cages into the impacted cancellous bone.

Both cortical allografts and PEEK cages are highly effective in promoting interbody fusion, maintaining postoperative disc space height, and achieving desirable clinical outcomes in patients who undergo fusion surgery. However, the advantages of PEEK cages include a lower incidence of subsidence and their radiolucency, which permits easier visualization of bone growth. The common design is either cylindrical or trapezoid in shape and often uses serrated anchorages on the upper and lower surfaces to prevent loosening or subsidence of the cage [66-69].

In general, there are several features of this kind of device (Figure 2.16). First, the spinal

fusion cage is made of a variety of biocompatible materials, including stainless steel, titanium alloy, carbon fiber-reinforced polymer (CFRP), and PEEK [70]. Due to the high mechanical strength of these materials, a spinal interbody fusion cage can provide better longitudinal support than a traditional bone graft, without causing collapse. Second, rough or specific designs can be found on the contact surfaces of spinal cages. In order to prevent cage slippage, rough contact surfaces, saw teeth, spikes or threads have been designed to increase stability between fusion devices and endplates. Third, these implants are usually designed to be hollow, with small pore or openings on the wall. These hollow cages can be filled with bone grafts to promote bone growth. Furthermore, only small amounts of cancellous bone are required, because there is no longer need for the cubic graft to be a spacer. The small pores and openings on the wall allow the growth of bone through the cage, resulting in bony fusion. Therefore, spinal fusion cages can avoid donor site morbidity and increase fusion rates.

Currently, many kinds of spinal cage designs are available on the market, which can be classified by the various surgical approaches used in their implantation. Large single lumbar cage designs are used for the ALIF procedure (Figure 2.16 A). Some paired cage designs are used strictly for PLIF procedures (Figure 2.16 B). In addition, some specific shapes of cages are designed for minimally invasive surgical techniques such as the TLIF procedure (Figure 2.16 C).



Figure 2. 16: Various lumbar interbody fusion cages: (A) SynCage-Open (Synthes Spine, Inc., PA, USA); (B) O.I.C. (Stryker Spine, Mahwah, New Jersey, USA); (C) AVS-TL (Stryker Spine, Mahwah, New Jersey, USA).

2.2.6. Minimally invasive techniques and stand-alone implant

Since 1991, when Obenchain described the first laparoscopic lumbar discectomy [3], the field of minimally invasive spine surgery has continued to evolve. Surgeon and patient alike have been attracted by the advantages of minimally invasive surgery, including less tissue trauma during the surgical approach, less postoperative pain, shorter hospital stays, and faster return to activities of daily living.

The reported advantages of minimally invasive surgery led to the laparoscopic anterior lumbar approach and mini-open ALIF becoming commonly performed procedures [71-80]. However, when examining the researches that have been performed to date, the results showed that ALIF has provided less than desirable stability in unstable spinal segments [81]. Presently, it is common to clinically perform an additional posterior fixation to recover the stability of spinal segments, as well as to enhance the fusion. The construct stability can be further enhanced by the supplementation of posterior fixation such as pedicle or facet screws [82, 83]. However, the significant morbidities of the combined anterior and posterior approaches have been mentioned [84]. Therefore, if sufficient stability can be provided in a single surgery, the problems that arise from extensive anterior and posterior approaches can be reduced.

The stand-alone implants can be inserted *via* anterior or lateral approach with minimal operative morbidity and without causing damage to posterior bony elements and neural, vascular, and muscular tissues [85]. These stand-alone implants could reduce the postoperative pain and number of days of hospitalization, and could lead to a quick return to one's daily routine.

Development of cages combining with integrated fixation may provide surgeons with sufficient construct stability to allow stand-alone use, removing the need for additional fixation. These stand-alone devices generally comprise a interbody cage with single or multiple integrated fixation such as locking screws that thread through the cage and into the

adjacent inferior and superior vertebral bodies [85, 86] (Figure 2.17). The stand-alone implants have been used in ALIF treatment and their ability to stabilize the intervertebral motion has been reported to be superior in flexion and bending compared to extension and rotation [81, 87].

In the literatures [71, 72, 81], comparisons between different conventional stand-alone ALIF cages have been extensively conducted by the experimental, numerical, and clinical methods. Using human cadavers as specimens, the three-dimensional stiffness tests in Schleicher's study [71] demonstrated the effective stabilization ability of the stand-alone SynFix cage in all physiological motion directions. In Chen's study [88], the numerical results showed no differences of ROM in extension and lateral bending between the SynCage-Open and the stand-alone Stabilis cage. Except for the differences among cage frames, the stabilizing mechanism might contribute to the postoperative outcome of the stand-alone ALIF [85]. Cho *et al.* [72] demonstrated that the stand-alone ALIF cage could assure good clinical results in the surgical treatment of symptomatic lumbar intervertebral foraminal stenosis in a mid-term follow up. From the biomechanical viewpoint, however, the insertion depth and holding power were quite different between the plate, screw, and cylinder, thus, potentially affecting the stabilizing ability of the stabilizing mechanisms [89]. At present, there has been no extensive study devoted to investigate the kinematic and mechanical differences between the plate-, screw-, and thread-type stand-alone cages.

The current study describes a novel, minimally disruptive spine device called the Latero (Figure 2.17 A). This novel device can be used to gain access to the lumbar spine via a lateral approach that passes through the retroperitoneal fat and psoas major muscle. Hence, the potential complications with an anterior approach to the lumbar spine can be avoided, major vessels are not encountered. In this study, two conventional stand-alone cages, consisting of trapezoid frames that incorporates the stabilizing components were also investigated. The SynFix implant (Figure 2.17 B) uses four screws to lock the adjacent vertebrae. The Stabilis

implant (Figure 2.17 C) accommodates a threaded cylinder to anchor the superior and inferior endplates. Simultaneously, SynCage-Open (Figure 2.17 D) interbody cage supplementation with posterior pedicle screw fixation was selected to represent the traditional fusion model in this study.

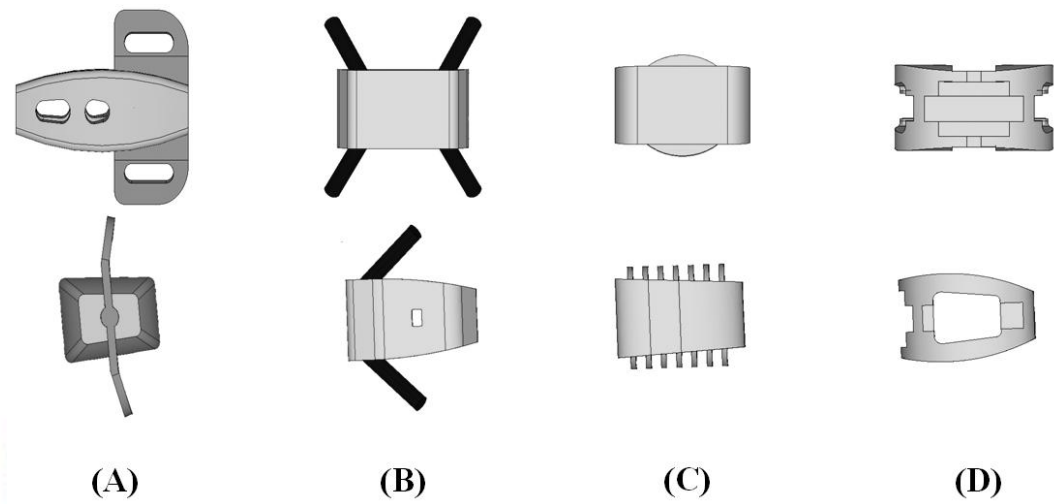


Figure 2. 17: Front and left side views of the four ALIF cages were used in this study. (A) Latero. (B) SynFix. (C) Stabilis. (D) SynCage-Open.

Chapter 3 Materials and Methods

3.1 Part-1 of this study

Initial promise of a stand-alone interbody fusion cage to treat chronic back pain and restore disc height has not been fully realized. In some instances, a posterior spinal fixation has been used to enhance stability and increase fusion rate. In the part-1 of this study, a new stand-alone cage is compared with two conventional stand-alone implants and one conventional fixation method (ALIF plus pedicle screws: A+P) based on the finite element analysis, with a focus on investigating cage-bone interface mechanics and stress distribution on the adjacent tissues.

3.1.1. The establishment of intact lumbar spine model (INT model)

To create a three-dimensional FE model, computed tomography scan DICOM files of the L1 to L5 lumbar spine of a middle-aged male were obtained at 1-mm intervals. The commercially available visualization software Amira 3.1.1 (Mercury Computer Systems, Inc., Berlin, Germany) was used to describe cross-section contours of each spinal component in accordance with gray scale value (Figure 3.1). Then, the three-dimensional surface geometries were constructed through sequential processed cross-section contours as shown in Figure 3.2 A. Each spinal component was exported as a Drawing Exchange Format (DXF) file and converted to the Initial Graphics Exchange Specification (IGES) file as shown in Figure 3.2 B. The FE analysis software ANSYS 14.0 (ANSYS Inc., Canonsburg, PA) was used to reconstruct the FE model by converting the IGES file to ANSYS Parametric Design Language (APDL) code in Figure 3.2 C. The INT model was an osseo-ligamentous lumbar spine, which included the vertebrae, intervertebral discs, endplates, posterior bony elements, and all seven ligaments (Figure 3.3).

Eight-node solid element (SOLID185) were used for modeling the cortical bone, cancellous bone, posterior bony element, cartilage endplate, and annulus ground substance. The cortical bone and cancellous bone were assumed to be homogeneous and transversely isotropic [90]. The posterior bony element and cartilage endplate were assumed to be homogeneous and isotropic [90]. The intervertebral disc consisted of annulus ground substance, nucleus pulposus and collagen fibers embedded in the ground substance. The nonlinear annulus ground substance was simulated by using a hyper-elastic Mooney-Rivlin formulation [91, 92]. The collagen fibers simply connected between nodes on adjacent endplates to create an irregular criss-cross configuration. These irregular angles of collagen fibers were oriented within the range of the Marchand's study [93]. In the radial direction, twelve double cross-linked fiber layers were defined to decrease elastic strength proportionally from the outermost layer to the innermost. Therefore, the collagen fibers in different annulus layers were weighted (elastic modulus at the outermost layers 1-3: 1.0, layers 4-6: 0.9, layers 7-9: 0.75, and at the innermost layers 10-12: 0.65; cross sectional areas at the outermost layers 1-3: 1.0, layers 4-6: 0.78, layers 7-9: 0.62, and at the innermost layers 10-12: 0.47) based on previous studies [94, 95]. The nucleus pulposus was modeled as an incompressible fluid with a bulk modulus of 1666.7 MPa by eight-node fluid elements (FLUID80) [90]. 43 % of the cross-sectional area in the disc was defined as the nucleus, which was within the range of the study by Panagiotacopoulos (30-50 %) [96]. Therefore, approximately 47 % to 49 % disc volume was assigned to nucleus pulposus. All seven ligaments and collagen fibers were simulated by using two-node bilinear link elements (LINK10) with uniaxial tension resistance only, which were arranged in an anatomically correct direction [97]. The cross-sectional area of each ligament was obtained from previous studies [94, 98, 100], and material properties of the spine are listed in Table 3.1. The facet joint was treated as having sliding contact behavior using three-dimensional eight-node surface-to-surface contact elements (CONTA174), which may slide between three-dimensional target elements (TARGE170). The coefficient of friction was set at 0.1 [101]. The initial gap

between a pair of facet surfaces was kept within 0.5 mm [90]. The stiffness of the spinal structure changes depending on the contact status, so the standard contact option in ANSYS was adopted to account for the changing-states nonlinear problem in this study. In addition, the element's shape will change after applying bending moments, thus changing the individual element stiffness. Therefore, the large displacement analysis option in ANSYS was chosen to solve this geometric nonlinear problem. The INT model consisted of 112,174 elements and 94,162 nodes [102, 103].

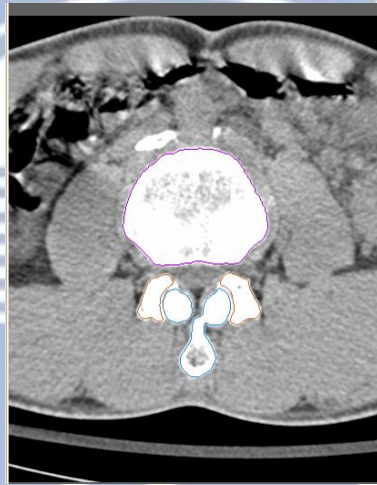


Figure 3. 1: Each spinal component was selected from computed tomography scan DICOM file to create material-related contours.

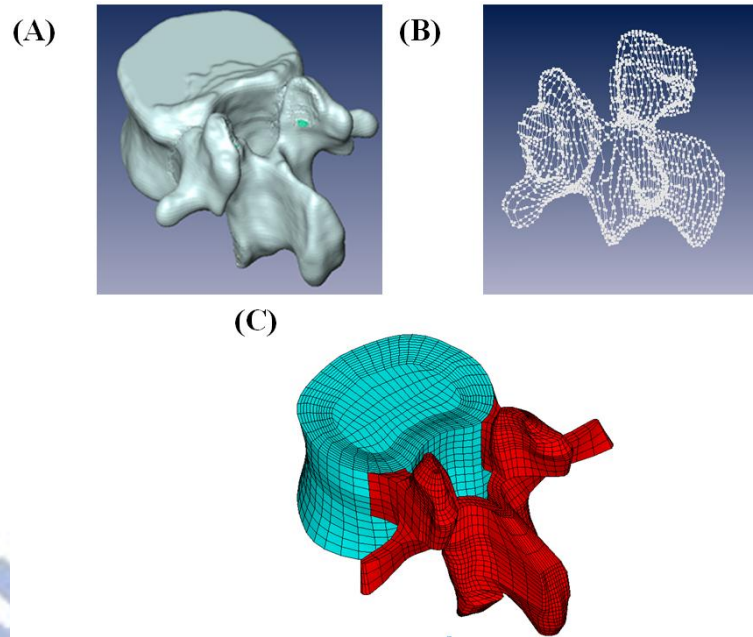


Figure 3. 2: Modeling process of the L3 vertebra: (A) surface geometries of vertebra were reconstructed through sequential processed computed tomography scan DICOM file; (B) surface geometry was exported to the DXF file; (C) FE model of the L3 vertebra.

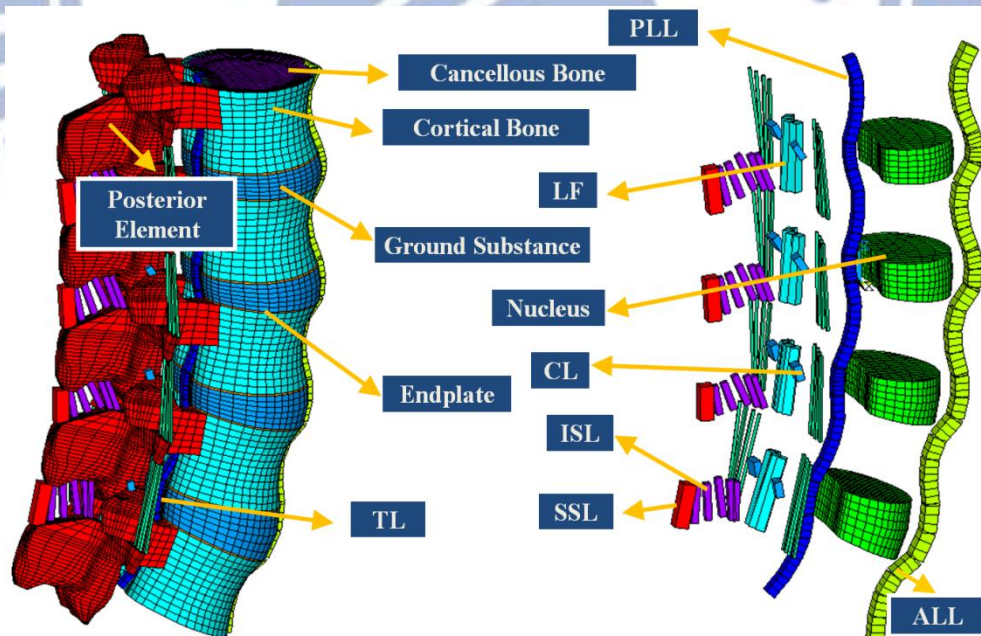


Figure 3. 3: The lumbar finite element model used in this study (Intact model from L1 to L5 levels)

Table 3. 1: Material properties used in the FE model

Material	Element type	Young's modulus (MPa)	Poisson's ratio	Area (mm ²)	References
Vertebral					
Cortical	8node-Solid 185	E _x =11300 E _y =11300 E _z =22000 G _x =3800 G _y =5400 G _z =5400	$\nu_{xy}=0.484$ $\nu_{xz}=0.203$ $\nu_{yz}=0.203$	-	[90]
Cancellous	8node-Solid 185	E _x =140 E _y =140 E _z =200 G _x =48.3 G _y =48.3 G _z =48.3	$\nu_{xy}=0.45$ $\nu_{xz}=0.315$ $\nu_{yz}=0.315$	-	[90]
Posterior bony element	8node-Solid 185	3500	0.25	-	[90]
Disc					
Nucleus pulposus	8node-Fluid 80	1666.7	-	-	[90]
Annulus Ground substance	8node-Solid 185	C ₁₀ =0.42 C ₀₁ =0.105	-	-	[98, 91]
Annulus fibers	2node-Link 10				[94, 95]
Outmost (1-3 layers)		550	-	0.76	
Second (4-6)		495	-	0.5928	
Third (7-9)		412.5	-	0.4712	
Innermost (10-12)		357.5	-	0.3572	
Cartilaginous endplates	8node-Solid 185	24	0.4	-	[90]
Ligaments*	2node-Link 10				[98,95,98]
ALL		7.8	-	24	[100]
PLL		10	-	14.4	
TL		10	-	3.6	
LF		15	-	40	
ISL		10	-	26	
SSL		8	-	23	
CL		7.5	-	30	

*ALL, anterior longitudinal ligament; PLL, posterior longitudinal ligament; TL, transverse ligament; LF, ligamentum flavum; ISL, interspinous ligament; SSL, supraspinous ligament; CL, capsular ligament.

3.1.1.1. Convergence test of INT model

In order to get reliable data, convergence test were conducted. Three mesh densities (coarse model: 4,750 elements / 4,960 nodes; normal model: 27,244 elements / 30,630 nodes;

finest model: 112,174 elements / 94,162 nodes) were selected to test ROM in the intact model (Figure 3.4). The boundary and loading conditions of the test were that the inferior surface of L5 vertebra was fixed, and 10 Nm moment and a 150 N pressure preload were applied to the superior surface of L1 vertebra.

Compared with normal model and finest model, the variation of ROM was within 1.03% in flexion (less than 0.2°), 4.39% in extension (less than 0.5°), 0.01% in axial rotation (less than 0.2°), and 0.001% in lateral bending (less than 0.1°). From the simulation results, the normal model only required fewer computational times to complete. However, several contact surfaces in facet joint have stress concentration owed to the lower smooth geometry for fewer elements and nodes. Therefore, the appropriate mesh density (finest model) was selected in this study.

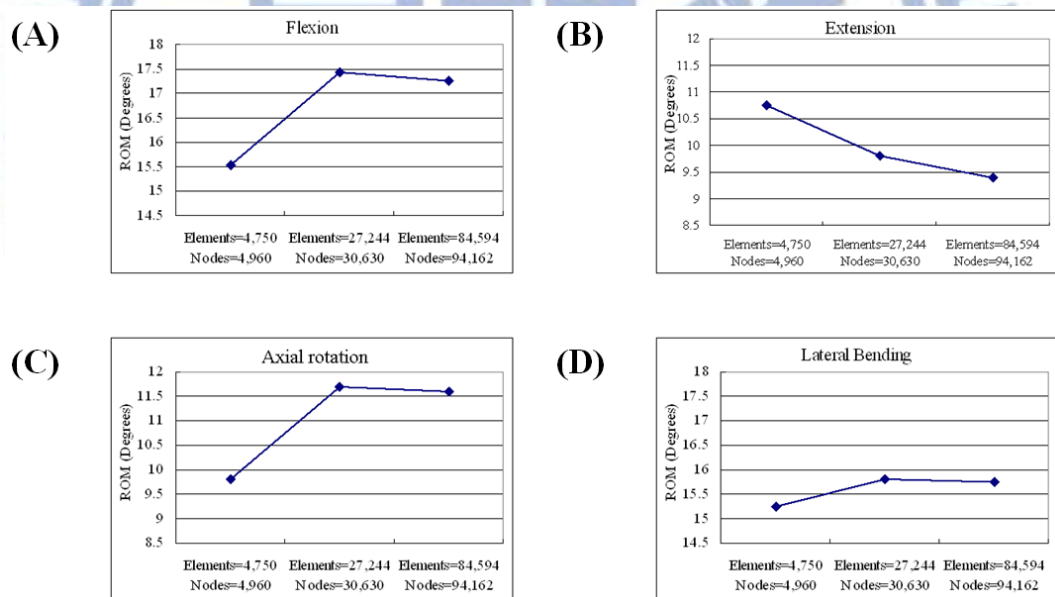


Figure 3. 4: Convergence test of the intact model: (A) result of motion changes under flexion; (B) result of motion changes under extension; (C) result of motion changes under axial rotation; (D) result of motion changes under lateral bending.

3.1.1.2. Follower load setting

During tasks of daily living the lumbar spine withstands compressive loads of very high magnitude along with significant amounts of motion. Compressive loads can easily approach several thousand Newtons during some lifting tasks [104]. Physiologic compressive loads applied to individual lumbar motion segments and the stiffening effect of compressive preload on single functional spine units has been investigated [107]. For the *in vitro* test, difficulty arises in terms of stability of the lumbar spine when physiologic compressive loads are applied to the entire lumbar spine. The traditional vertical preloads are unable to stabilize the whole lumbar spine specimens under higher physiologic magnitude because the spine without active musculature is unstable at around 100-200 N of vertical preload [108]. The follower load technique, described by Patwardhan et al. [14], applied compressive preload along a path following the lordotic curve of the lumbar spine, and allowed the *in vitro* spinal models to support higher physiologic loads without damage or instability (Figure 3.5)[14, 109].

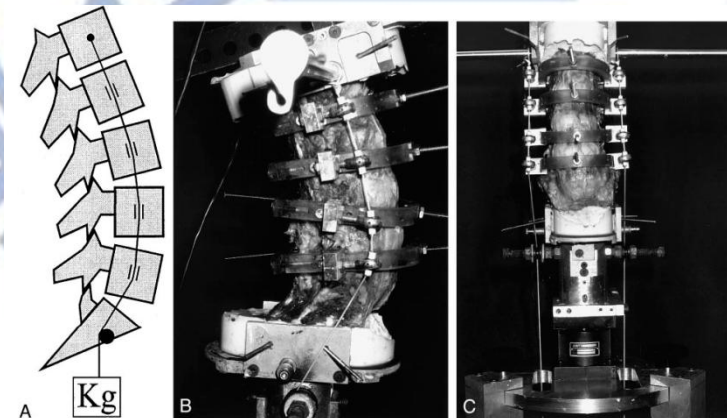


Figure 3. 5: (A)The illustration of applying follower load; The experiment setting of follower load ((B) lateral view and(C) front view) [14].

Based on Patwardhan's [14] study, Rohlman [110] used ten fresh-frozen human cadaveric lumbar spines to determine the influence of different loading conditions on

intradiscal pressure and intersegmental rotation at all levels of the lumbar spine by applying loads, including pure moments of 3.75, 7.5, and 7.5 Nm plus a follower load of 280 N (140 N on each lateral side)(Figure 3.6). The 280 N corresponds to the partial body weight above the L1 vertebra of a person weighing 66 kg. The results showed that a follower load in the range of the partial body weight is sufficient to stabilize the spine.

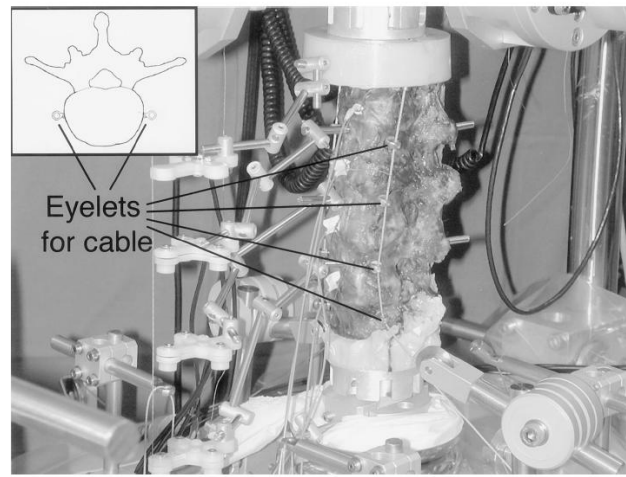


Figure 3. 6: Lumbar spine specimen mounted in a spine tester and loaded with a pure moment plus a follower load [110].

Because of the technical limitation of the current experimental set-up, a physiologic compressive preload was applied only while assessing the kinematics in flexion and extension, and was not applied in lateral bending or axial rotation. The preload resulting from muscle activity has a stabilizing effect on a motion segment; therefore, the results pertaining to lateral bending and axial rotation may be viewed as a worst-case scenario.

In finite element studies, the application of a great number of muscle forces is not a problem, but still seldom used as the muscle forces are not known. The influence of muscle forces on the biomechanical behavior of the lumbar spine was investigated using the finite

element method. Patwardhan [14] support the following hypothesis concerning the action of muscles in the context of a frontal plane model: Muscle activation causes the internal force resultant to follow a path approximating the tangent of the spinal curve, thereby minimizing the internal shear forces and bending moments and loading the whole lumbar spine in nearly pure compression.

Various numerical models have been used to show the follower load activation effectively on the lumbar spine. Shirazi-Adl [111, 112] developed a method to apply physiologic compression to the lumbar spine through the use of posture changes and “wrapping” elements which wrap around prescribed spatial targets in the center of the endplates of each motion segment such that the compressive load remains perpendicular to the mid-plane of each disc (Fig 3.7). The caudal vertebra S1 is fixed while the remaining vertebrae L1-L5 are unconstrained. Axially fixed compression loads of up to 2800 N are incrementally applied at all L1-L5 vertebral centers (80% at the L1 and the rest evenly distributed among remaining L2-L5 vertebrae to account for differential compression loads along the lumbar spine).

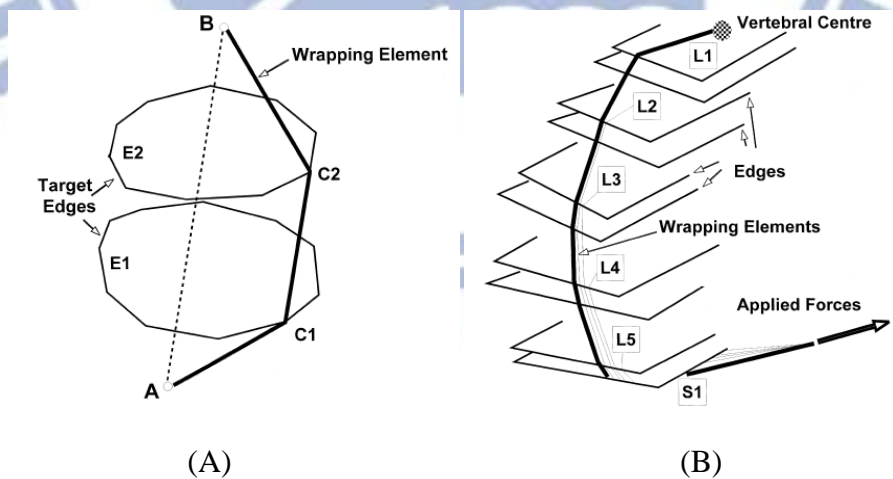


Figure 3. 7: (A)The illustration of wrapping element; (B)the wrapping element applied on the five levels lumbar spine [111,112].

In Renner's [113] study, A follower load was simulated at each motion segment in the

model through a pair of two-node thermo-isotropic truss elements. The follower load trusses were attached bilaterally to the cortical shell of the vertebrae of each motion segment such that each truss spanned the disc, approximately passing through the instantaneous center of rotation of each motion segment, optimizing the follower load path (Figure 3.8). Compressive load was applied to each motion segment by inducing contraction in each of these truss elements by decreasing the temperature in each truss. The results demonstrate that the ability of a large follower load to stiffen the spine in all three planes. Because the follower load concept acts to mimic optimized muscles forces, this study illustrates the important role of muscles in providing spinal stability.

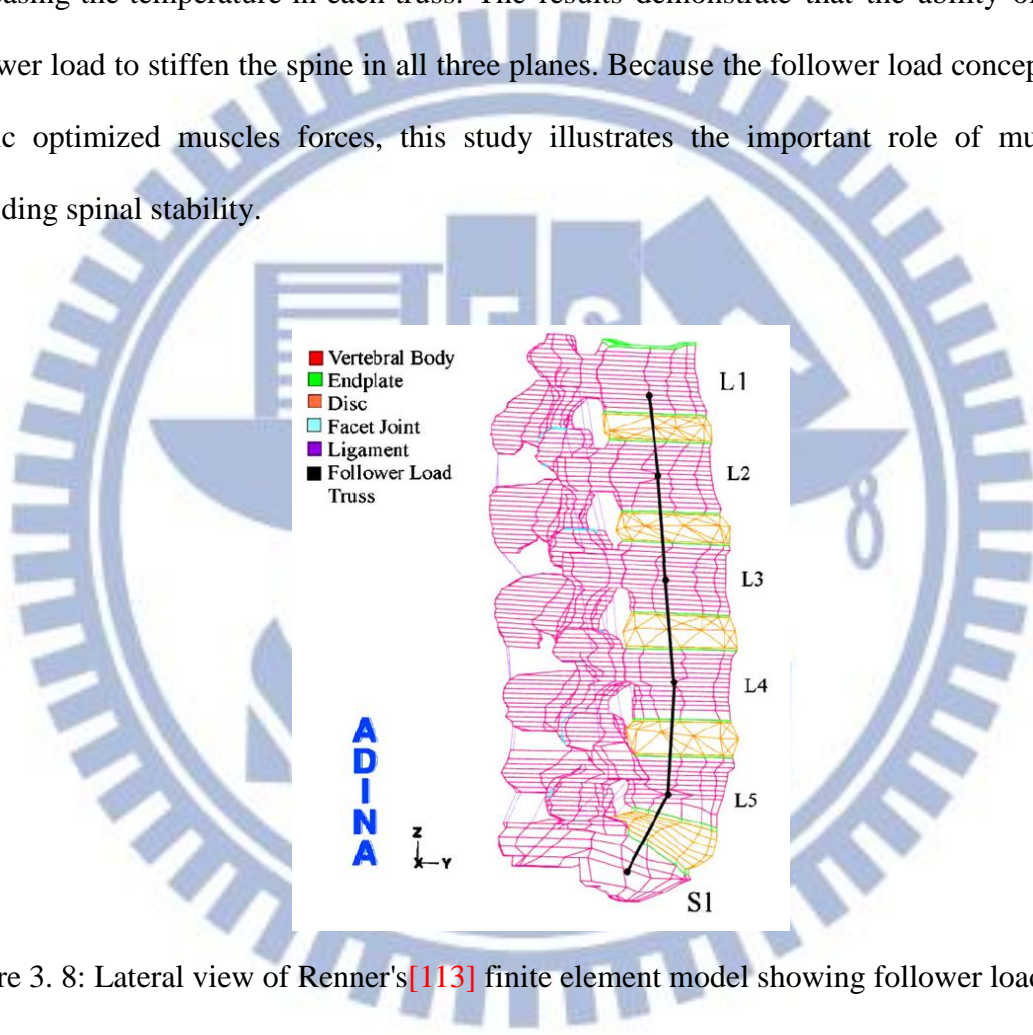


Figure 3. 8: Lateral view of Renner's [113] finite element model showing follower load trusses at each vertebra.

In Rohlmann's [114] study, the weight of the upper body acts in the center of gravity. Since flexion and extension occur in the sagittal plane, only four muscle groups were simulated: left and right erector spinae, plus left and right rectus abdominis. A compressive follower load was applied to substitute for the unknown stabilizing effect of local muscles

(Figure 3.9). The follower load was accomplished by forces of constant magnitude acting in the centers of adjacent vertebral bodies (Figure 3.10).

Applying a follower load instead of a great number of small forces simulating the local dorsal muscles makes realistic loading in *in vitro* studies feasible. It seems that for sagittal plane motion few global muscle forces are sufficient to achieve realistic results. Rohlmann's [114] results showed that the follower load is a suitable tool to adjust the intradiscal pressure to physiological values without significantly affecting intersegmental motion. However, the local muscles act at a larger lever arm to the center of rotation than a follower load and thus have a greater stabilizing effect. Therefore, local muscles contribute somewhat more to the equilibrium of spinal moments than the follower load.

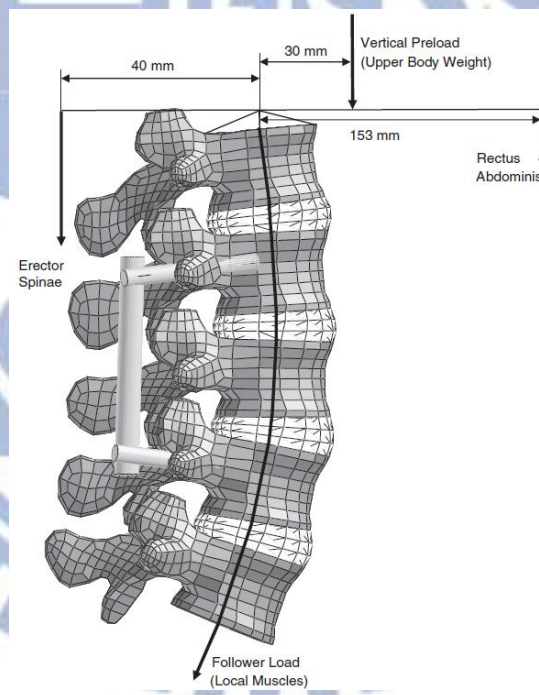


Figure 3. 9: Finite element model of the lumbar spine with the loads applied in Rohlman's study[114].

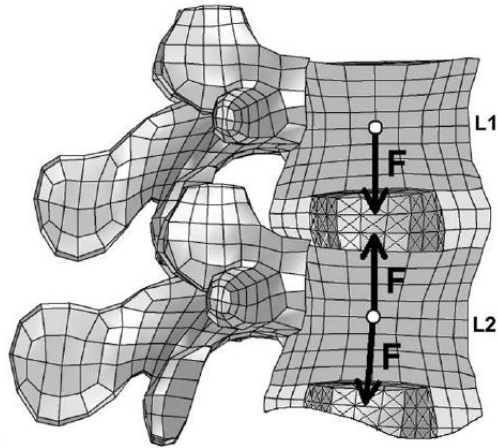


Figure 3. 10: The illustration of follower load of Rollman's model [114].

In this study, two kinds of follower load setting for the finite element analysis were proposed. In order to obtain a suitable setting for the follower load. The simplified follower load was applied on the center of the vertebra (Figure 3.11). In this setting, two hypotheses are used. Firstly, a follower load was applied in the centers of vertebral bodies to substitute for the unknown stabilizing effect of local muscles [114]. Secondly, the thermo-isotropic truss element is used to guarantee the resultant force always toward the center of the next vertebra [113]. The second follower load setting is more close to the experimental set-up. The bilateral follower load was applied through the cable guides on the both side of the spine (Figure 3.12). The two-node truss element is used to present the cable. The downward force was applied at the end of the cable.

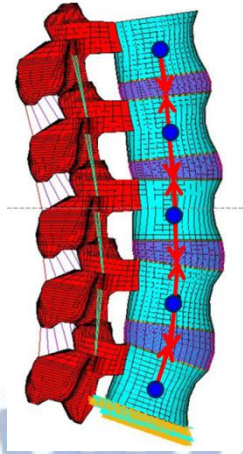


Figure 3. 11: The illustration of follower load (simplified: applied in the center).

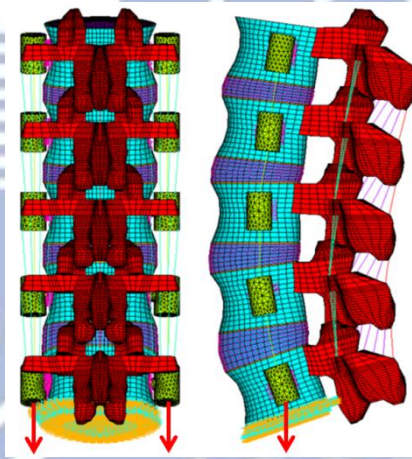


Figure 3. 12: The illustration of follower load (bilateral: applied bilaterally)

In order to estimate both kinds of follower loads, a 10 Nm moments for four physiological motions were applied. And there are four kinds of loading: 0 N (pure moment), 150 N (vertical load), 400 N (follower load: simplified) and 400 N (follower load: bilateral). The results are shown in [Figure 3.13](#). The results show that the simplified and the bilateral follower load have similar performance in flexion, extension and rotation. But the bilateral follower load setting shows significantly high stiffness in lateral bending. It is because of the technical limitation of this set-up. Therefore, the results pertaining to lateral bending has the worst correlation to the realistic case. Also, for further research, the position of the lateral plate

of the Latero device is going to interfere with the guide device for the cable. Finally, since the bilateral follower load setting is worse, the simplified follower load setting was used in further study.

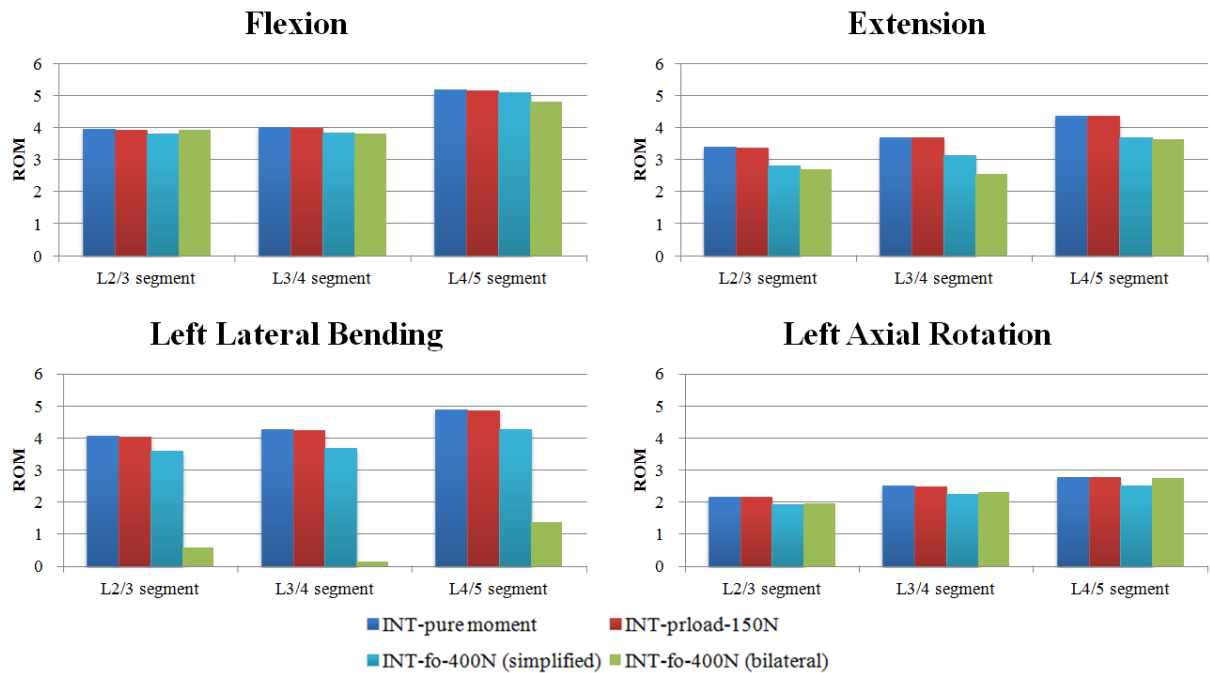


Figure 3. 13: Range of motion (ROM) calculated for the L1-L5 segments of intact lumbar spine is compared to four kinds of preload condition.

3.1.1.3. Validation of INT model

For the validation of the INT model with follower load, the ROM of the intact model under different loading moments was compared to Rohlmann's [104] *in vitro* cadaveric study. Under 7.5 N-m moments without preload and with a 280 N follower load, the total ROM of five segments lumbar were within one standard deviation in flexion-extension, axial rotation, and lateral bending. The results are shown in Figure 3.14. The present model was verified for further simulations.

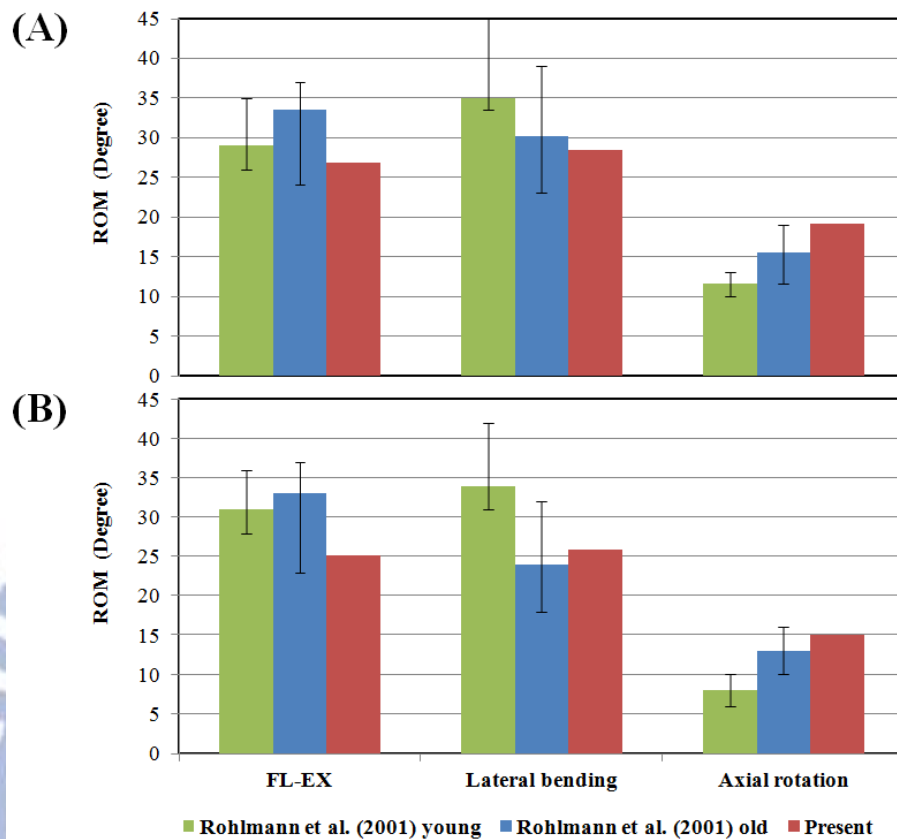


Figure 3. 14: Range of motion (ROM) calculated for the L1-L5 segments of intact lumbar spine is compared to previous *in vitro* experiments. (A)Intact lumbar spine without follower load; (B)intact lumbar spine with simplified follower load.

3.1.2. The establishment of implant models

In order to establish the implant models, the geometric appearances of the implant devices should be obtained. The implant devices were re-created by CAD software from the real product and then transferred into the ANSYS software to construct the implant FE models. [Figure 3.15](#) shows the interbody fusion devices which were used in this study:

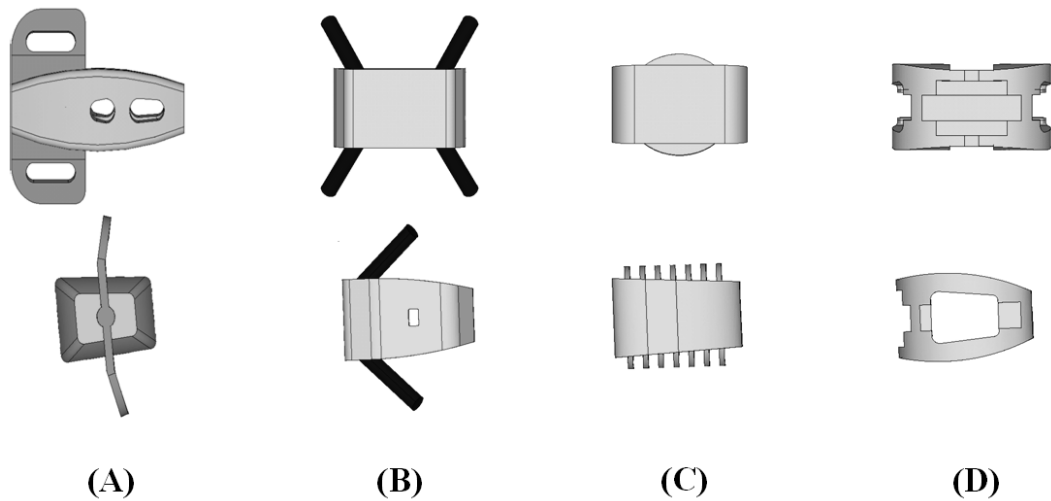


Figure 3. 15: The implant devices used in this study. (A)Latero. (B) SynFix. (C)Stabilis.
(D)SynCage-Open

3.1.2.1. FE model of Latero implant (Latero model)

This model was a spine model implanted with the Latero device at the L3-L4 segment (Figure 3.16). The Latero integrates a lateral vertebral plate into the trapezoid frame which is bent to be parallel to the coronal plane. The geometry of the Latero device was re-created by CAD software from the real product and then transferred into the ANSYS software to construct the Latero FE model. The surface between the plate and the cage was modeled as full bonding. The surface between the bones and the Latero device was modeled as a surface-to-surface contact. The effect of teeth on the cage and the lateral plate of the Latero device was simplified by assigning a higher coefficient of friction (0.8) to the contact area. The higher coefficient of friction (0.8) was used in the contact interface to prevent device slip motion [94]. The material used for the Latero device was Titanium alloy for the lateral plate and PEEK for the main cage. The Young's modulus and Poisson's ratio were listed on Table 3.2.

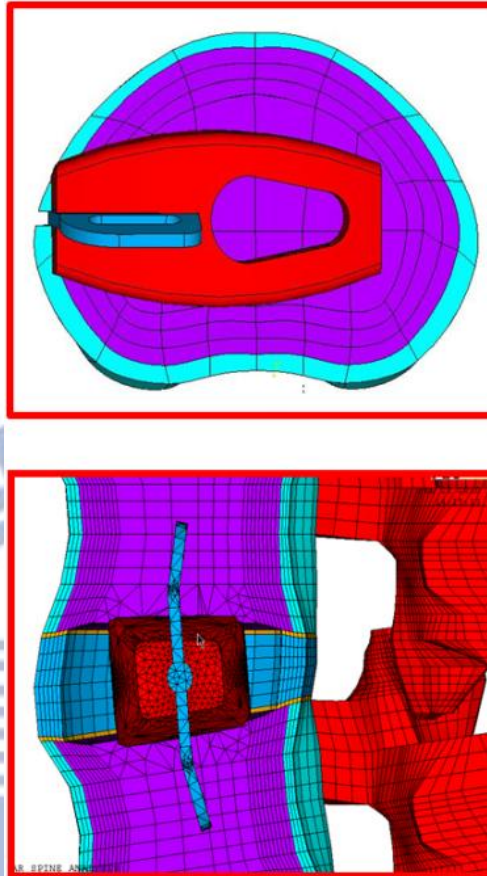


Figure 3. 16: The vertical view and lateral cross-sectional view of Latero implanted into L3-L4 segment

3.1.2.2. FE models of conventional stand-alone ALIF implants (SynFix model and Stabilis model)

The SynFix and Stabilis devices were implanted at the L3-L4 segment for the conventional stand-alone models (Figure 3.17). The SynFix system uses four screws to lock the adjacent vertebrae (Figure 3.17 A). The Stabilis system accommodates a threaded cylinder to anchor the superior and inferior endplates (Figure 3.17 B). The contact surfaces of the screw with the bone and with the cage are set to be full bonding. The coefficient of friction of the bone-cage interfaces was 0.8 to mimic a serrated surface for the initial stability of the trapezoid frame, and the coefficient of friction for the rest of the contact regions was set to 0.1. The

material used for the Stabilis and the screw part of the SynFix were Titanium alloy. PEEK is used for the cage part of the SynFix. The Young's modulus and Poisson's ratio were listed on Table 3.2.

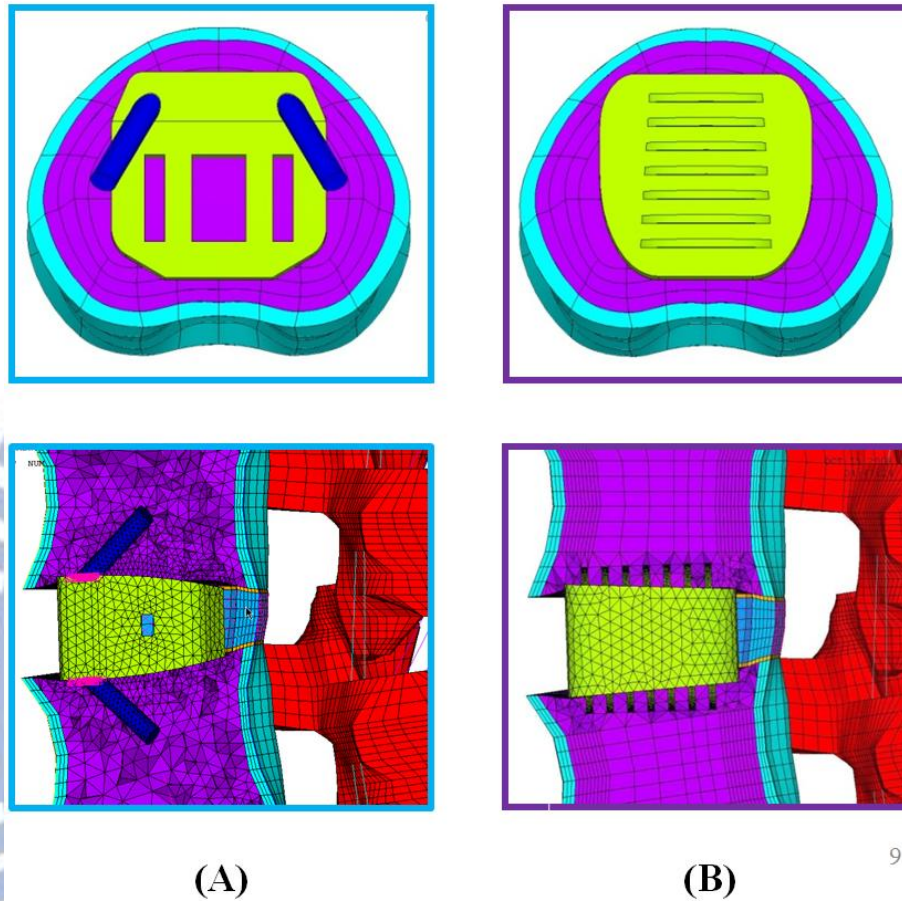


Figure 3. 17: The vertical view and lateral cross-sectional view of (A) SynFix and (B) Stabilis implanted into L3-L4 segment

3.1.2.3. FE model of conventional fixation method (A+P Model)

The traditional fusion surgery always accompanied the pedicle screws. This model was implanted with SynCage-Open with pedicle screw at the L3-L4 segment to present the traditional fixation model (Figure 3.18). This model was denoted as A+P (ALIF plus Pedicle screws) model. The difference between the A+P model and the above stand-alone implantation models was that the pedicle screw fixation model demand more complicate surgical procedure.

The A+P model consisted of two rods (diameter, 4.5 mm) and four pedicle screws (diameter, 6 mm). The pedicle screws were inserted through the pedicles of the L3 and L4 vertebrae bilaterally. The pedicle screws were simplified as cylinders. The screw-bone interfaces were assigned to be fully constrained. The material used for the cage and pedicle screws were Titanium alloy. The Young's modulus and Poisson's ratio were listed on [Table 3.2](#).

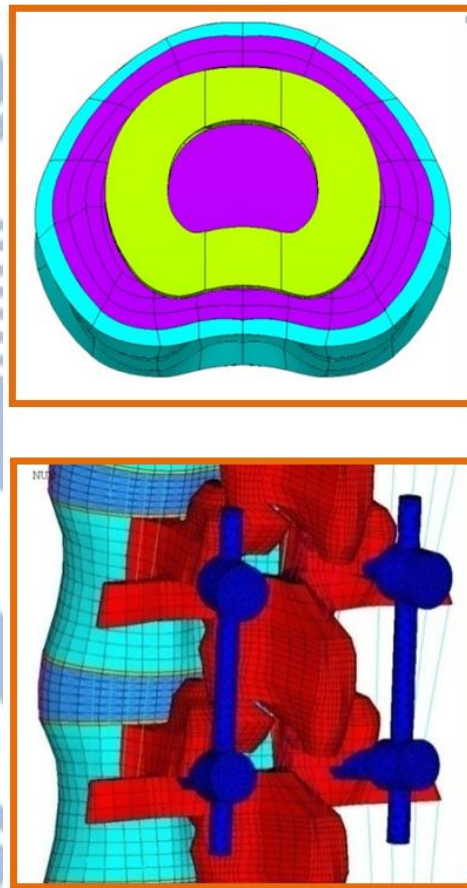
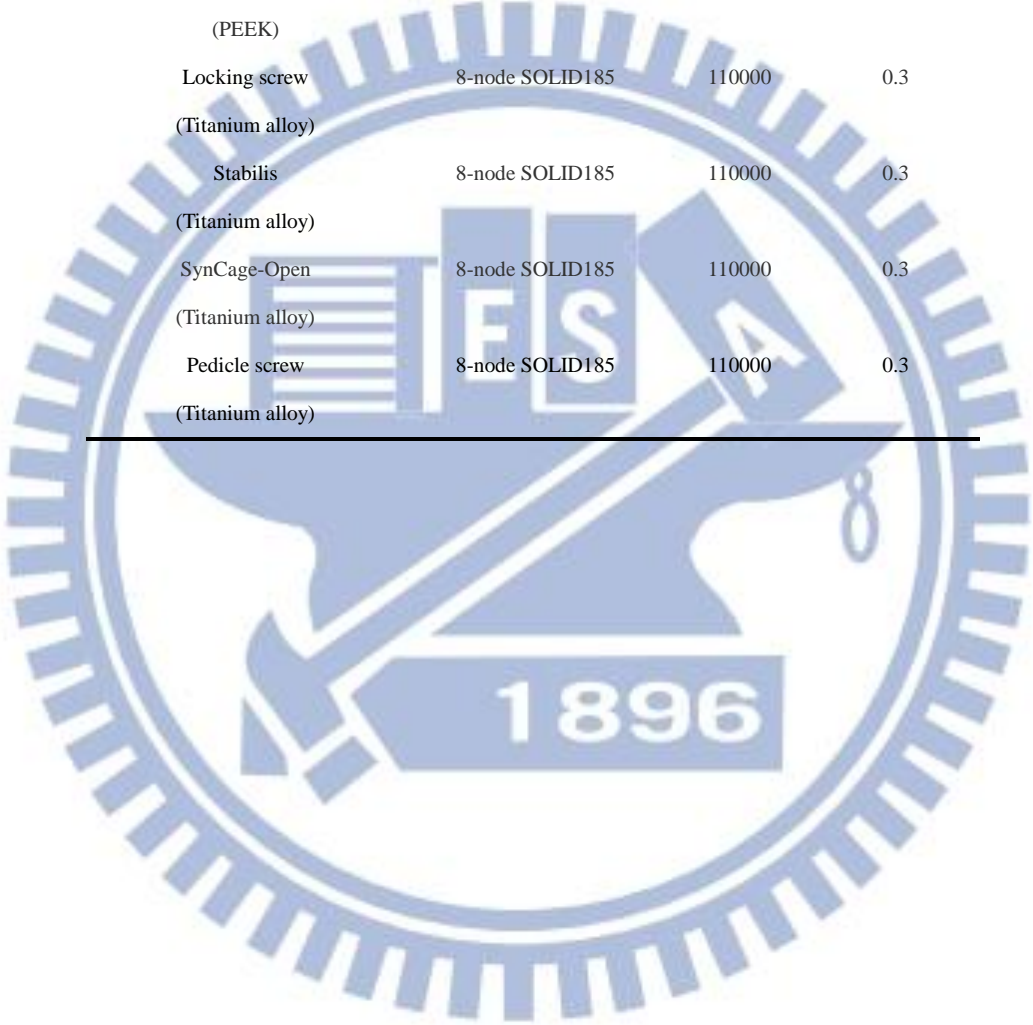


Figure 3. 18: The vertical view and rear view of SynCage-Open and the pedicle screws implanted into L3-L4 segment

Table 3. 2: Material properties of the implants.

Material	Element Type	Young's Modulus (MPa)	
			Poisson's Ratio
Latero (PEEK)	8-node SOLID185	6500	0.2
Latero-plate (Titanium alloy)	8-node SOLID185	110000	0.3
SynFix-LR (PEEK)	8-node SOLID185	6500	0.2
Locking screw (Titanium alloy)	8-node SOLID185	110000	0.3
Stabilis (Titanium alloy)	8-node SOLID185	110000	0.3
SynCage-Open (Titanium alloy)	8-node SOLID185	110000	0.3
Pedicle screw (Titanium alloy)	8-node SOLID185	110000	0.3



3.2 Part-2 of this study

In the part-2 of this study, two improvement parameters for the Latero device were proposed: position of implant and bending angle of lateral plate. The subject of following sections includes FE models for the improvement for the Latero device. The position of the implants should be an important factor for the surgery. In this study, three positions were proposed to compare the differences of the stability for the spine. Anterior (Latero-A), middle (Latero-M) and posterior (Latero-P) positions were used. The middle part (Latero-M) is the Latero model mentioned in part-1. The bending angle of the lateral plate is also an important design factor for the Latero model. The original bending angle of the lateral plate is 15 degree. In this study the bending angle of 30 degree (Latero-(30)) is proposed to check the effect of the plate.

3.2.1. Different insert positions of Latero model

These models were spine models implanted with the Latero device at the L3-L4 segment (Figure 3. 19). The Latero model in the part-1 was denoted as Latero-M in part-2. The letter “M” was used to emphasize that the implant is in the middle position. For the Latero-A model, the position of Latero is moved forward. In the limitation of keeping the same layers of annulus as Latero-M, the implant is moved as far as possible. For the Latero-P model (Figure 3. 20 B), the position of Latero is moved backward. In the limitation of keeping the same layers of annulus as Latero-M, the implant is moved as far as possible. The letter “A” and “P” were used to emphasize that the implant were in the anterior position and posterior position. The surface between the plate and the cage was modeled as full bonding. The surface between the bones and the Latero device was modeled as a surface-to-surface contact. The effect of teeth on the cage and the lateral plate of the Latero device was simplified by assigning a higher coefficient of friction (0.8) to the contact area.

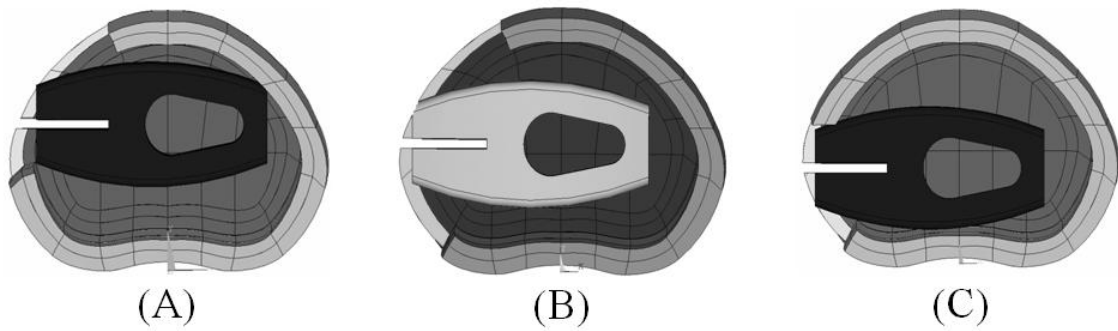


Figure 3. 19: The different positions of Latero model:(A)Anterior; (B)Middle; (C)Posterior

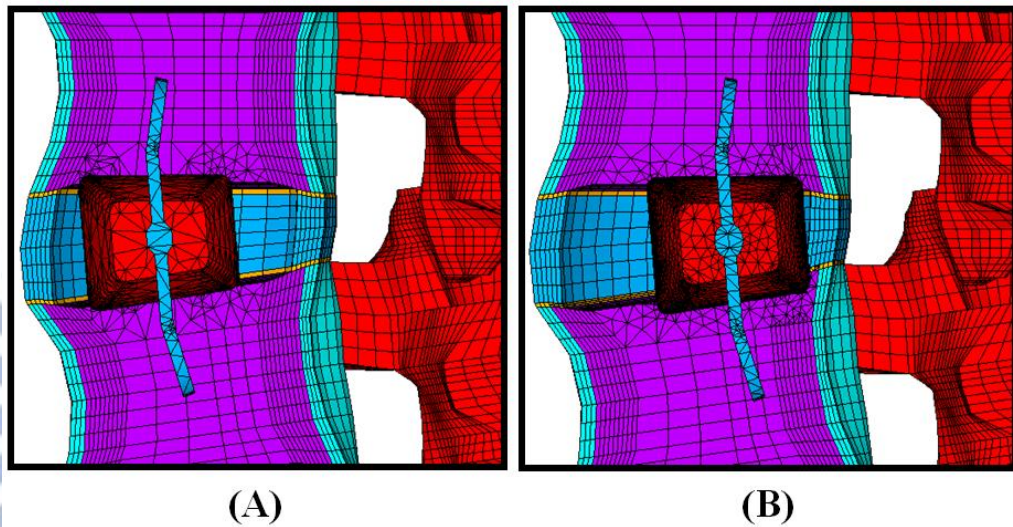


Figure 3. 20: The lateral view of (A)Latero-A and (B)Latero-P

3.2.2. Different angle of the lateral plate of the Latero

This model was model implanted with the Latero device at the L3-L4 segment (Figure 3. 21). In the Latero-M model, the lateral plate is bended at upper and lower part (Figure 3. 22 B). The angle between the plate and the vertical line is 15 degree. For the Latero-(30) degree model, the angle is changed into 30 degree (Figure 3. 22 C). The contact conditions are the same as Latero-M model. The surface between the plate and the cage was modeled as full bonding. The surface between the bones and the Latero device was modeled as a surface-to-surface contact. The effect of teeth on the cage and the lateral plate of the Latero device was simplified by assigning a higher coefficient of friction (0.8) to the contact area.

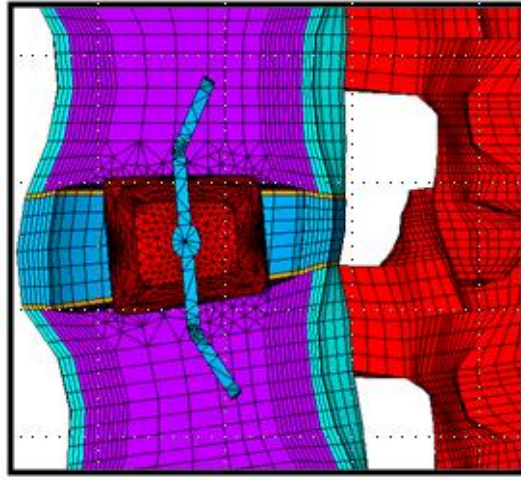


Figure 3. 21: The lateral view of Latero-(30).

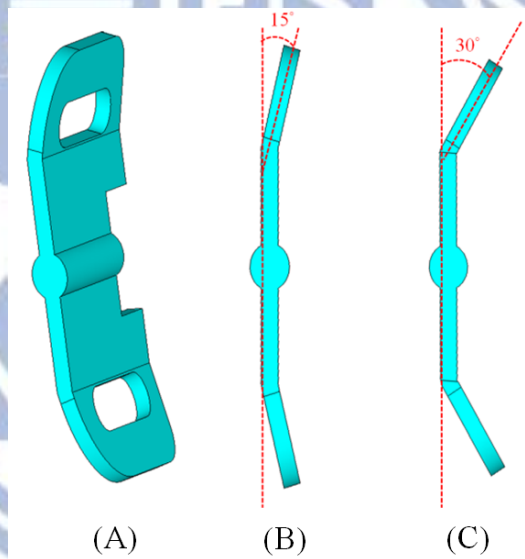


Figure 3. 22: The different bending angle of lateral plate:(A)Oblique view of original plate;
 (B)Lateral view of original plate; (C) Lateral view of modified plate.

3.3. Boundary and loading conditions

In the past, several finite element and cadaver studies have used the traditional load-controlled method (LCM) to evaluate the characteristics of adjacent level effects (ALEs) on spinal constructs with fusion or non-fusion spinal implants [105]. This loading method applied the same pure moment to all the spinal constructs, and then the motions in each level were calculated. In recent years, Panjabi *et al.* [106] have introduced a new testing protocol that is similar to the displacement-controlled method (DCM), called the hybrid approach. This approach applies different moments so that the same overall ranges of motions (ROMs) are achieved for both intact and implant models. Currently, spinal implants in vitro test has been advanced from traditional LCM to DCM. It is still not clear whether the LCM or the DCM is more suitable to reveal the reality of fusion versus non-fusion spinal implants at the surgical and adjacent levels. Recently, Zhong's study [103] suggested that these two analytical methods can be used to predict specific conditions in the patient's daily life. The DCM is suitable for evaluation of the patient's daily life motions during restoration after surgery. The LCM is suitable for evaluation of the patient's normal lifting work-loading condition after surgery. In this study, for the clarity of presentation, only one control method was used. Therefore, the LCM which used in the validation models [104] was used in this study.

In both parts of this study, a 400 N compressive follower load was applied to each motion segment through induced contraction in these thermo-isotropic truss elements by decreasing the temperature [113, 114]. And then, a 10 Nm moment was applied to obtain the six physiological motions (Flexion, extension, left/right lateral bending, and left/right axial rotation) (Figure 3.23). The ROMs of the INT model are a baseline with which to match the total lumbar motion among the implantation models.

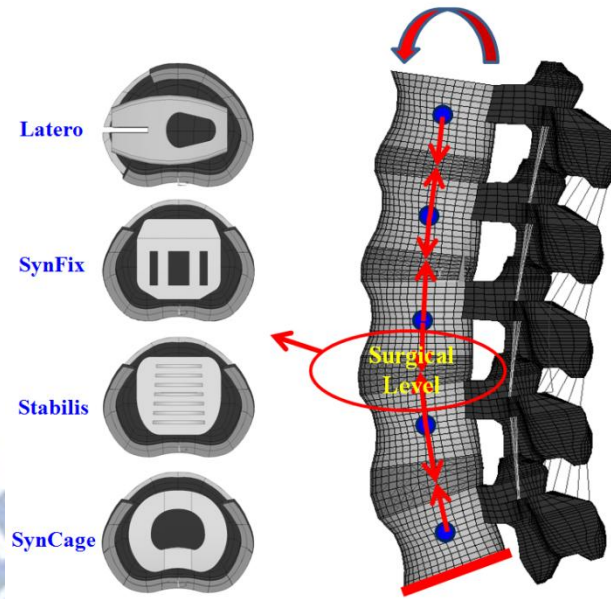


Figure 3. 23: The boundary and loading conditions of the simulation were that the inferior surface of L5 vertebra was fixed, and 10 Nm moment and a 400 N follower load were applied to the superior surface of L1 vertebra.

Chapter 4 Results

4.1. Part-1 Results

The stand-alone implant for interbody fusion is gaining popularity because of its minimally invasive nature. The acute biomechanical stability of the stand-alone implant for interbody fusion is dependent on the type of supplemental internal fixation used. For the Latero device, the lateral plate has been approved for clinical use for added stabilization after cage implantation. Five parameters were used as the indices for the comparison of Latero and other stand-alone implants, including intersegmental range of motion (ROM), annulus stress, facet contact forces, implant stress and endplate stress. There were five models used in this study: one intact (INT), three stand-alone cages (Latero, SynFix, and Stabilis), and one traditional fusion model (A+P). The ROM comparisons of the instrumented models were normalized by the corresponding value of the intact model.

4.1.1. ROM

Referring to the formula used in Panjabi's study [106] ($ROM_{normalized} = (ROM_{implant} - ROM_{INT}) / ROM_{INT} * 100 \%$), the restricted ROM of the instrumented model was compared with the corresponding ROM value of the INT model (Figure 4.1). For the sake of clarity, the percentages of restricted ROM for the models of the normal lumbar at the surgical level are given below:

FL : A+P (-90%) > Latero (-82%) > SynFix (-67%) > Stabilis (-60%)

EX : A+P (-94%) > Latero (-92%) > SynFix (-51%) > Stabilis (-11%)

LLB: A+P (-77%) > SynFix (-72%) > Latero (-59%) > Stabilis (-21%)

RLB: A+P (-77%) > SynFix (-72%) > Latero (-37%) > Stabilis (-21%)

LAR: A+P (-77%) > SynFix (-57%) > Latero (-50%) > Stabilis (-34%)

RAR: A+P (-77%) > SynFix (-57%) > Latero (-48%) > Stabilis (-34%)

The A+P model had the maximal capability in restricting ROM from -76.5% to -93.8% in all motions. The Latero model performed ROM control similar to that of A+P, and superior to that of the SynFix model in flexion and extension. Moreover, the Latero model performance was similar to that of the SynFix model in bilateral axial rotation and left lateral bending, but inferior in right lateral bending. The asymmetrical design of the Latero model with the vertebral plate placed on the left side explained the different behaviors in left *versus* right lateral bending. The Stabilis model had the lowest values in all motions, especially in controlling lateral bending (-21.0%) and extension (-10.6%). This finding is consistent with the result of the Chen's study [102].

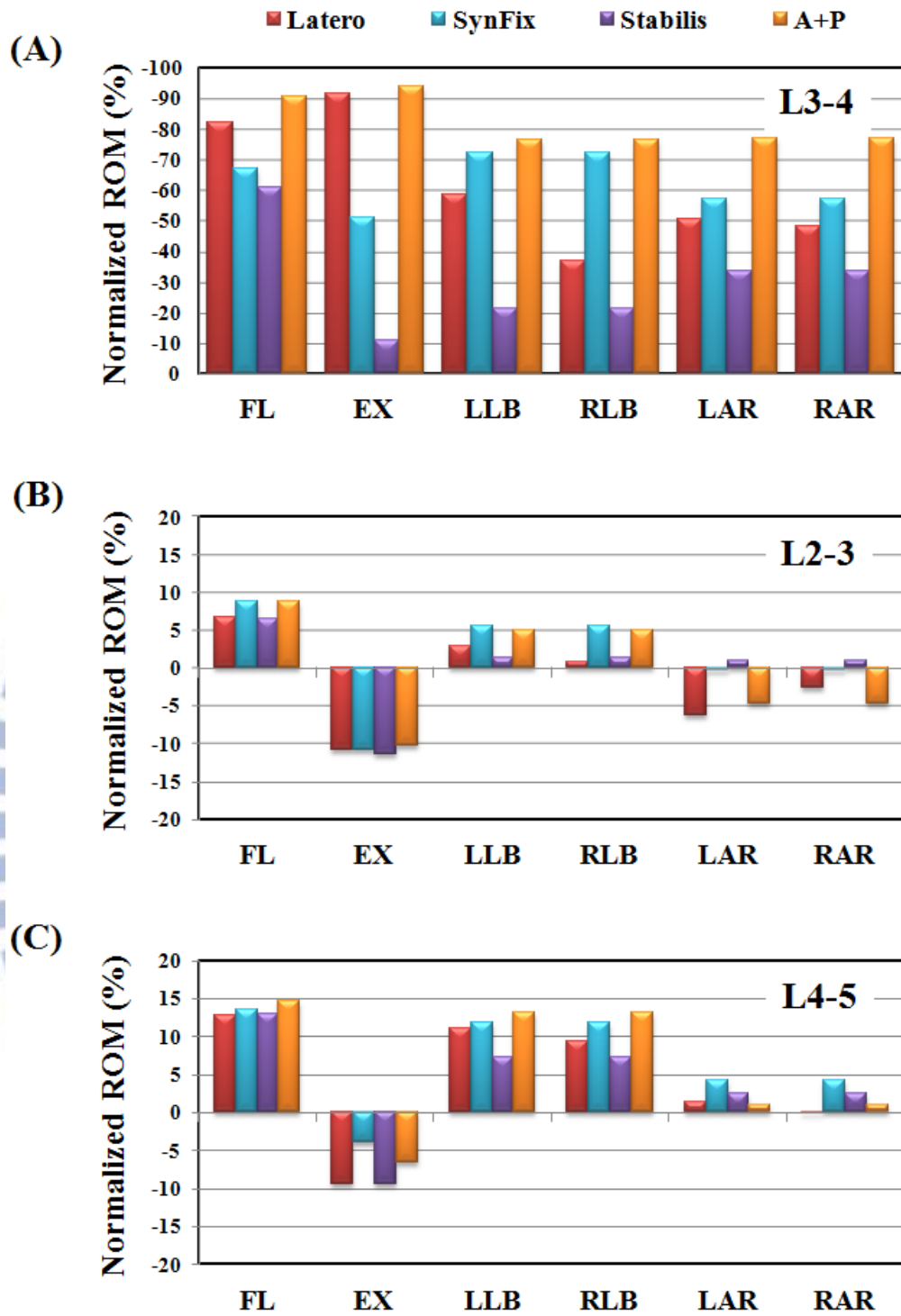


Figure 4. 1: Comparison of the normalized intersegmental ROM among all models under six motions. (A) Surgical level. (B) Upper adjacent levels. (C) Lower adjacent level

4.1.2. Annulus stress

Referring to the formula used in Panjabi's study [106], the normalized percentages of the maximum annulus stress at the surgical level of all models are shown in Figure 4.2. At the surgical level, the normalized annulus stress and intersegmental ROM can be well correlated for each model. The Latero model had maximum annulus stress similar to the A+P model, and was superior to the SynFix model in flexion and extension. It was also similar to the SynFix model in bilateral axial rotation and left lateral bending, but inferior in right lateral bending.

Under the normal condition, the annulus stress distribution of the four instrumented models was shown in extension, left and right lateral bending (Figure 4.3A-C). The Latero had annulus stress distribution similar to the A+P model in extension (Figure 4.3A), similar to the Stabilis model in right lateral bending (Figure 4.3B), and similar to the SynFix model in left lateral bending (Figure 4.3C). The Stabilis model showed the highest annulus stress in all motions, with the stress being concentrated at the posterior annulus in extension (Figure 4.3A) and at the lateral annulus in bilateral lateral bending (Figure 4.3B, C). In contrast, the annulus stress was more evenly distributed in the other three models. However, at the adjacent L2/L3 and L4/L5 levels, there was no obvious difference in annulus stress distribution among the four instrumented models.

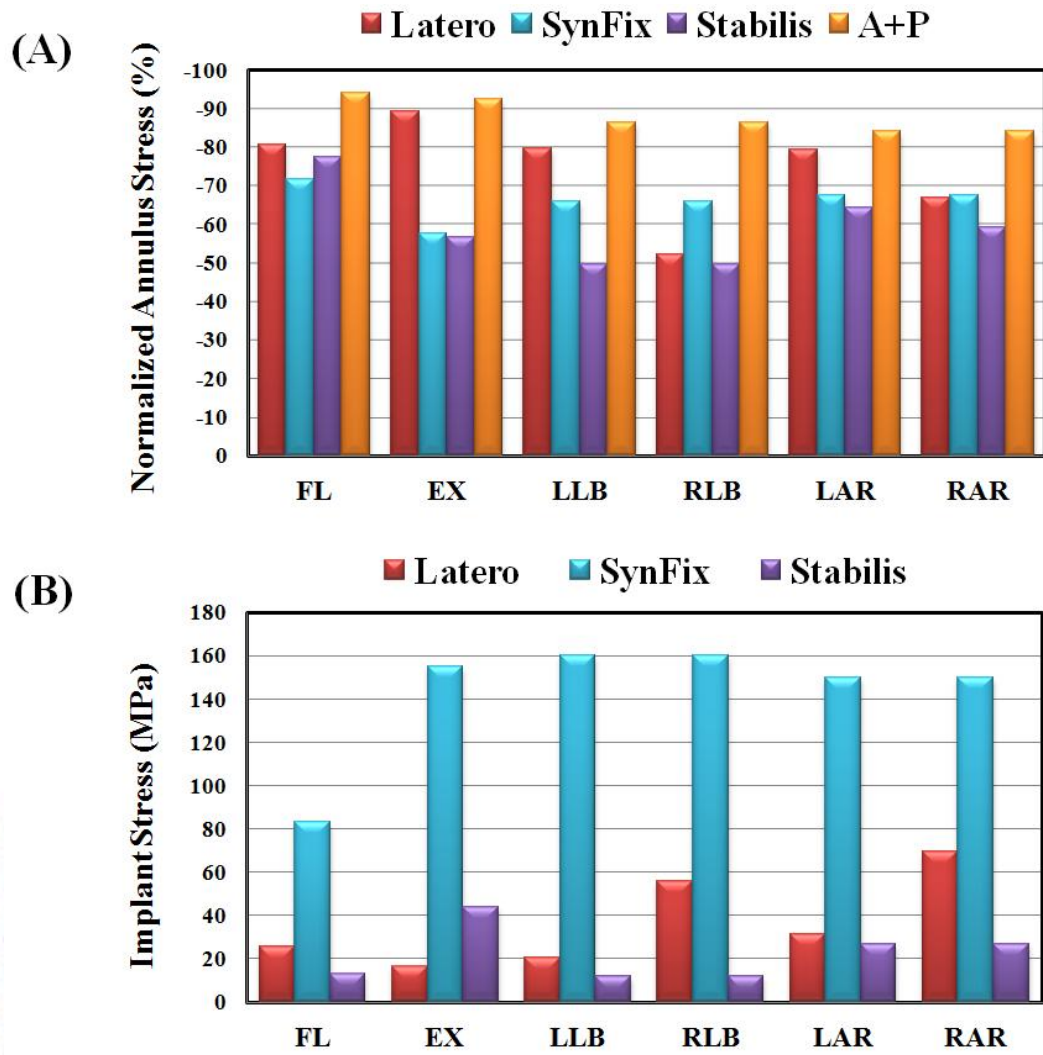


Figure 4. 2: Stress comparison of the normalized stress among all models under six motions. (A) Annulus stress. (B) Implant stress.

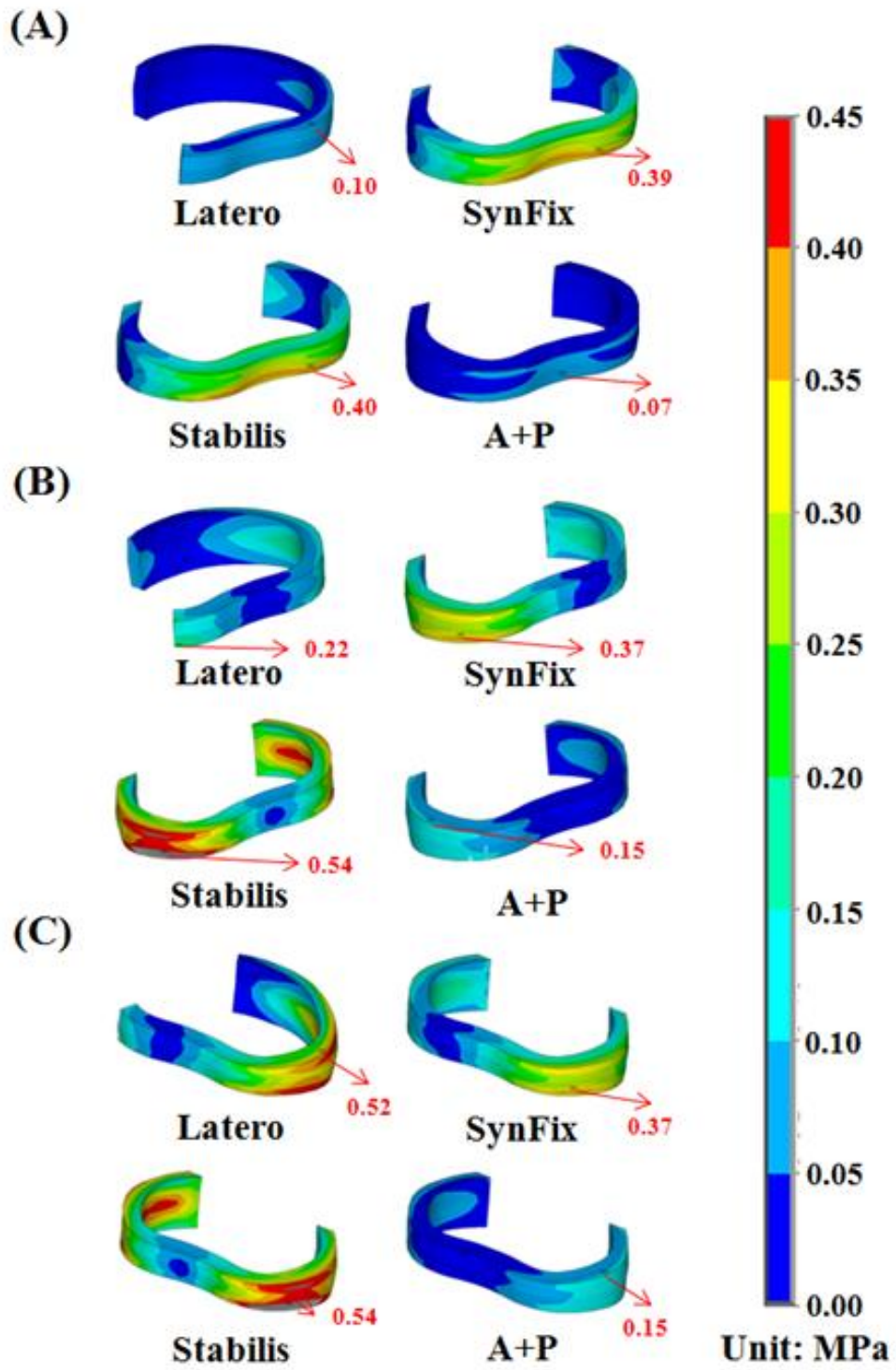
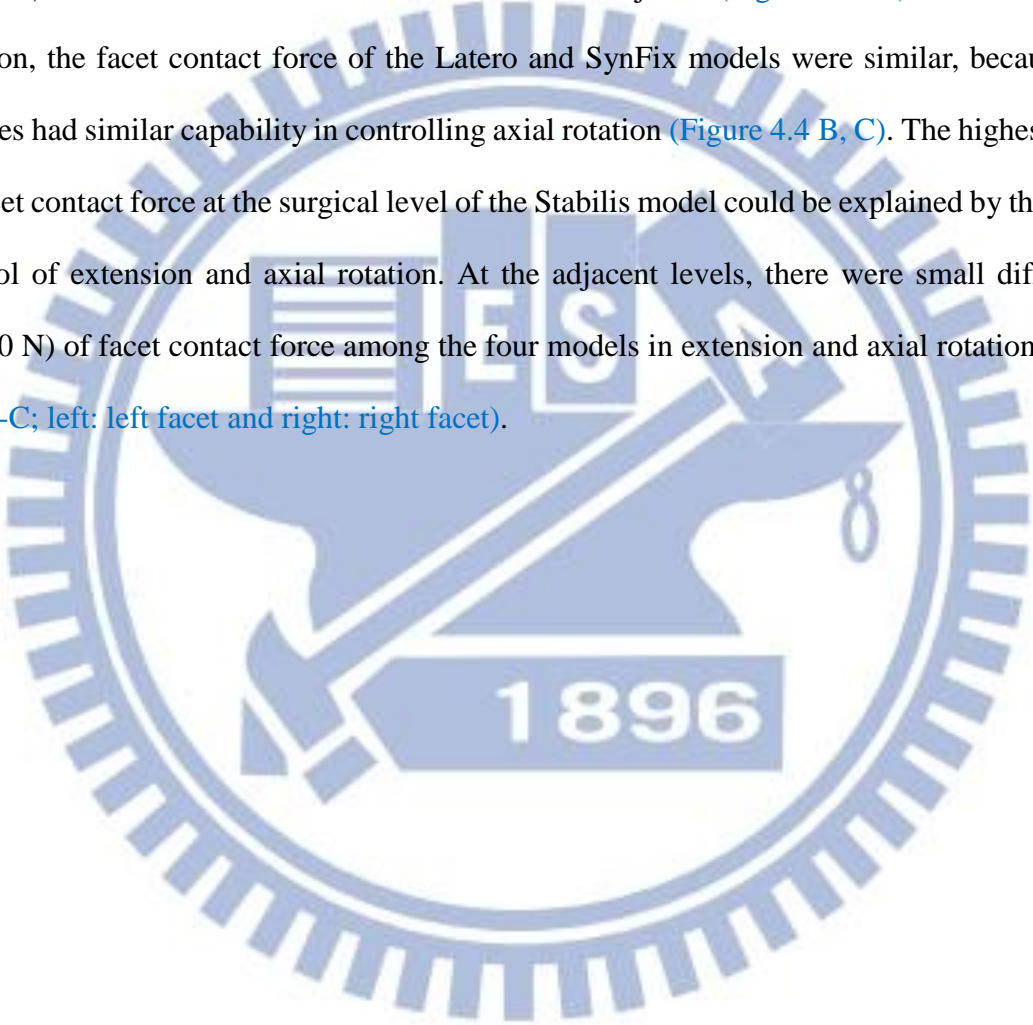


Figure 4. 3: Distribution of the annulus stress for the four models. (A) Extension (B) Left lateral bending. (C) Right lateral bending.

4.1.3. Facet contact force

The facet contact forces at the surgical and adjacent levels of all models are shown in extension and bilateral rotation (Figure 4.4A-C). The A+P model had nearly zero facet contact force at the surgical level in all motions, because the relative motions of the facets joint were restricted by the pedicle screw. In extension, the Latero model could control most of extension (-91.6%) and there was little force shifted to the facet joints (Figure 4.4 A). In bilateral axial rotation, the facet contact force of the Latero and SynFix models were similar, because both devices had similar capability in controlling axial rotation (Figure 4.4 B, C). The highest values of facet contact force at the surgical level of the Stabilis model could be explained by the poorer control of extension and axial rotation. At the adjacent levels, there were small differences (<15.0 N) of facet contact force among the four models in extension and axial rotation (Figure 4.4 A-C; left: left facet and right: right facet).



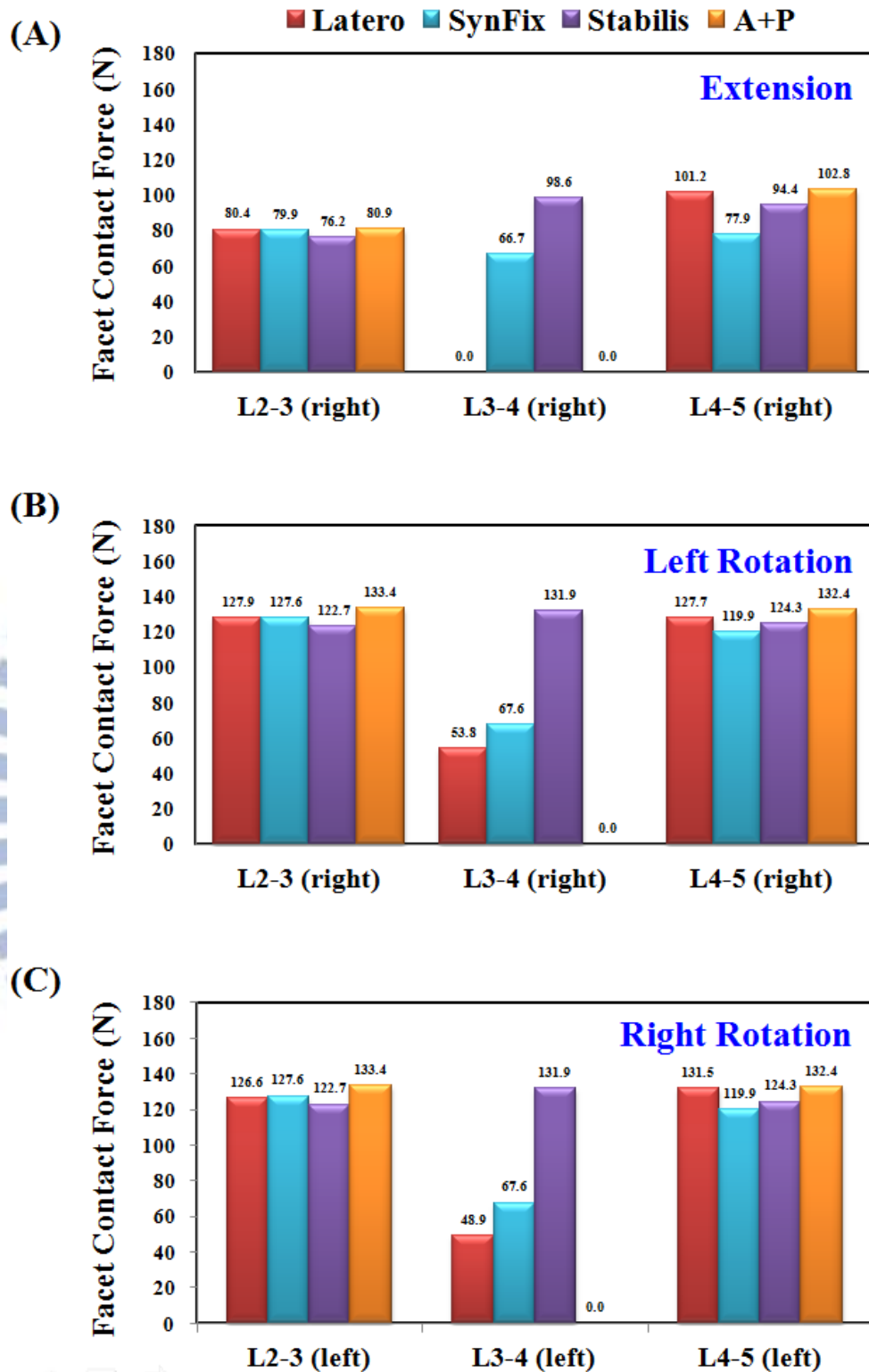
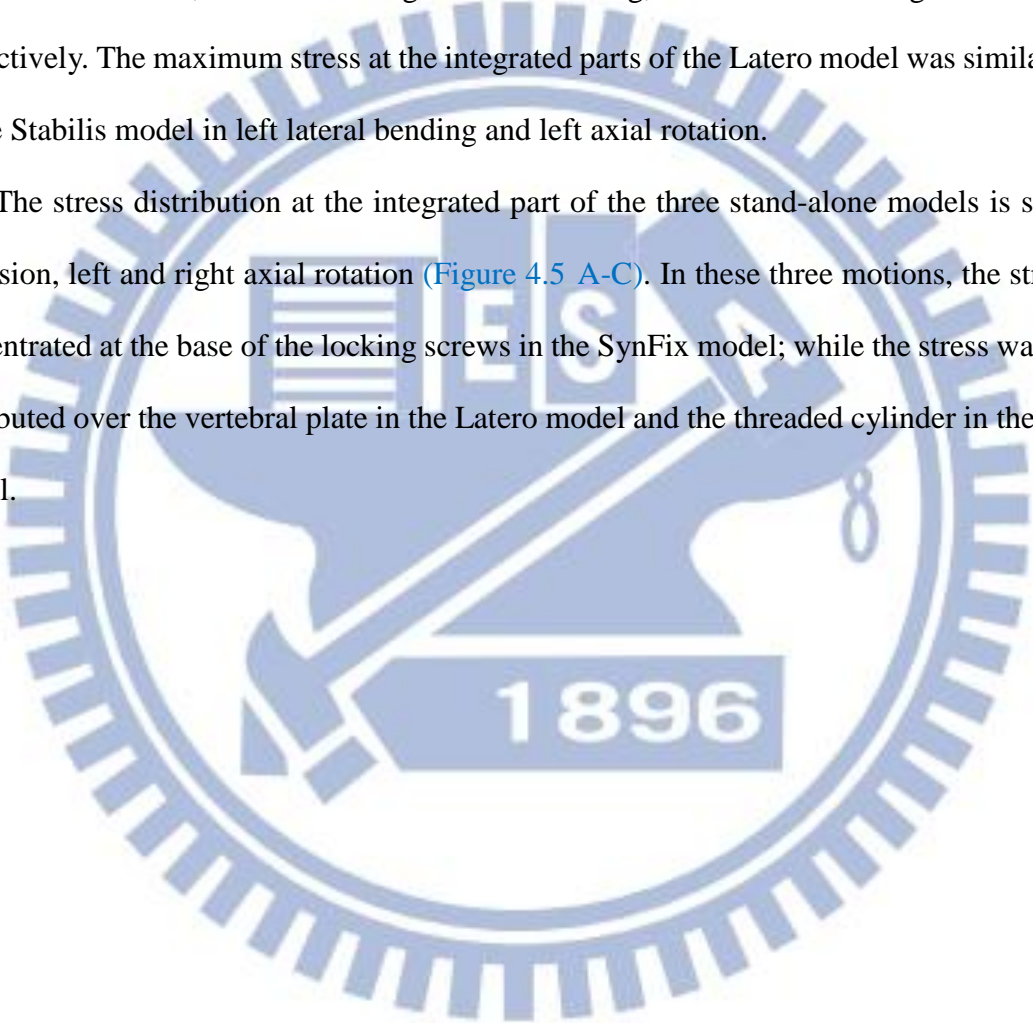


Figure 4. 4: Comparison of facet contact force among all models. (A) Extension. (B) Left axial rotation. (C) Right axial rotation. Middle bars are the surgical level (L3-L4); left and right bars are the adjacent levels (L2-L3 and L4-L5).

4.1.4. Implant stress

The maximum stresses sustained by the integrated parts of three stand-alone cages are shown in [Figure 4.2 B](#). The locking screws of the SynFix model had higher stress than the vertebral plate of Latero and the threaded cylinder of Stabilis models in all motions. The ratios of maximum stresses at the integrated parts among Latero, SynFix and Stabilis models were 1: 9.6: 2.7 in extension, 1: 2.9: 0.2 in right lateral bending, and 1: 2.2: 0.4 in right axial rotation, respectively. The maximum stress at the integrated parts of the Latero model was similar to that of the Stabilis model in left lateral bending and left axial rotation.

The stress distribution at the integrated part of the three stand-alone models is shown in extension, left and right axial rotation ([Figure 4.5 A-C](#)). In these three motions, the stress was concentrated at the base of the locking screws in the SynFix model; while the stress was evenly distributed over the vertebral plate in the Latero model and the threaded cylinder in the Stabilis model.



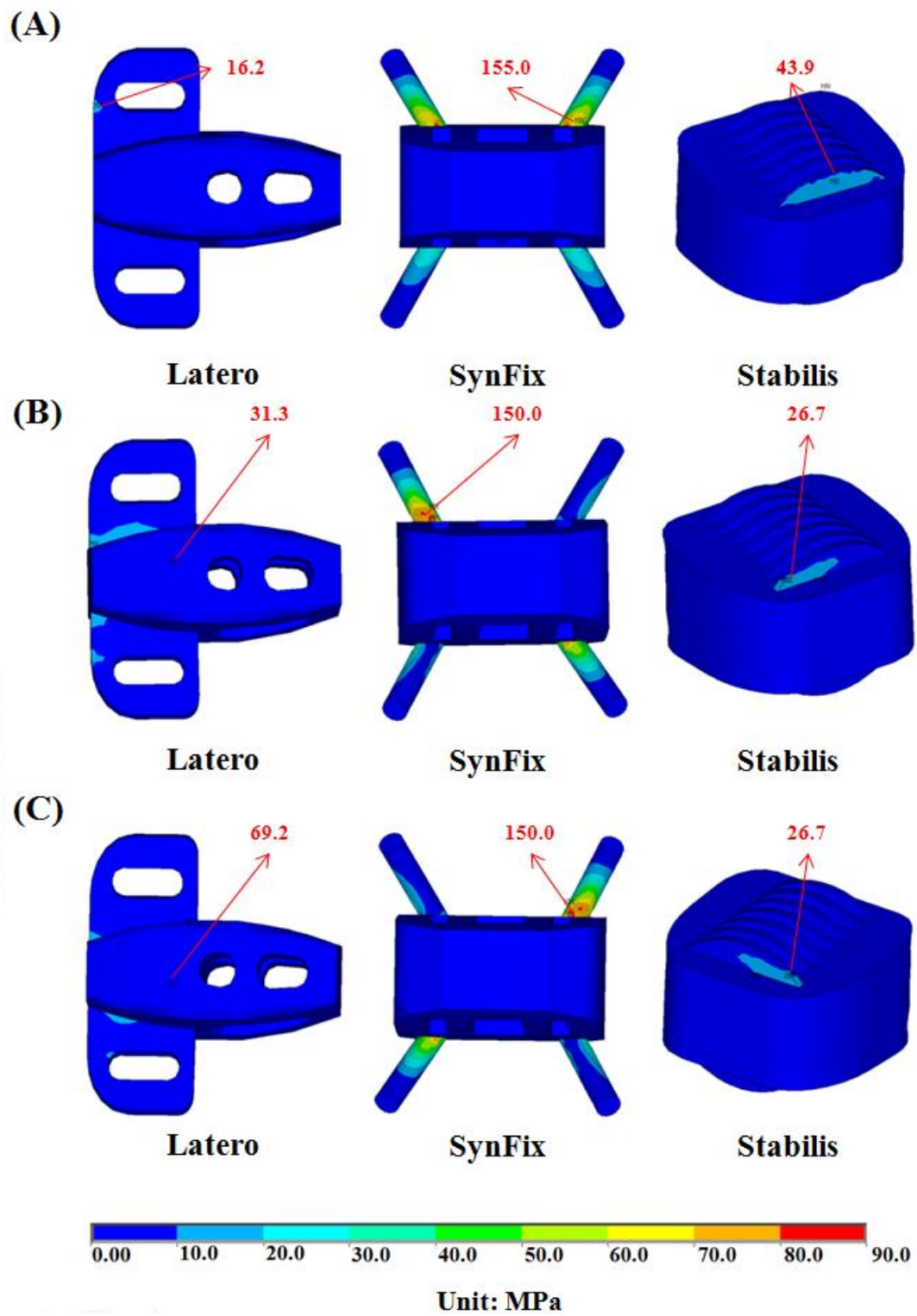


Figure 4. 5: Distribution of implant stress for the Latero, SynFix, and Stabilis models. (A) Extension. (B) Left axial rotation. (C) Right axial rotation.

4.1.5. Endplate stress

Since cage subsidence most commonly occurs at the lower endplate of the upper vertebra [72], only the maximum stress on the L3 endplate was calculated. All models consistently showed that the maximum stress occurs at the top surface of the L3 vertebra (Figure 4.6). The adjacent endplate of the Latero model was more stressed than the other models in axial rotation. Among all motions, the L3 endplate was most stressed in flexion at the SynFix model. In extension, the stress ratios of the contact surface on L3 between the three stand-alone cage models in extension equal to 1:1.07:1.15 in Latero, SynFix, and Stabilis, respectively. The aforementioned stress ratios were 1:1.47:0.53, 1:0.48:0.53 and 1:0.31:0.34 in flexion, left axial rotation and right axial rotation, respectively. The highly stressed endplate of the Latero model in axial rotation might be attributed to the smaller contact surface of the Latero cage.

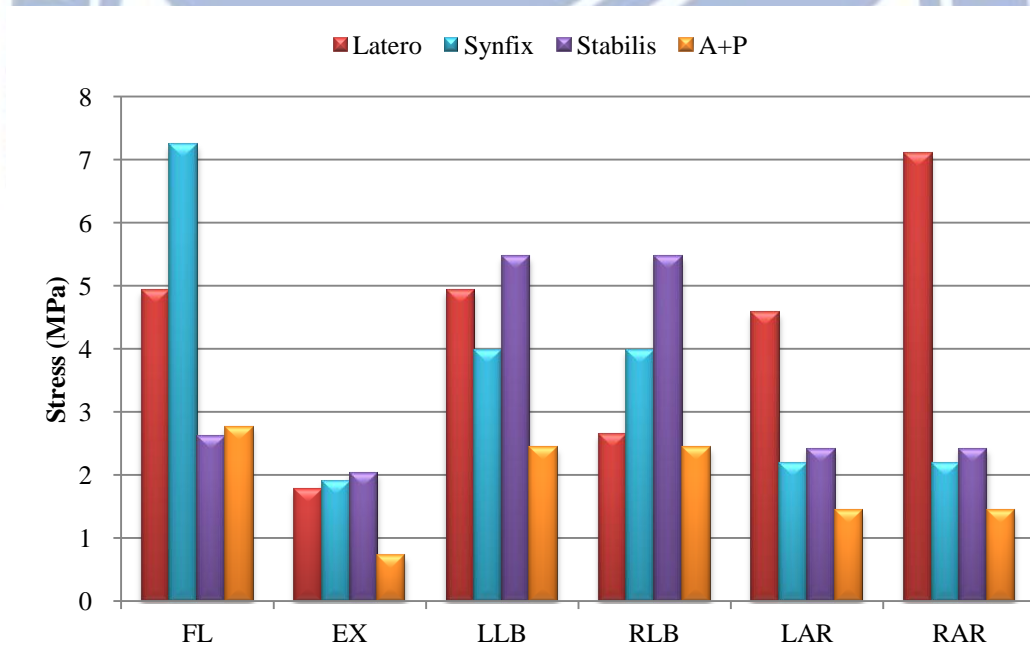


Figure 4. 6: Comparison of endplate stress on the lower surface of the L3 vertebra for all models.

4.2. Part-2 Results

This study used two parameters as the comparison indices for the improvement of Latero implantation, including implant position and plate angle. There were four models: Latero-A, Latero-M, Latero-P and Latero-(30). The ROM comparison of the instrumented models was normalized by the corresponding value of the intact model.

4.2.1. ROM of different positions

Biomechanical behaviors of the Latero models with different positions were compared. Data were normalized with respect to the intact model as percentage values under each loading condition (Figure 4.7). For the sake of clarity, the percentages of restricted ROM for the models of the normal lumbar at the surgical level are given below:

FL : Latero-M (-82%) > Latero-A (-67%) > Latero-P (-33%)

EX : Latero-M (-92%) > Latero-P (-48%) > Latero-A (-31%)

LLB: Latero-M (-59%) > Latero-P (-55%) > Latero-A (-53%)

RLB: Latero-M (-37%) > Latero-A (-24%) > Latero-P (14%)

LAR: Latero-M (-50%) > Latero-A (-45%) > Latero-P (-43%)

RAR: Latero-M (-48%) > Latero-A (-43%) > Latero-P (-40%)

The Latero-M model had the maximal capability in restricting ROM from -47.9% to -91.6% in flexion, extension and left/right axial rotation. The middle position of the Latero model provide better stability than anterior (Latero-A) and posterior (Latero-P) position in flexion and extension. Moreover, all Latero models performance were similar in left/right axial rotation and left lateral bending.

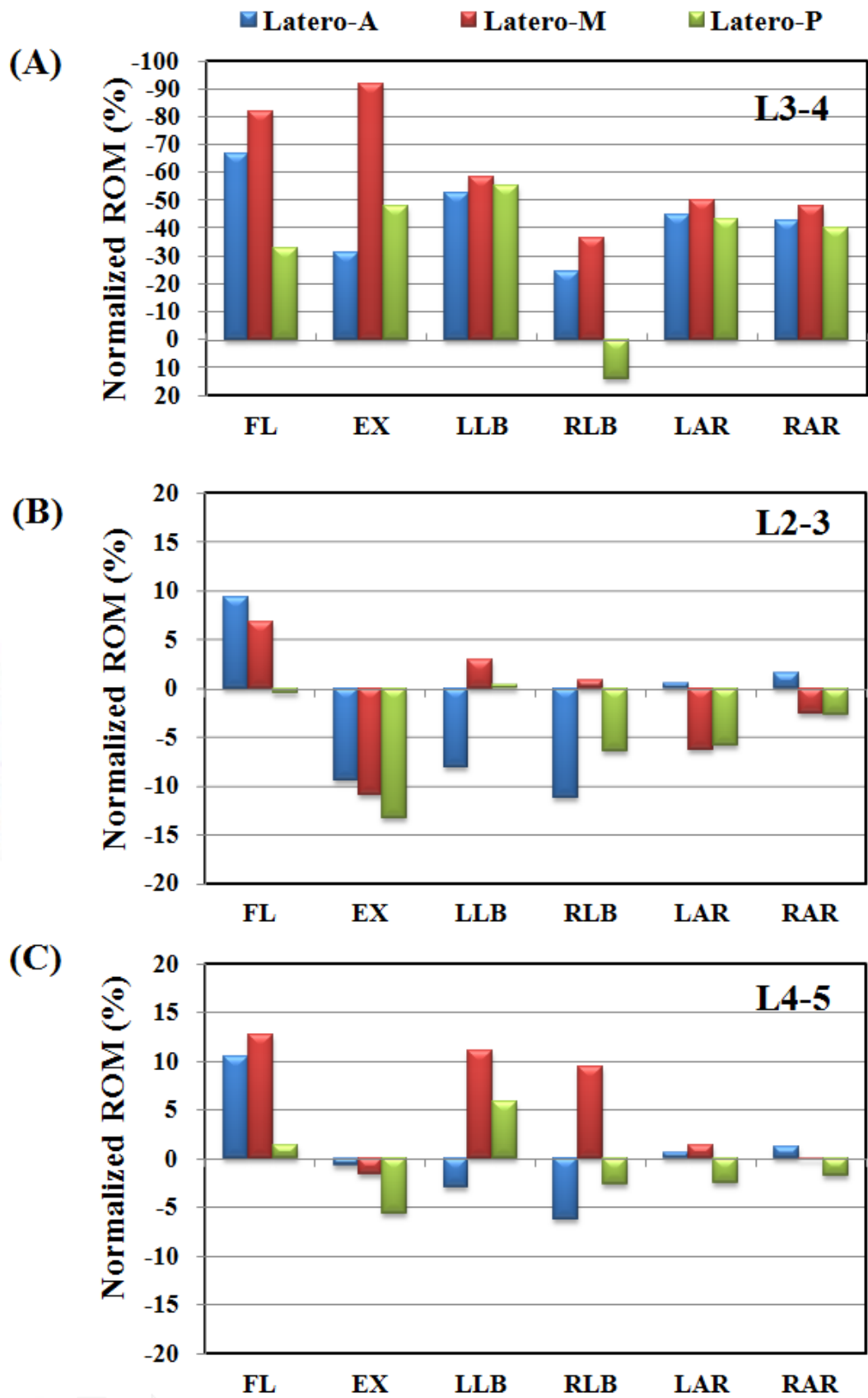


Figure 4. 7: Comparison of the normalized intersegmental ROM among Latero models under six motions. (A) Surgical level. (B) Upper adjacent levels. (C) Lower adjacent level

4.2.2. ROM of different lateral plate angles

Biomechanical behaviors of the Latero models with different lateral plate angle were compared. Data were normalized with respect to the intact model as percentage values under each loading condition (Figure 4.8). For the sake of clarity, the percentages of restricted ROM for the models of the normal lumbar at the surgical level are given below:

FL : Latero-M (-82%) > Latero-(30) (-71%)

EX : Latero-M (-92%) > Latero-(30) (-84%)

LLB: Latero-(30) (-62%) > Latero-M (-59%)

RLB: Latero-(30) (-43%) > Latero-M (-37%)

LAR: Latero-M (-50%) > Latero-(30) (-45%)

RAR: Latero-M (-48%) > Latero-(30) (-38%)

The Latero-M model had the better capability in restricting ROM from -47.9% to -91.6% in flexion, extension and left/right axial rotation. The Latero-(30) model performed ROM control similar to that of Latero-M, and superior to Latero-M model in left/right lateral bending. Moreover, both models performed similar in left/right axial rotation and left lateral bending.

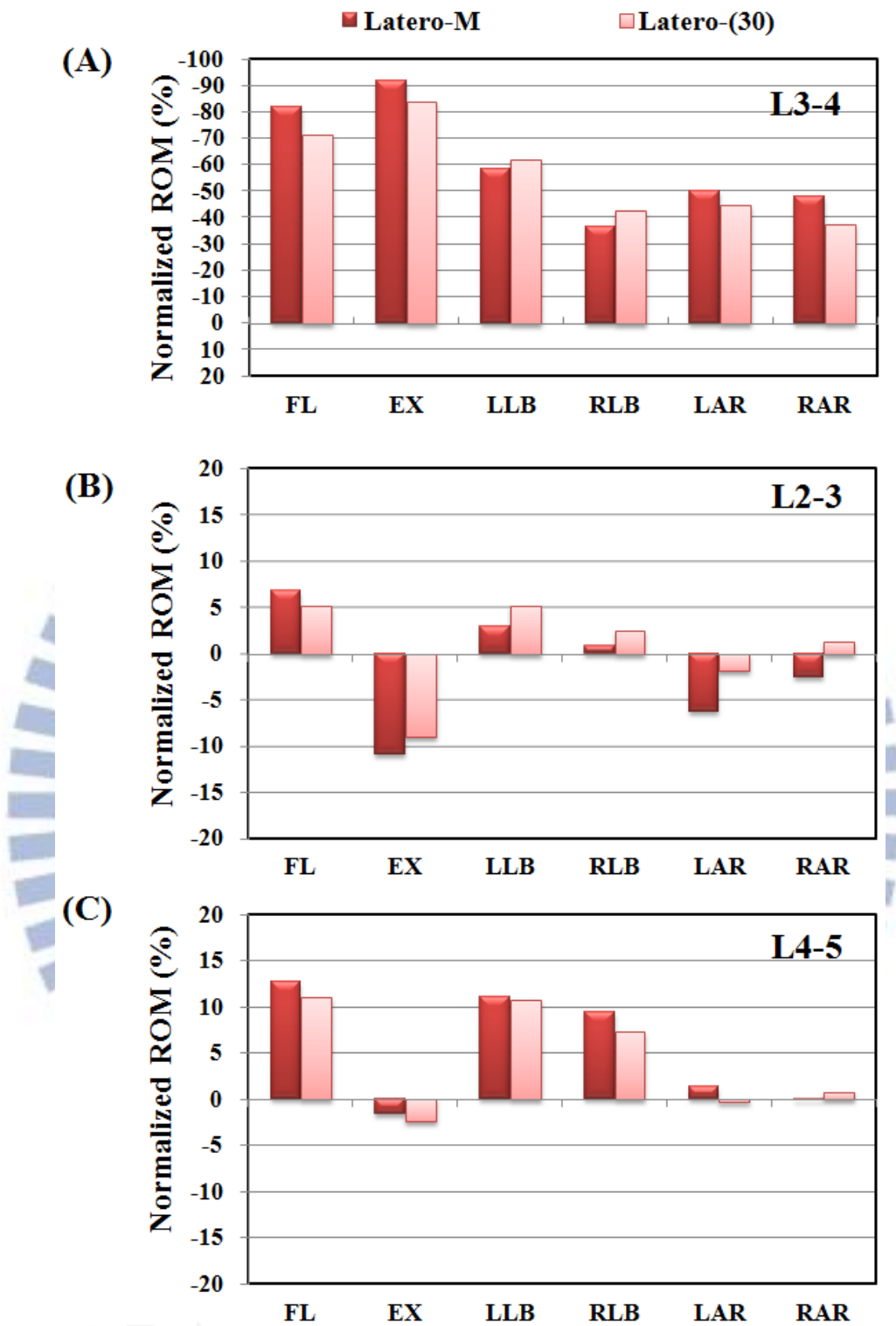


Figure 4. 8: Comparison of the normalized intersegmental ROM among different lateral plate angles of Latero models under six motions. (A) Surgical level. (B) Upper adjacent levels. (C) Lower adjacent level

Chapter 5 Discussion

The purpose of this investigation is to conduct a comprehensive characterization of the three-dimensional kinematic behavior of a new stand-alone implant. In the part-1, the Latero was compared with conventional stand-alone implants and determine their different performances in various physiological motions. With this finite element model using the follower load, it will be possible to study the differences in intersegmental rotation, facet loading, intradiscal pressure, implant stress, and stress concentration on the adjacent vertebrae. In the part-2, the design factors of Latero were investigated. The ROM was used to be the criterion to estimate the modified models.

5.1. Part-1: Comparison with stand-alone implants and conventional fixation method

Recently, surgical trends have shifted using minimally invasive techniques through alternative approaches and reduced loads of fixation devices to mitigate the issues of concern. Examples of such techniques are stand-alone cages coupled with self-stabilizing mechanisms, such as the Latero plate, SynFix screw, and Stabilis cylinder, which eliminate the need of posterior fixation.

5.1.1. ROM

In this study, the results of ROM control showed that the A+P model had the best overall performance and the Stabilis model had the weakest ROM control. Both Latero and SynFix models were shown to have $<(-50\%)$ of ROM control in all motions except for that of the Latero model, which demonstrated a weak control of right lateral bending (-37%). The asymmetrical design of the Latero cage and its instrumentation in the left side of interspace may explain the

different left and right bending behaviors. In practice, this discrepancy might be compensated for by adding bone grafts or elongating the cage to cover the right side of the interspace. Various biomechanical studies have shown that stand-alone cages lack control of extension and axial rotation but not of flexion and lateral bending [81]. The Latero model (-92%) had comparable control in extension as the A+P model (-94%) and was significantly superior to the SynFix model (-51%). This could be explained by the force vector of extension which was directly perpendicular to the Latero plate. This also accounts for the excellent control of extension and axial rotation by the Latero plate in comparison to the other counterparts (Figure 4. 1).

Although the rigidity of the screw-bone interface may be enhanced by injecting cement, there is the possibility of cement-related hazards. In Stabilis, the bony endplates might be compromised by threading in the cylindrical cage, and a higher incidence of cage subsidence than in other cages has been reported [72]. At the adjacent levels, their segmental ROMs were indeed changed when compared with the intact state. However, the changes were small among these four models, even in the stiffest A+P model which is known to have a higher incidence of adjacent segment disease at long-term follow up. This finite element study cannot reflect the consequences of clinical cyclic loading. It can only reveal the ROM changes of adjacent levels.

The varying design concepts of the integrated parts in the self-stabilizing cages not only affect their ROM control, but also influence the stress distribution on the device and the adjacent tissues. In this study, the stress distribution on the Latero plate was much lower and more evenly distributed than that of the SynFix screws (Figure 4. 5). The SynFix screws sustained 3.75 to 9.57 times greater stresses than the Latero plate, with the stress concentrated at the cage-screw junctions. For the Latero and SynFix models, the difference in modes and amounts of distributed stress might be explained by the different configurations of the stabilizing components: sizes, contact areas, and the distance to the center of rotation. In cyclic loading, the Latero plate might be less likely to have fatigue failure than the SynFix screws. The cylindrical cage of the Stabilis model sustained the lowest stress as a result of its relatively

suboptimal ROM control.

5.1.2. von-Mises stress at the vertebra

Stress distribution on the vertebra-cage interface represents vertical compression force exerted on the bony endplate. The Latero model exerted the highest stress on the L4 endplate compared to the other models (Figure 5. 1). This might be due to the stress not being fully shielded by the intervertebral plate and being redistributed by the plate and transmitted onto the L4 endplate. Comparatively, the stress was shielded by the screws of the SynFix and A+P models and thus less stress was distributed on the endplate. In the Stabilis model, because of its relatively poor ROM control, the distributed stress on the endplate was less than in the other three models. There were two biomechanical implications in the Latero model, which had higher vertical load on the L4 endplate than the other counterparts. The first implication indicates that higher vertebral stress may increase the incidence of cage subsidence particularly in suboptimal bone density. On the other hand, unshielded vertical load may be beneficial for graft consolidation according to Wolff's law.

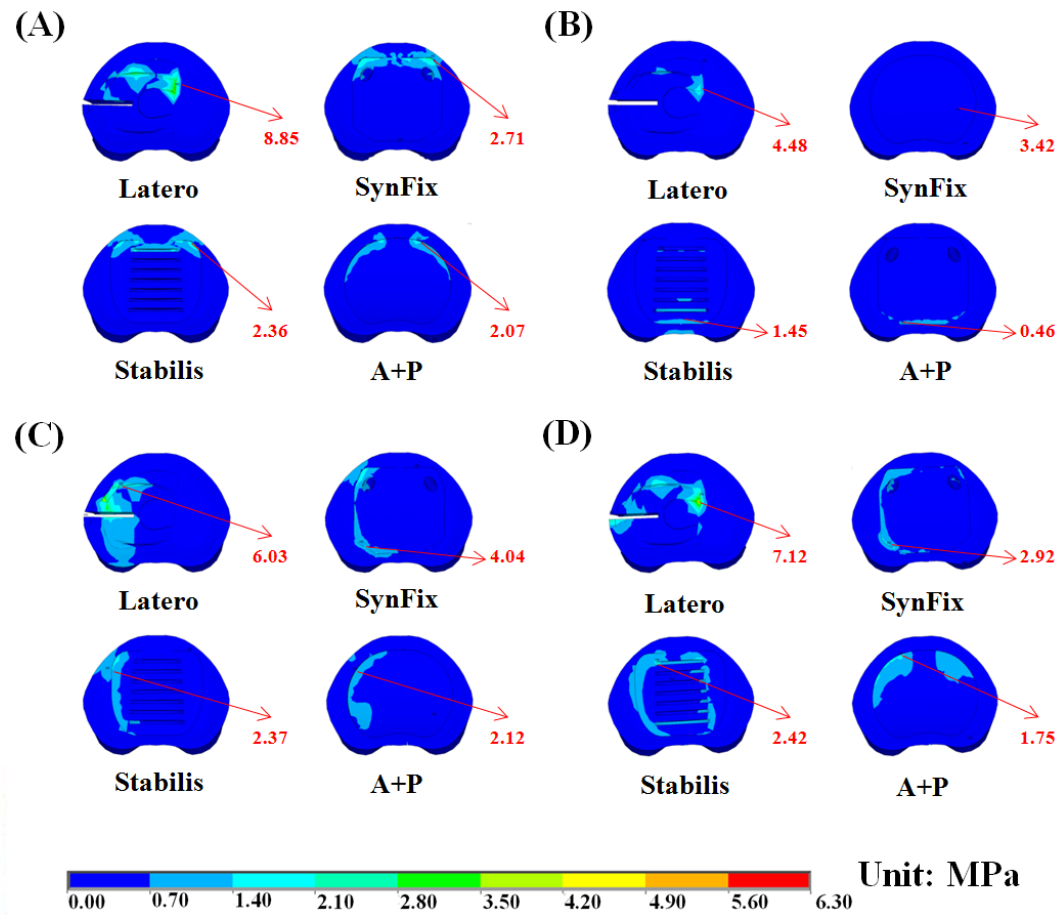


Figure 5. 1: Distribution of endplate stress on the upper surface of the L4 vertebra for all models.

(A) Flexion. (B) Extension. (C) Left lateral bending. (D) Left axial rotation.

5.1.3. Facet contact force

After interbody fusion, abnormally high transmission of loads to the facet joints may ultimately result in arthritic changes. At the surgical level, when comparing the three stand-alone cage models, the Latero model was shown to have the lowest values of facet contact force in bilateral rotation and was near absent in extension (Figure 4. 4). The facet joints at the surgical level seemed to be relatively well protected in the Latero model in comparison to the SynFix and Stabilis models. At the adjacent levels, there were only few differences of facet contact force among all four instrumented models. This may indicate that the reasons for the degenerative facet joints at the adjacent levels might not be attributed to the facet contact force

but other clinical factors.

5.1.4. Stress distribution at the annulus

Distribution of annulus stress can provide the clinical implication that higher stress may result in annulus disruption and disc herniation. At the surgical level for the four instrumented models, the distribution of annulus stress was well correlated inversely to their ROM control (Figure 4. 3). At right lateral bending, the highest annulus stress was found in the Latero model, where it was concentrated at the right annulus. This corresponded to the relatively inferior control of the Latero due to its asymmetrical design. The posterior and left sides of annulus in the Stabilis model sustained the highest stress at extension and lateral bending, which manifested in its inferior control of those moments.

5.1.5. von-Mises stress at the cages

For the stresses of integrated parts, the locking screws of the SynFix model experienced extreme values under extension and lateral bending, and the stress concentrated at the connection area between the cage frame and the screws. In contrast, the thread of Stabilis had relatively lower stress under extension and lateral bending. In Latero and SynFix models, the maximum stresses of the implants occurred on the side plate and locking screws, respectively. However, the stress on the locking screws is larger than that on the side plate. The stress on the locking screws is even 9.57 times of the stress on the side plate under extension. So, the fracture may occurred in the position of the locking screws. The fatigue tests with detailed boundary conditions can be simulated in the future.

5.2. Part-2: The effects of different design factors for Latero device

The aim of part-2 was to modified the Latero device and evaluate the biomechanics of different finite element models for cages with different positions and shapes. In the part-1,

compared to other stand-alone fusion devices, the Latero-M model shown the comparable stability for lumbar spine. In order to improve current design, different positions (Latero-A and Latero-P) and plate angle (Latero-(30)) were proposed to compare the differences of the stability for the spine.

The result of comparing different cage positions suggested that cages placed in the central aspect were 4%-36% stronger than cages placed in anterior aspect or posterior aspect in all physiological motions except rotation. However, all models performed similar stability in rotation (difference within 8%).

The increased value for the bending angle of the lateral plate is one of biomechanical interests, because it implies a more efficient force transfer mechanism in lateral bending and still sufficient stability in other motions. The Latero-(30) model showed sufficient ROM reduction to every physiological motion. It implies that a larger plate angle may present the better combination for the Latero device.

5.3. Limitations

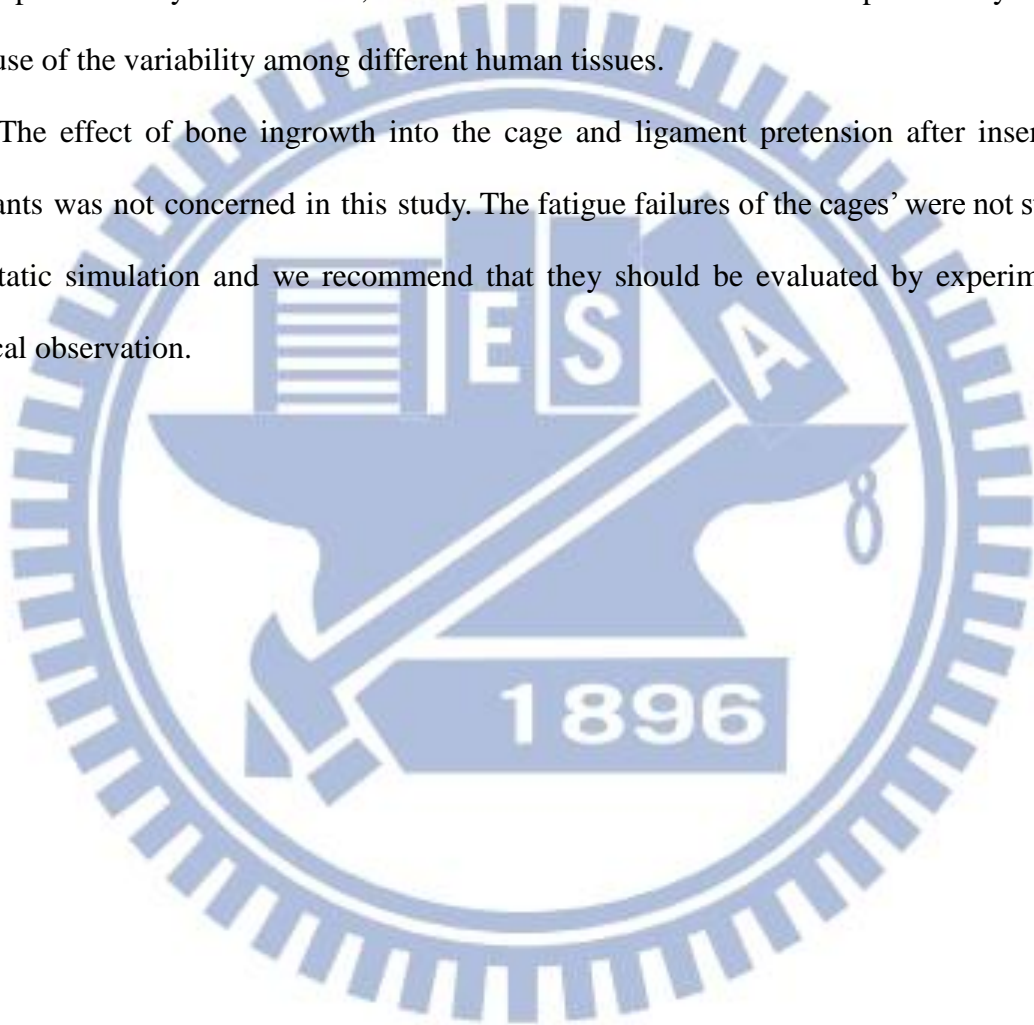
Several limitations in this study are related to the simplified and idealized material properties during simulation, such as the linearized behavior of the spinal ligaments and pure elastic intact discs without degeneration [102, 103]. Degenerative discs are common in most patients with fusion surgery. The various grades of degeneration in the disc, such as delamination, dehydration or reduced disc height, do not allow for exact replication of the unique material properties of a degenerated disc. The osteoporotic bone condition is not considered in this study, either.

In a real spine, the size of vertebra and the orientation of the facet joint are different for each segments. In this study, the CT-scanning images of only one vertebra were used to build the entire lumbar column. The other vertebrae are duplicated and spanned by the intervertebral discs that are manually developed by the CAD software. This makes the

vertebral bodies, posterior elements, and associated processes quite similar in shape and size. In addition, the coefficient of friction used here was based on the results of a previous study about friction parameters between the cage and the bone [102].

The loading conditions in the present finite element simulations were similar to those of the traditional *in vitro* tests. Thus, muscle contraction and pelvic movement were not included in the present study. Furthermore, finite element models should be interpreted only as a trend because of the variability among different human tissues.

The effect of bone ingrowth into the cage and ligament pretension after inserting the implants was not concerned in this study. The fatigue failures of the cages' were not studied in the static simulation and we recommend that they should be evaluated by experimental or clinical observation.



Chapter 6 Conclusion and Future Work

6.1 Part-1: Conclusion

In the stand-alone fusion surgery, the Latero implantation can provide stability in flexion (ROM decreased 82%), extension (ROM decreased 22%), lateral bending (ROM decreased 59% and 37%), and axial rotation (ROM decreased 50% and 48%) at the surgical segment. It had no influence at adjacent segments except during extension (ROM increased 20~24%). In the minimally invasive fusion surgery, the Latero can provide sufficient stability of the surgical segment in lateral bending and axial rotation.

The numerical results of this study have shown that Latero is a stable and effective device. It has the benefits of a minimally invasive procedure, with quick recovery and improvements in pain and function scales. Disc heights were restored and stability maintained by inserting the interbody implant and preserving ligamentous structures. This can indirectly improve the foraminal volume and result in reduction of radiculopathy.

When compared with the ALIF, the lateral approach has two advantages. First, a general surgeon is not needed for access. A lateral approach eliminates the need to violate or retract the peritoneum, or to retract the great vessels. Second, a lateral approach avoids many of the known complications of ALIF, such as damage to the great vessels during mobilization.

In conclusion, this study extensively compared the stabilizing mechanisms of three stand-alone fusion cages. The vertebral plate of the Latero model provided sufficient ability in stabilizing intersegmental motions: it was comparable to the A+P model in flexion and extension, comparable to the SynFix in bilateral axial rotation and left lateral bending, and inferior but compensable in right lateral bending. In contrast, the Stabilis model was less favorable due to its poorer control in extension and lateral bending. Further experimental and clinical studies should be conducted to validate the numerical observations.

6.2 Part-2: Conclusion

In the comparison of different modified Latero models, the Latero-(30) implantation can provide stability in flexion (ROM decreased 71%), extension (ROM decreased 84%), lateral bending (ROM decreased 62% and 43%), and axial rotation (ROM decreased 45% and 38%) at the surgical segment. It improve the stability of Latero-M under right lateral bending (-37% => -43%). Under other motions, the Latero-(30) still provide sufficient stability (-38%~-82%). The Latero-P showed the worse stability in all modified Latero models except in extension. Therefore, the sagittal balances were maintained or improved by placement of the implant in central or anterior position. The coronal balances were corrected by modified (bigger) plate bending angle.

In conclusion, the part-2 of this study found that: (1) The Latero in the middle position can provide better stability to other positions in all physiological motions. (2) Larger plate bending angle can provide better stability in lateral bending.

6.3 Future work

The above studies are focused on single segment disease only. However, the disc degeneration disease occurs sometime in the multi-segment or adjacent segment after fusion surgery. Adjacent segment degeneration is the tendency for clinical symptomatic changes to occur following fusion surgery. It is widely believed that spinal fusion significantly alters the biomechanical environment of the adjacent spinal motion segments leading to an acceleration of the normal degenerative process. However, the outcomes of the combined use with pedicle screws and the multi-segment use of Latero device are unknown. The models instrumented with multiple levels can be a major topic in the further works.

In this study, the size of the implanted cages were decided by the surgeon. However, the lumbar geometry difference of every individual may lead to different analysis result. The size effect of the cages can be considered in the future works. Therefore, the surgeon can select

more appropriate cage size for each patient.

Topics can also be extended for new fusion surgery processes comparing with the Latero device. Ozgur et al. [118] described a minimally disruptive spine procedure called the Extreme Lateral Interbody Fusion or XLIF. The technique is used to gain access to the lumbar spine passing through the retroperitoneal fat and psoas major muscle. It is the other kind of lateral approach. The XLIF® cage (NuVasive Co., USA) is larger than Latero that it is can cross the whole vertebra (figure 6.1). The two-hole lateral plate has been used for clinical use for added stabilization after cage instrumentation. The two-hole lateral plate used here is not the same as the lateral plate in the Latero device. The two-hole lateral was not inserted into the vertebra. It attached on the lateral side of vertebra, and used the superior and inferior screws to stabilize the vertebra (see figure 6.1). The XLIF® device and Latero device are similar in some way. However, no finite element literature exists defining the stabilizing role of XLIF® by far. Therefore, the study of comparing the Latero device and XLIF® device can be investigated in the further.



Figure 6. 1: The XLIF® device (anterior view)

References

1. Weinstein JN, Lurie JD, Tosteson TD et al., “Surgical versus nonsurgical treatment for lumbar degenerative spondylolisthesis”, *New England Journal of Medicine* 2007, vol. 356, no. 22, pp. 2257–2270.
2. Weinstein JN, Lurie JD, Tosteson TD et al., “Surgical compared with nonoperative treatment for lumbar degenerative spondylolisthesis: four-year results in the Spine Patient Outcomes Research Trial (SPORT) randomized and observational cohorts”, *Journal of Bone and Joint Surgery A* 2009, vol. 91, no. 6, pp. 1295–1304.
3. Obenchain TG, “Laparoscopic lumbar discectomy: case report”, *J Laparoendosc Surg* 1991;1:145–9.
4. Regan JJ, Aronoff RJ, Ohnmeiss DD, Sengupta DK. “Laparoscopic approach to L4–L5 for interbody fusion using BAK cages”, *Spine* 1999;4:2171–4.
5. Lieberman IH, Willsher PC, Litwin DE, Salo PT, Kraetschmer BG. “Transperitoneal laparoscopic exposure for lumbar interbody fusion”, *Spine* 2000;25:509–14.
6. Ozgur BM, Aryan HE, Pimenta L, Taylor WR, “Extreme Lateral Interbody Fusion (XLIF): a novel surgical technique for anterior lumbar interbody fusion”, *Spine Journal* 2006, vol. 6, no. 4, pp. 435–443.
7. Oliveira L, Marchi L, Coutinho E, Pimenta L, “A radiographic assessment of the ability of the extreme lateral interbody fusion procedure to indirectly decompress the neural elements”, *Spine* 2010, vol. 35, pp. S331–S337.
8. Oliveira L, Marchi L, Coutinho E, Abdala N, Pimenta L, “The use of rh-BMP2 in standalone eXtreme Lateral Interbody Fusion (XLIF): clinical and radiological results after 24 months follow-up”, *World Spinal Column Journal* 2010, vol. 1, no. 1, pp. 19–25.
9. Ozgur BM, Agarwal V, Nail E, and Pimenta L, “Two-year clinical and radiographic

- success of minimally invasive lateral transpoas approach for the treatment of degenerative lumbar conditions”, SAS Journal 2010, vol. 4, no. 2, pp. 41–46.
10. Billingham J, Akbarnia BA, “Extreme lateral interbody fusion - XLIF”, Current Orthopaedic Practice 2009, vol. 20, no. 3, pp. 238–251.
 11. Rodgers WB, Cox CS, Gerber EJ, “Early complications of extreme lateral interbody fusion in the obese”, Journal of Spinal Disorders and Techniques 2010, vol. 23, no. 6, pp. 393–397.
 12. Amaral R, Marchi L, Oliveira L, “Minimally invasive lateral alternative for thoracolumbar interbody fusion”, Coluna/ Columna 2011, vol. 10, no. 3.
 13. Pimenta L, Oliveira L, Schaffa T, Coutinho E, Marchi L, “Lumbar total disc replacement from an extreme lateral approach: clinical experience with a minimum of 2 years’ followup: clinical article”, Journal of Neurosurgery: Spine 2011, vol. 14, no. 1, pp. 38–45.
 14. Patwardhan AG, Havey RM, Meade KP, Lee B, Dunlap B “A follower load increases the load-carrying capacity of the lumbar spine in compression”, Spine 1999, 24(10), 1003-1009.
 15. http://www.backpain-guide.com/Chapter_Fig_folders/Ch05_Anatomy_Folder/4OverallSpine.html
 16. Hall SJ. Basic Biomechanics, 4th edition, McGraw-Hill, New York, 2004.
 17. McBroom RJ, Hayes WC, Edwards WT, Goldberg RP, White AA 3rd. “Prediction of vertebral body compressive fracture using quantitative computed tomography”, J Bone Joint Surg Am 1985, 67(8), pp.1206-1214.
 18. http://www.karger.com/gazette/65/anderson2/art_2_p.htm
 19. Gower WE, Pedrini V. “Age-related variations in protein polysaccharides from human nucleus pulposus, annulus fibrosus, and costal cartilage”, J Bone Joint Surg Am 1969, 51, pp.1154-1162.

20. Panagiotacopoulos ND, Pope MH, Krag MH, Block R. "Water content in human intervertebral discs. Part I. Measurements by magnetic resonance imaging", *Spine* 1987, 12, pp. 912-917.
21. Marchand F, Ahmed AM. "Investigation of the laminate structure of lumbar disc annulus fibrosus", *Spine* 1990, 15, pp. 402-410.
22. Adams M, Bogduk N, Burton K, Dolan P. "The biomechanics of back pain", 2nd edition, Churchill Livingstone, Edinburgh, 2006.
23. Skaggs DL, Weidenbaum M, Iatridis JC, Ratcliffe A, Mow VC. "Regional variation in tensile properties and biochemical composition of the human lumbar annulus fibrosus", *Spine* 1994, 19(12), pp. 1310-1319.
24. Setton LA, Zhu W, Weidenbaum M, Ratcliffe A, Mow VC. "Compressive properties of the cartilaginous end-plate of the baboon lumbar spine", *J Orthop Res* 1993, 11, pp. 228-239.
25. Farfan H. "Mechanical disorders of the low back", Philadelphia, 1937, Lea & Febiger.
26. Hutton WC, Stott JRR, Cyron BM. "Is spondylolysis a fatigue fracture?" *Spine* 1977, 2, pp. 202-209.
27. <http://www.spineuniverse.com/anatomy/ligaments>
28. <http://www.health.com/health/library/mdp/0,,zm2325,00.html>
29. Zucherman J, Hsu K, Picetti G 3rd, White A, Wynne G, Taylor L. "Clinical efficacy of spinal instrumentation in lumbar degenerative disc disease", *Spine* 1992, 17(7), pp. 834-837.
30. Verbiest H. "A radicular syndrome from developmental narrowing of the lumbar vertebral canal", *J Bone Joint Surg Br* 1954, 36-B (2), pp. 230-237.
31. Arbit E, Pannullo S. "Lumbar stenosis: a clinical review", *Clin Orthop Relat Res* 2001, 384, pp. 137-143.
32. Kirkaldy-Willis WH, Wedge JH, Yong-Hing K, Reilly J. "Pathology and pathogenesis of

- lumbar spondylosis and stenosis”, *Spine* 1978, 3(4), pp. 319-328.
33. Christie SD, Song JK, Fessler RG. “Dynamic interspinous process technology”, *Spine* 2005, 30(16 Suppl), pp. S73-S78.
 34. Brantigan JW, Neidre A, Toohey JS. “The Lumbar I/F Cage for posterior lumbar interbody fusion with the variable screw placement system: 10-year results of a Food and Drug Administration clinical trial”, *Spine J* 2004, 4(6), pp. 681-688.
 35. Siebert E, Prüss H, Klingebiel R, Failli V, Einhäupl KM, Schwab JM. “Lumbar spinal stenosis: syndrome, diagnostics and treatment”, *Nat Rev Neurol* 2009. 5(7), pp.392-403.
 36. Schulte TL, Bullmann V, Lerner T, Schneider M, Marquardt B, Liljenqvist U, Pietilä TA, Hackenberg L. “Lumbar spinal stenosis”, *Orthopade* 2006, 35(6), pp.675-692.
 37. Simotas AC. “Nonoperative treatment for lumbar spinal stenosis”, *Clin Orthop Relat Res* 2001, 384, pp. 153-161.
 38. Vo AN, Kamen LB, Shih VC, Bitar AA, Stitik TP, Kaplan RJ. “Rehabilitation of orthopedic and rheumatologic disorders. Lumbar spinal stenosis”, *Arch Phys Med Rehabil* 2005, 86(3 Suppl 1), pp. S69-S76.
 39. Murphy DR, Hurwitz EL, Gregory AA, Clary R. “A non-surgical approach to the management of lumbar spinal stenosis: a prospective observational cohort study”, *BMC Musculoskelet Disord* 2006, 7, 16.
 40. van Tulder MW, Koes B, Malmivaara A. “Outcome of non-invasive treatment modalities on back pain: an evidence-based review”, *Eur Spine J* 2006,15 Suppl 1, pp. S64-S81.
 41. Wünschmann BW, Sigl T, Ewert T, Schwarzkopf SR, Stucki G. “Physical therapy to treat spinal stenosis”, *Orthopade* 2003, 32(10), pp. 865-868.
 42. Atlas SJ, Keller RB, Wu YA, Deyo RA, Singer DE. “Long-term outcomes of surgical and nonsurgical management of lumbar spinal stenosis: 8 to 10 year results from the maine lumbar spine study”, *Spine* 2005, 30(8), pp. 936-943.
 43. Armin SS, Holly LT, Khoo LT. “Minimally invasive decompression for lumbar stenosis

- and disc herniation”, *Neurosurg Focus* 2008, 25(2), pp. E11.
44. Weinstein JN, Tosteson TD, Lurie JD, Tosteson AN, Blood E, Hanscom B, Herkowitz H, Cammisa F, Albert T, Boden SD, Hilibrand A, Goldberg H, Berven S, An H; SPORT Investigators. “Surgical versus nonsurgical therapy for lumbar spinal stenosis”, *N Engl J Med* 2008, 358(8), pp. 794-810.
 45. Benz RJ, Ibrahim ZG, Afshar P, Garfin SR. “Predicting complications in elderly patients undergoing lumbar decompression”, *Clin Orthop Relat Res* 2001, 384, pp. 116-21.
 46. Mayer HM, List J, Korge A, Wiechert K. “Microsurgery of acquired degenerative lumbar spinal stenosis. Bilateral over-the-top decompression through unilateral approach”, *Orthopade* 2003, 32(10), pp. 889-895.
 47. Thomé C, Zevgaridis D, Leheta O, Bänzner H, Pöckler-Schöniger C, Wöhrle J, Schmiedek P. “Outcome after less-invasive decompression of lumbar spinal stenosis: a randomized comparison of unilateral laminotomy, bilateral laminotomy, and laminectomy”, *J Neurosurg Spine* 2005, 3(2), pp. 129-141.
 48. Ng LC, Tafazal S, Sell P. “The effect of duration of symptoms on standard outcome measures in the surgical treatment of spinal stenosis”, *Eur Spine J* 2007, 16(2), pp. 199-206.
 49. Postacchini F, Cinotti G. “Bone regrowth after surgical decompression for lumbar spinal stenosis”, *J Bone Joint Surg Br* 1992, 74(6), pp. 862-869.
 50. Jutte PC, Castelein RM. “Complications of pedicle screws in lumbar and lumbosacral fusions in 105 consecutive primary operations”, *Eur Spine J* 2002, 11(6), pp. 594-598.
 51. <http://www.orsoosti.com/procedure-information?id=228>
 52. Ploumis A, Transfeldt EE, Denis F. “Degenerative lumbar scoliosis associated with spinal stenosis”, *Spine J* 2007, 7(4), pp. 428-436,.
 53. Gelalis ID, Stafilas KS, Korompilias AV, Zacharis KC, Beris AE, Xenakis TA. “Decompressive surgery for degenerative lumbar spinal stenosis: long-term results”, *Int*

Orthop 2006, 30(1), pp. 59-63.

54. Ikuta K, Arima J, Tanaka T, Oga M, Nakano S, Sasaki K, Goshi K, Yo M, Fukagawa S. "Short-term results of microendoscopic posterior decompression for lumbar spinal stenosis. Technical note", J Neurosurg Spine 2005, 2(5), pp. 624-33.
55. Katz JN, Stucki G, Lipson SJ, Fossel AH, Grobler LJ, Weinstein JN. "Predictors of surgical outcome in degenerative lumbar spinal stenosis", Spine 1999, 24(21), pp. 2229-2233.
56. Mackay DC, Wheelwright EF. "Unilateral fenestration in the treatment of lumbar spinal stenosis", Br J Neurosurg 1998, 12(6), pp. 556-558.
57. Postacchini F. "Surgical management of lumbar spinal stenosis", Spine 1999, 24(10), pp. 1043-1047.
58. Postacchini F, Cinotti G, Perugia D, Gumina S. "The surgical treatment of central lumbar stenosis. Multiple laminotomy compared with total laminectomy", J Bone Joint Surg Br 1993, 75(3), pp. 386-392.
59. Spetzger U, Bertalanffy H, Reinges MH, Gilsbach JM. "Unilateral laminotomy for bilateral decompression of lumbar spinal stenosis. Part II: Clinical experiences", Acta Neurochir (Wien) 1997, 139(5), pp. 397-403.
60. Herkowitz HN, Garfin SR, Eismont FJ, Bell GR, Balderston RA, Rothman-Simeone the spine, 4th edition, Harcourt Publishers International Company, Singapore, 1999.
61. Brantigan JW, Steffee AD, Lewis ML, Quinn LM, Persenaire JM. "Lumbar interbody fusion using the Brantigan I/F cage for posterior lumbar interbody fusion and the variable pedicle screw placement system: two-year results from a Food and Drug Administration investigational device exemption clinical trial", Spine 2000, 25(11), PP. 1437-1446.
62. <http://www.spine-health.com/treatment/spinal-fusion/anterior-lumbar-interbody-fusion-alif-surgery>.
63. <http://www.spine-health.com/treatment/back-surgery/posterior-lumbar-interbody-fusion->

plif-surgery.

64. Ames CP, Acosta FL Jr, Chi J, Iyengar J, Muiro W, Acaroglu E, Puttlitz CM. “Biomechanical comparison of posterior lumbar interbody fusion and transforaminal lumbar interbody fusion performed at 1 and 2 levels”, *Spine* 2005, 30(19), pp.E562-E566.
65. http://www.spineuniversity.com/anterior_lumbar_fusion_with_cages
66. Brantigan JW, Steffee AD, Lewis ML, Quinn LM, Persenaire JM “Lumbar interbody fusion using the Brantigan I/F cage for posterior lumbar interbody fusion and the variable pedicle screw placement system: two-year results from a Food and Drug Administration investigational device exemption clinical trial”, *Spine* 2000, 25:1437-1446
67. Kuslich SD, Danielson G, Dowdle JD, Sherman J, Fredrickson B, Yuan H, Griffith SL “Four-year follow-up results of lumbar spine arthrodesis using the Bagby and Kuslich lumbar fusion cage”, *Spine* 2000, 25:2656-2662.
68. Pavlov PW, Spruit M, Havinga M, Anderson PG, van Limbeek J, Jacobs WC “Anterior lumbar interbody fusion with threaded fusion cages and autologous bone grafts”, *Eur Spine J* 2000, 9:224-229.
69. Steffen T, Tsantrizos A, Aebi M “Effect of implant design and endplate preparation on the compressive strength of interbody fusion constructs”, *Spine* 2000, 25:1077-1084
70. McAfee PC. “Interbody fusion cages in reconstructive operations on the spine”, *J Bone Joint Surg Am* 1999, 81(6), pp.859-880.
71. Schleicher P, Gerlach R, Schár B, Cain CM, Achatz W, Pflugmacher R, Haas NP, Kandziora F “Biomechanical comparison of two different concepts for stand alone anterior lumbar interbody fusion”, *Eur Spine J* 2008, 17:1757-1765.
72. Cho CB, Ryu KS, Park CK “Anterior lumbar interbody fusion with stand-alone interbody cage in treatment of lumbar intervertebral foraminal stenosis: comparative study of two different types of cages”, *J Korean Neurosurg Soc* 2010, 47:352-357.

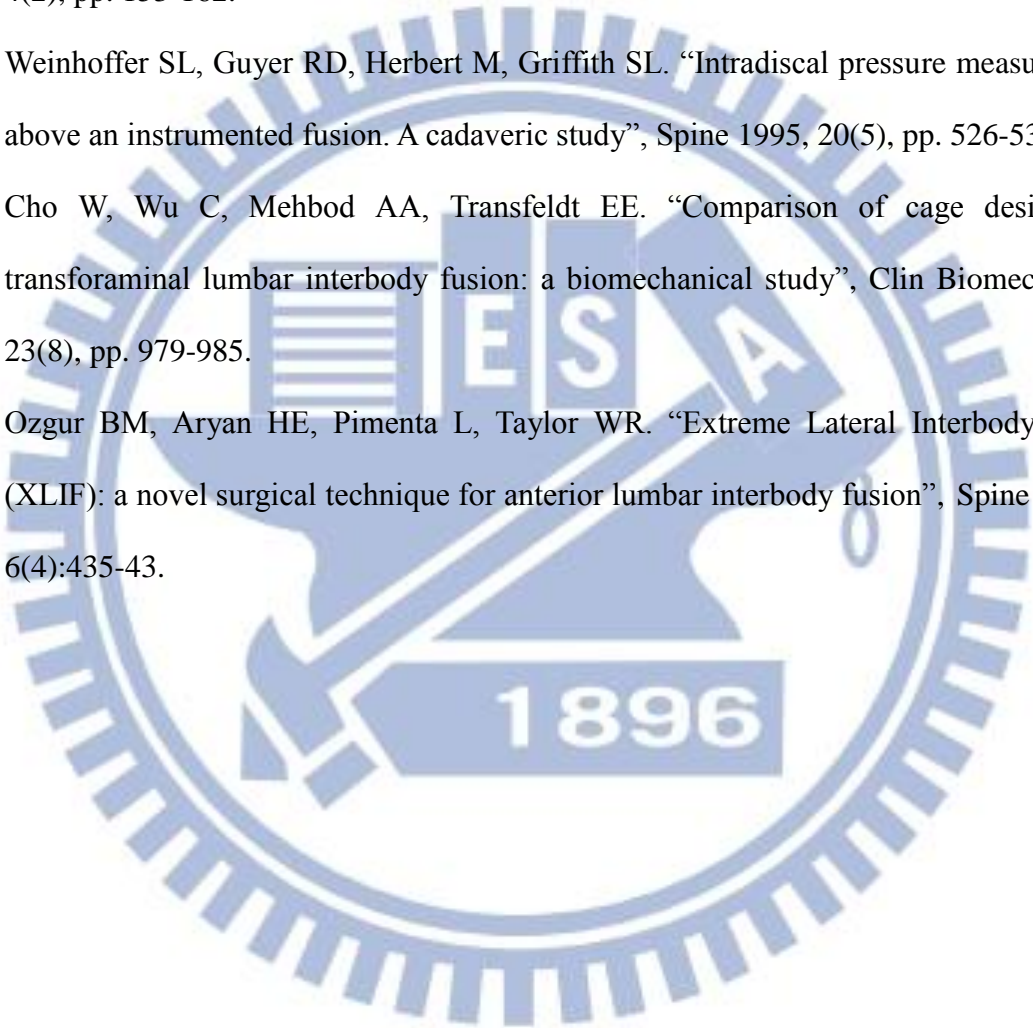
73. Regan JJ, Aronoff RJ, Ohnmeiss DD, Sengupta DK. "Laparoscopic approach to L4–L5 for interbody fusion using BAK cages", *Spine* 1999;4:2171–4.
74. Lieberman IH, Willsher PC, Litwin DE, Salo PT, Kraetschmer BG. "Transperitoneal laparoscopic exposure for lumbar interbody fusion", *Spine* 2000, 25:509–14.
75. Olsen D, McCord D, Law M. "Laparoscopic discectomy with anterior interbody fusion of L5–S1", *Surg Endosc* 1996, 10:1158–63.
76. Regan JJ, Yuan H, McAfee PC. "Laparoscopic fusion of the lumbar spine", *Spine* 1999, 24:402–11.
77. Zdeblick TA, David SM. "A prospective comparison of surgical approach for anterior L4–L5 fusion", *Spine* 2000, 25:2682–7.
78. Zucherman JF, Zdeblick TA, Bailey SA, Mahvi D, Hsu KY, Kahrs D. "Instrumented laparoscopic spinal fusion", *Spine* 1995, 20:2029–35.
79. Regan JJ, Aronoff RJ, Ohnmeiss DD, Sengupta DK. "Laparoscopic approach to L4-L5 for interbody fusion using BAK cages: experience in the first 58 cases", *Spine* 1999, 15;24(20):2171-4.
80. Baker JK, Reardon PR, Reardon MJ, Heggeness MH. "Vascular injury in anterior lumbar surgery", *Spine* 1993, 18(15):2227-30.
81. Oxland TR, Lund T. "Biomechanics of stand-alone cages and cages in combination with posterior fixation: a literature review", *Eur Spine J* 2000, 9:S95-S101.
82. Costa F, Sassi M, Ortolina A, Cardia A, Assietti R, Zerbi A, Lorenzetti M, Galbusera F, Fornari M. "Stand-alone cage for posterior lumbar interbody fusion in the treatment of high-degree degenerative disc disease: design of a new device for an "old" technique. A prospective study on a series of 116 patients", *Eur Spine J* 2011, 20:S46–S56.
83. Tsuang YH, Chiang YF, Hung CY, Wei HW, Huang CH, Cheng CK. "Comparison of cage application modality in posterior lumbar interbody fusion with posterior instrumentation—A finite element study", *Med Eng Phys* 2009, 31:565–570

84. Lin RM, Huang KY, Lai KA. "Mini-open anterior spine surgery for anterior lumbar diseases", *Eur Spine J* 2008, 17:691-697
85. Cain CM, Schleicher P, Gerlach R, Pflugmacher R, Scholz M, Kandziora F. "A new stand-alone anterior lumbar interbody fusion device: biomechanical comparison with established fixation techniques", *Spine* 2005, 30(23):2631-2636
86. Kim Y. "Finite element analysis of anterior lumbar interbody fusion: threaded cylindrical cage and pedicle screw fixation", *Spine* 2007, 32:2558-2568
87. Steffen T, Tzantrizos A, Fruth I, Aebi M. "Cage: designs and concepts", *Eur Spine J* 2000, 9: S89-S94
88. Chen SH, Tai CL, Lin CY, Hsieh PH, Chen WP. "Biomechanical comparison of a new stand-alone anterior lumbar interbody fusion cage with established fixation techniques - a three-dimensional finite element analysis", *BMC Musculoskeletal Disorders* 2008, 9:88.
89. Jost B, Cripton PA, Lund T, Oxland TR, Lippuner K, Jaeger P, Nolte LP. "Compressive strength of interbody cages in the lumbar spine: the effect of cage shape, posterior instrumentation and bone density", *Eur Spine J* 1998, 7:132-141.
90. Lu YM, Hutton WC, Gharpuray VM. "Do bending, twisting, and diurnal fluid changes in the disc affect the propensity to prolapse? A viscoelastic finite element model", *Spine* 1996, 21(22), pp.2570-2579.
91. Rohlmann A, Zander T, Bergmann G. "Effect of total disc replacement with ProDisc on intersegmental rotation of the lumbar spine", *Spine* 2005, 30(7), pp.738-743.
92. Schmidt H, Heuer F, Simon U, Kettler A, Rohlmann A, Claes L, Wilke HJ. "Application of a new calibration method for a three-dimensional finite element model of a human lumbar annulus fibrosus", *Clin Biomech (Bristol, Avon)* 2006, 21(4), pp. 337-344.
93. Marchand F, Ahmed AM. "Investigation of the laminate structure of lumbar disc annulus fibrosus", *Spine* 1990, 15, pp. 402-410.
94. Polikeit A, Ferguson SJ, Nolte LP, Orr TE. "Factors influencing stresses in the lumbar

- spine after the insertion of intervertebral cages: finite element analysis”, *Eur Spine J* 2003, 12(4), pp. 413-420.
95. Shirazi-Adl A, Ahmed AM, Shrivastava SC. “Mechanical response of a lumbar motion segment in axial torque alone and combined with compression”, *Spine* 1986, 11, pp. 914-927.
 96. Panagiotacopoulos ND, Pope MH, Krag MH, Block R. “Water content in human intervertebral discs. Part I. Measurements by magnetic resonance imaging”, *Spine* 1987, 12: pp. 912-917.
 97. Agur AMR, Lee MJ. *Grant’s atlas of anatomy*, 10th edition, Lippincott Williams & Wilkins, Philadelphia, Pennsylvania, 1999.
 98. Goel VK, Monroe BT, Gilbertson LG, Brinckmann P. “Interlaminar shear stresses and laminae separation in a disc. Finite element analysis of the L3-L4 motion segment subjected to axial compressive loads”, *Spine* 1995, 20(6), pp. 689-698.
 99. White AA, Panjabi MM. *Clinical biomechanics of the spine*, 2nd edition, J.B. Lippincott Company, Philadelphia, Pennsylvania 1990.
 100. Lee KK, Teo EC, Fuss FK, Vanneville V, Qiu TX, Ng HW, Yang K, Sabitzer RJ. “Finite-element analysis for lumbar interbody fusion under axial loading”, *IEEE Trans. Biomed Eng* 2004, 51, pp. 393-400.
 101. Polikeit A, Ferguson SJ, Nolte LP, Orr TE. “Factors influencing stresses in the lumbar spine after the insertion of intervertebral cages: finite element analysis”, *Eur Spine J* 2003, 12(4), pp.413-420.
 102. Chen SH, Zhong ZC, Chen CS, Chen WJ, Hung C. “Biomechanical comparison between lumbar disc arthroplasty and fusion”, *Med Eng Phys* 2009, 31(2), pp. 244-253.
 103. Zhong ZC, Chen SH, Hung CH. “Load- and displacement-controlled finite element analyses on fusion and non-fusion spinal implants”, *Proc Inst Mech Eng* 2009, 223(2), pp. 143-157.

104. Rohlmann A, Neller S, Claes L, Bergmann G, Wilke HJ. "Influence of a follower load on intradiscal pressure and intersegmental rotation of the lumbar spine", *Spine* 2001, 26(24), pp. E557-E561.
105. Lafage V, Gangnet N, Senegas J, Lavaste F, Skalli W. "New interspinous implant evaluation using an in vitro biomechanical study combined with finite-element analysis", *Spine* 2007, 32(16), 1706-1713.
106. Panjabi MM. "Hybrid multidirectional test method to evaluate spinal adjacent-level effects", *Clin. Biomech.* 2007, 22:257-265.
107. Gardner-Morse M, Stokes IAF. "Structural behavior of human lumbar spinal motion segments", *Journal of Biomechanics* 2004, 37, 205–212.
108. Crisco JJ, Panjabi MM, Yamamoto I, Oxland, TR. "Euler stability of the human ligamentous lumbar spine, Part I: theory", *Clinical Biomechanics* 1992a, 7: 19–26.
109. Rohlmann A, Zander T, Bergmann G. "Effects of total disc replacement with ProDisc on intersegmental rotation of the lumbar spine", *Spine* 2005, 30(7), 738-743.
110. Rohlmann A, Neller S, Claes L, Bergmann G, Wilke HJ. "Influence of a follower load on intradiscal pressure and intersegmental rotation of the lumbar spine", *Spine* 2001, 26(24), E557-E561.
111. Shirazi-Adl A, Parnianpour M. "Load-bearing and stress analysis of the human spine under a novel wrapping compression loading", *Clinical Biomechanics* 2000, 15, 718–725.
112. Shirazi-Adl A. "Analysis of large compression loads on lumbar spine in flexion and in torsion using a novel wrapping element", *Journal of Biomechanics* 2006, 39, 267–275.
113. Renner SM, Natarajan RN, Patwardhan AG, Havey RM, Voronov LI, Guo BY, Andersson GB, An HS. "Novel model to analyze the effect of a large compressive follower pre-load on range of motions in a lumbar spine", *J Biomech* 2007, 40(6), pp. 1326-1332.

114. Rohlmann A, Bauer L, Zander T, Bergmann G, Wilke HJ. "Determination of trunk muscle forces for flexion and extension by using a validated finite element model of the lumbar spine and measured in vivo data", *J Biomech* 2006, 39(6):981-9.
115. Little JS, Ianuzzi A, Chiu JB, Baitner A, Khalsa PS. "Human lumbar facet joint capsule strains: II. Alteration of strains subsequent to anterior interbody fixation", *Spine J* 2004, 4(2), pp. 153-162.
116. Weinhoffer SL, Guyer RD, Herbert M, Griffith SL. "Intradiscal pressure measurements above an instrumented fusion. A cadaveric study", *Spine* 1995, 20(5), pp. 526-531.
117. Cho W, Wu C, Mehbod AA, Transfeldt EE. "Comparison of cage designs for transforaminal lumbar interbody fusion: a biomechanical study", *Clin Biomech* 2008, 23(8), pp. 979-985.
118. Ozgur BM, Aryan HE, Pimenta L, Taylor WR. "Extreme Lateral Interbody Fusion (XLIF): a novel surgical technique for anterior lumbar interbody fusion", *Spine J*, 2006, 6(4):435-43.



Vita

個人簡介

中文姓名	江銘傑	
英文姓名	Ming-Chieh Chiang	
性別	男	
出生日期	民國 70 年 9 月 27 日	
E-mail	jmj.me93g@nctu.edu.tw	
電話	0919-690-372	
地址	520 彰化縣員林鎮鎮興里員東路一段 98 巷 52 號之 3	

學歷

學校名稱	國別	主修學門系所	學位	起訖年月(西元年/月)
國立交通大學	中華民國	機械工程系	博士	2006 / 09 – 2013 / 11
國立交通大學	中華民國	機械工程系	碩士	2004 / 09 – 2006 / 06
國立清華大學	中華民國	動力機械工程系	學士	2000 / 09 – 2004 / 06
國立員林高中	中華民國		高中	1997 / 09 – 2000 / 06

Publication List

Journal Papers

1. Chen SH, **Chiang MC**, Lin JF, Lin SC, Hung CH. “Biomechanical comparison of three stand-alone lumbar cages --- a three-dimensional finite element analysis”, BMC Musculoskelet Disord 2013, 14(1):281. DOI: 10.1186/10.1186/1471-2474-14-281 [Epub ahead of print]
2. Chen SH, **Chiang MC**, Hung CH, Lin SC, Chang HW. “Finite element comparison of retrograde intramedullary nailing and locking plating fixation with/without an intramedullary allograft for distal femur fracture following total knee arthroplasty”, Knee 2013. DOI: 10.1016/j.knee.2013.03.006. [Epub ahead of print]
3. Chen SH, **Chiang MC**, Zhong ZC, Hung C. “The finite element analysis using a follower load on fusion and non-fusion spinal implants”, Journal of Orthopaedic Surgery Taiwan 2009, Vol. 26 No. 4 p170-179.

4. Chien CY, Tan CH, Lin SC, Chuang WH, **Chiang MC**, Luh YP, Chen YJ. “Pretension Effects of the Dynesys Cord on the Tissue Responses and Screw-Spacer Behaviors of the Lumbosacral Construct With Hybrid Fixation”, Spine 2013, 1;38(13):E775-E782

Conference Papers

1. Chen SH, Zhong ZC, **Chiang MC**, Chen WJ, Hung C. “The load and displacement controlled finite element analyses on fusion and non-fusion spinal implants”, 53rd Congress of Taiwan Orthopaedic Association, Taoyuan, Taiwan, October 27-28 2007.
2. Chen SH, Zhong ZC, **Chiang MC**, Chen WJ, Hung C. “The load and displacement controlled finite element analyses with follower load on fusion and non-fusion spinal implants”, 55th Congress of Taiwan Orthopaedic Association, Taoyuan, Taiwan 2008.
3. Lo CC, Zhong ZC, Chen SH, **Chiang MC**, Hung C. “Biomechanical effect of TLIF combined with Coflex-F or with unilateral pedicle screw fixation for minimally invasive surgery - A finite element study”, ESB2010, 17th Congress of the European Society of Biomechanics. University of Edinburgh, UK. July 5 - 8, 2010.
4. Lo CC, Zhong ZC, Chen SH, **Chiang MC**, Hung C. “Biomechanical effect after interspinous process device (Coflex) implantation for multilevel decompression surgery - A finite element study”, ESB2010, 17th Congress of the European Society of Biomechanics. University of Edinburgh, UK. July 5 - 8, 2010.